

1 Response to the reviewers' comments on

2 **Atmospheric energy budget response to idealized aerosol perturbation in tropical cloud**
3 **systems**

4 We would like to thank the revisers for their constructive and thoughtful reviews that helped
5 us improve our paper.

6 Below please find a point by point reply to all of the reviewers' comments (in blue).
7

8 **Reviewer #1:**

9 The authors have run some fairly large-domain cloud resolving simulations over the tropical
10 Atlantic, in order to investigate how aerosol indirect effects contribute to the radiative impact
11 of aerosols. They note a non-negligible contribution that depends on the cloud regime being
12 examined. The regime and location dependence of aerosol forcing is something that is not well
13 captured in climate models, since most don't include aerosol effects on convection. This study
14 is straightforward and worthwhile, as it begins to break down these differences in the radiation
15 budgets. I believe it is a good contribution and have only a few suggestions to help improve
16 the manuscript.

17 Reply: we would like to thank the reviewer again for the effort and the constructive comments.
18 We are happy that the reviewer found our paper to be straightforward and worthwhile.
19

20 **Comments:**

21 Changing CDNC is, you even admit, a rather simplistic way to approach aerosol effects. In
22 addition to neglecting the activation and scavenging effects that you mention, another missing
23 piece is the direct effect. This can be especially important in the eastern Atlantic where you are
24 looking since a lot of the aerosols that would be present in this region are dust. Have you
25 considered how the direct effect would fit into this?

26 Reply: Thank you for this comment. Indeed, the direct effect of aerosol is interesting and
27 important [and is a main focus of our work, i.e. (Dagan et al., 2019)] but is not included in this
28 study. We believe that separating the overall response of the atmospheric energy budget to the
29 radiative and microphysical aerosol effects is a necessary first step in studying this complex
30 system. This is the approach we are taking in the current study. However, we are currently
31 working on implementing the aerosol model HAM (Stier et al., 2005) into the regional version
32 of ICON. This will allow studying the mutual interaction between the aerosol radiative and
33 microphysical effects in a cloud and aerosol resolving simulations.

34 Following this comment, we have added to the revised manuscript the following:

35 *“The different CDNC scenarios serve as a proxy for different aerosol conditions (as the first*
36 *order effect of increased aerosol concentration on clouds is to increase the CDNC, Andreae,*
37 *2009). This also allows to separate the cloud response from the uncertainties involved in the*
38 *representation of the aerosols in numerical models (Ghan et al., 2011; Simpson et al., 2014;*
39 *Rothenberg et al., 2018). However, it limits potential feedbacks between clouds and aerosols,*
40 *such as the removal of aerosol levels by precipitation scavenging and potential aerosol effects*
41 *thereon. In addition, the fixed CDNC framework does not capture the differences in aerosol*
42 *activation between shallow and deep clouds, due to differences in vertical velocity. Another*
43 *aerosol effect that is not included in our simulations is the direct interaction between aerosol*
44 *and radiation. In future work we plan to examine the mutual interaction between microphysical*
45 *effects and the direct aerosol radiative effects.”*

46

47 In the conclusions:

48 *“Furthermore, we do not include the temporal evolution of the aerosol concentration.*
49 *Feedbacks between the aerosol concentration and clouds processes (such as wet scavenging),*
50 *as well as the direct effects of aerosol on radiation would add another layer of complexity that*
51 *should be accounted for in future work.”*

52

53 **You held SST constant in these simulations. Do you have a sense for how much this might**
54 **have affected the overall energy budgets? I would suspect at least the sensible heat flux might**
55 **show some differences.**

56 Reply: We agree that including interactive SST would predominantly affect the sensible heat
57 flux. However, please note that in both cases the sensible heat flux is an order of magnitude
58 smaller than the rest of the terms (Figs. 4 and 12 in the manuscript). Hence, we do not believe
59 that the effect on the total energy budget would be large. In addition, due to the large heat
60 capacity of the ocean, over two days of simulation the SST is not expected to dramatically
61 change. For example, in the deep-cloud dominated case, the difference in the surface radiative
62 fluxes between the clean and polluted conditions is about 12 W/m². Considering the heat
63 capacity of 50m deep ocean mixed layer results in about 0.005K difference in the SST between
64 the two cases over the two days simulation. In the shallow-cloud dominated case the difference
65 in surface radiative fluxes is about half of the deep-cloud dominated case (6 W/m²), resulting
66 in half the temperature change.

67 Following this argument, we added a clarification about this point to the revised manuscript:

68 “Additional details, such as the surface and atmospheric physics parameterizations, are
69 described in Klocke et al., (2017) and include an interactive surface flux scheme and fixed sea
70 surface temperature (SST). We note that using a fixed SST does not include feedbacks of
71 aerosols on the SST evolution that could change the surface fluxes. However, due to the large
72 heat capacity of the ocean, we do not expect the SST to dramatically change over the two days
73 simulations.”

74

75 Your ‘residual’ term is rather large, especially in the deep convective case. You make the point
76 earlier that this term would become negligible on longer time and spatial scales, however an
77 important point in this paper is how large the differences can be on smaller scales. Do you have
78 thoughts on what is largely making up this residual term? How much of it is physical processes
79 that you are not considering, versus the fact that the model simulations are not going to be
80 perfectly balanced, considering the scales and the boundary forcing.

81 Reply: What was previously called a “residual” term was changes in the revised manuscript to
82 be refer to as “energy imbalance” as it better describes it. A recent study shows that in order to
83 get close to energy balance the spatial scale should be on the order of ~5000km (Jakob et al.,
84 2019) and the time scale longer than a month (we found a similar scale using GCMs). Our
85 simulations operate on smaller spatial-temporal scales than that and hence it is not surprising
86 that we obtain an imbalance.

87 The energy imbalance is composed of changes in the storage term and local divergence or
88 convergence of dry-static energy into the domain. In our case, almost the entire imbalance is
89 simply dry static energy that moves in or out of the domain. For example, in the deep-cloud
90 dominated case there is a net production of dry-static energy in the domain by precipitation
91 (which is not entirely balanced by the radiative cooling). This extra dry-static energy is then
92 advected out of the domain.

93 An explanation about this point was added to the revised manuscript:

94 “The total column atmospheric energy budget can be described as follows:

$$95 \quad LP + Q_R + Q_{SH} = \text{div}(s) + ds/dt \quad (1)$$

96 Equation 1 presents a balance between the latent heating rate (LP - latent heat of condensation
97 [L] times the surface precipitation rate [P]), the surface sensible heat flux (Q_{SH}), the atmospheric
98 radiative heating (Q_R), the divergence of dry static energy ($\text{div}(s)$, which will become negligible
99 on sufficiently large spatial scales), and the dry static energy storage term (ds/dt , which will
100 become negligible on long [inter-annual] temporal scales). Throughout the rest of this paper we

101 will refer to the right-hand side of Equation 1 ($\text{div}(s)+ds/dt$) as the energy imbalance (which is
102 calculated as the residual $[R]$ of the left-hand side).”

103

104 “In this shallow-cloud dominated case the radiative cooling of the atmosphere is significantly
105 larger than the warming due to precipitation (mean of -114.7 W/m^2 compared to 90.1 W/m^2),
106 hence the energy imbalance (R) is negative. Negative R means that there must be some
107 convergence of dry static energy into the domain and/or decrease in the storage term, in this
108 case it is mostly due to convergence of dry static energy.”

109

110 “Next, we analyse the atmospheric energy budget for the deep-cloud dominated case (Fiona
111 tropical storm – Fig. 12). As opposed to the shallow-cloud dominated case, in this case the LP
112 contribution dominates over the radiative cooling and hence the energy imbalance R is positive
113 and large, suggesting divergence of dry static energy out of the domain.”

114

115

116 Your mass flux in Fig 11 - how is this calculated? Is this just a total over the whole domain?
117 Or only in updrafts? If this is domain-wide, I imagine the largest reason for the increase is
118 simply the larger amount of deep convection.

119 Reply: Thank you for your comment that helped us clarify this point. Calculating the relative
120 change in the cloud fraction and in the water content between clean and polluted conditions
121 demonstrate the dominate role of the latter in the increase in mass flux. This calculation
122 demonstrates that the cloud fraction (total water content) increases by 20% (72%) at 500mb in
123 the simulation with $\text{CDNC}=200\text{cm}^{-3}$ compared with the simulations with $\text{CDNC}=20\text{cm}^{-3}$ in the
124 deep-convection dominated case. Similarity, in the shallow dominated case the cloud fraction
125 (total water content) increases by 22% (85%) at 500mb in the simulation with $\text{CDNC}=200\text{cm}^{-3}$
126 compared with the simulations with $\text{CDNC}=20\text{cm}^{-3}$. These calculations demonstrate that about
127 80% of the increase in mass flux under polluted conditions occur due to the increase in water
128 content and only about 20% occur due to the increase in cloud fraction (recalling that the
129 vertical velocity is similar between the two simulations). The increase in total water content is
130 caused by warm rain suppression at the lower troposphere.

131 This is now better explained in the revised manuscript:

132 “Both the increase in water vapor and ice content in the upper troposphere are driven by an
133 increase in upward water (liquid and ice) mass flux with increasing CDNC (Fig. 11). An

134 *increase in mass flux could be caused by an increase in vertical velocities and/or by an increase*
135 *in cloud (or updraft) fraction and/or by an increase in cloud water content. In our case, the*
136 *increases in mass flux is driven partially by the small increase in vertical velocity (especially*
137 *for updraft between 5 and 10 m/s – Fig. 11), partially by the small increase in cloud fraction at*
138 *this level (Fig. 9) and mostly due to the larger water mass mixing ratio (Fig. 9) that leads to*
139 *an increase in mass flux even for a given vertical velocity.”*

140

141 *“Analysis of the upward water mass flux from the warm to the cold part of the clouds (at 500*
142 *mb) in the different simulations (Fig. 19), demonstrates a substantial increase with the increase*
143 *in CDNC (Chen et al., 2017), which occurs due to the increase in the water content (Fig. 17)*
144 *and the delay in the rain formation to higher levels (Heikenfeld et al., 2019), even without a*
145 *large change in the vertical velocity or cloud fraction at this level (Fig.17).”*

146

147

148 *The paper is a bit long and I think you could consider getting rid of a few of the figures that*
149 *tell a redundant story. The inclusion of the 2nd, deep convective case is important because of*
150 *this point you make on page 32 "Our results demonstrate that regional atmospheric energy*
151 *budgets can be significantly perturbed by changes in CDNC and that the magnitude of the*
152 *effect is cloud regime dependent (even for a given geographical region and given time of the*
153 *year as the two cases are separated by less than a week)." However, the physical mechanisms*
154 *for the changes in cloud amount and radiative fluxes are consistent between the two cases, so*
155 *some of the figures and discussion here are a bit repetitive.*

156 Reply: Thank you for this comment. We did consider shortening the paper and not including
157 the figures of the second case but eventually we decided to keep them in as it demonstrate an
158 important point of this paper that the aerosol effect on the atmospheric energy budget is
159 meteorological conditions dependent.

160

161 *In general this could use some copy-editing. Nothing that prevents understanding, but there are*
162 *a number of small typos and verb agreement issues.*

163 Reply: Thank you. The manuscript went through copy editing and corrected accordingly.

164

165

166

167

168 **Reviewer #2:**

169 This paper studies the differences in the radiative and energy budgets in a tropical environment
170 when the cloud droplet number concentration (CDNC) is changed (as a proxy for changes to
171 the environmental aerosol concentration). The simulated periods are two separate 2-day within
172 the same week where the convection is either predominantly shallow or predominantly deep -
173 each case is simulated with CDNC values. The authors find substantial changes in amount of
174 energy absorbed by the atmosphere by changing the CDNC and find substantial differences in
175 the response between the two sets of simulations.

176 The main component of the paper is a breakdown of the energy budget into radiative, sensible
177 heating and heating through precipitation formation. The radiative component is later broken
178 down into shortwave and longwave fluxes at both the surface and top of the atmosphere. The
179 differences are also quantified in the time evolution of near- surface temperature, precipitation,
180 cloud fraction and in-cloud water contents.

181 Overall, I find the study to be well formulated with a clear motivation and simple but successful
182 strategy for breaking apart the components contributing to the changes in the atmospheric
183 energy budget. There are no substantial shortcomings that should prevent the publication of
184 this study; however, I have a few suggestions that could improve this contribution which are
185 explained below.

186 Reply: we would like to thank the reviewer again for the effort and for the suggestions. We are
187 happy that the reviewer found that our paper well formulated.

188

189 Primarily my suggestions are aimed to help the authors achieve their stated aim of better
190 understanding the physical processes behind aerosol effects on the atmospheric energy budget.
191 I see that their study does indeed achieve this, at least partly, but that these results are not
192 clearly expressed in the abstract nor the conclusions. Throughout the paper, the authors do a
193 good job of describing the differences between their simulations and quantifying these
194 differences (although in parts the quantification could be improved) - however, it is mostly left
195 to the reader to put these pieces of information together to get an understanding of the physical
196 processes involved. As a result, my overall impression of the authors conclusions and abstract
197 are: "we found another case where aerosol-cloud interactions behave differently under different
198 environmental conditions," which could be relatively simply converted to "these processes
199 (*see below) contribute to the different energy budget changes for shallow and deep convection
200 when CDNC is changed"

201 (1) From my understanding of the presented results, it seems that the large difference between
202 the shallow case and the deep case is the potential for a large upper-level cloud fraction change
203 in the deep case. I understand this as an increase of the anvil area, resulting in reduced LW
204 emission from the surface/lower atmosphere and therefore a warming contribution of the larger
205 anvil. In the shallow case, the upper level cloud fraction also has a systematic change, but
206 because it occupies a smaller part of the model domain - the overall change in the energy budget
207 is controlled by the change in low cloud fraction and the Twomey effect. If the authors agree
208 with this, I suggest adding a paragraph into the conclusions and a sentence in the abstract
209 clarifying these physical changes in the model and their impact on the energy budget.

210 Reply: Thank you for this suggestion that help us clarify this point. The reviewer's point is a
211 main conclusion of our paper; however, we believe that our results present more than just that
212 and include (among other) the effect of the thermodynamic evolution on radiation under
213 different CDNC conditions, the effect of CDNC on surface fluxes and so on. Nevertheless,
214 following the reviewer's comment, we have added a clarification to the revised manuscript.

215 In the abstract:

216 *"It is shown that the total column atmospheric radiative cooling is substantially reduced with*
217 *CDNC in the deep-cloud dominated case (by $\sim 10.0 \text{ W/m}^2$), while a much smaller reduction*
218 *($\sim 1.6 \text{ W/m}^2$) is shown in the shallow-cloud dominated case. This trend is caused by an increase*
219 *in the ice and water vapor content at the upper troposphere that leads to a reduced outgoing*
220 *longwave radiation, an effect which is stronger under deep-cloud dominated conditions."*

221

222 In the conclusions section:

223 *"Both the increase in water vapor and ice content in the upper troposphere are driven by an*
224 *increase in water mass flux with increasing CDNC to these levels (Fig. 19, (Koren et al., 2005;*
225 *Rosenfeld et al., 2008; Altaratz et al., 2014; Chen et al., 2017)), which is caused mostly by the*
226 *increase in the water mixing ratio in the mid-troposphere rather than by increase in vertical*
227 *velocity (Fig. 19) or in cloud fraction (Fig. 17). The ice content in the upper troposphere is*
228 *also increased due to reduction in the ice falling speed (Grabowski and Morrison, 2016), while*
229 *the increased relative humidity at these levels, further increases the ice particle lifetime due to*
230 *slower evaporation."*

231 *"In the shallow-cloud dominated case (which also contains a significant amount of deep*
232 *convection), the response of Q_R is weaker but still substantial (a total decrease in the*
233 *atmospheric radiative cooling of 1.6 W/m^2 - Fig. 20). The weaker total response under the*
234 *shallow-cloud dominated conditions is due to the smaller role of the ice part in this case."*

235

236 (2) Breakdown of the vertical mass flux changes with CDNC into component parts

237 The vertical mass flux of water is shown to change between the simulations with different
238 CDCN. What is the cause for this change? Either the vertical velocity should be increasing
239 (which seems not to be the case from the vertical velocity distributions in Figures 11 and 19),
240 so either the updraft area is increasing [implying wider updrafts?] or the in-cloud water mass
241 is increasing [because of a less efficient precipitation-forming processes?]. To what extent are
242 these two factors important? Furthermore, what happens to the vertical mass flux at (e.g.) 800
243 hPa - where the total water content is quite similar between all CDNC concentrations - is there
244 still an increased vertical mass flux?

245 Reply: Thank you for this comment that helped us clarify this point. Calculating the relative
246 change in the cloud fraction and in the water content between clean and polluted conditions
247 demonstrate the dominate role of the later in the increase in mass flux. This calculation
248 demonstrates that the cloud fraction (total water content) increases by 20% (72%) at 500mb in
249 the simulation with $CDNC=200\text{cm}^{-3}$ compared with the simulations with $CDNC=20\text{cm}^{-3}$ in the
250 deep convection dominated case. Similarity, in the shallow dominated case the cloud fraction
251 (total water content) increases by 22% (85%) at 500mb in the simulation with $CDNC=200\text{cm}^{-3}$
252 compared with the simulations with $CDNC=20\text{cm}^{-3}$. These calculations demonstrate that about
253 80% of the increase in mass flux under polluted conditions occur due to the increase in water
254 content and only about 20% occur due to the increase in cloud fraction (recalling that the
255 vertical velocity is similar between the two simulations). The increase in total water content is
256 caused by warm rain suppression at the lower troposphere.

257 This is now better explained in the revised manuscript:

258 *“Both the increase in water vapor and ice content in the upper troposphere are driven by an*
259 *increase in upward water (liquid and ice) mass flux with increasing CDNC (Fig. 11). An*
260 *increase in mass flux could be caused by an increase in vertical velocities and/or by an increase*
261 *in cloud (or updraft) fraction and/or by an increase in cloud water content. In our case, the*
262 *increases in mass flux is driven partially by the small increase in vertical velocity (especially*
263 *for updraft between 5 and 10 m/s – Fig. 11), partially by the small increase in cloud fraction at*
264 *this level (Fig. 9) and mostly due to the larger water mass mixing ratio (Fig. 9) that leads to*
265 *an increase in mass flux even for a given vertical velocity.”*

266

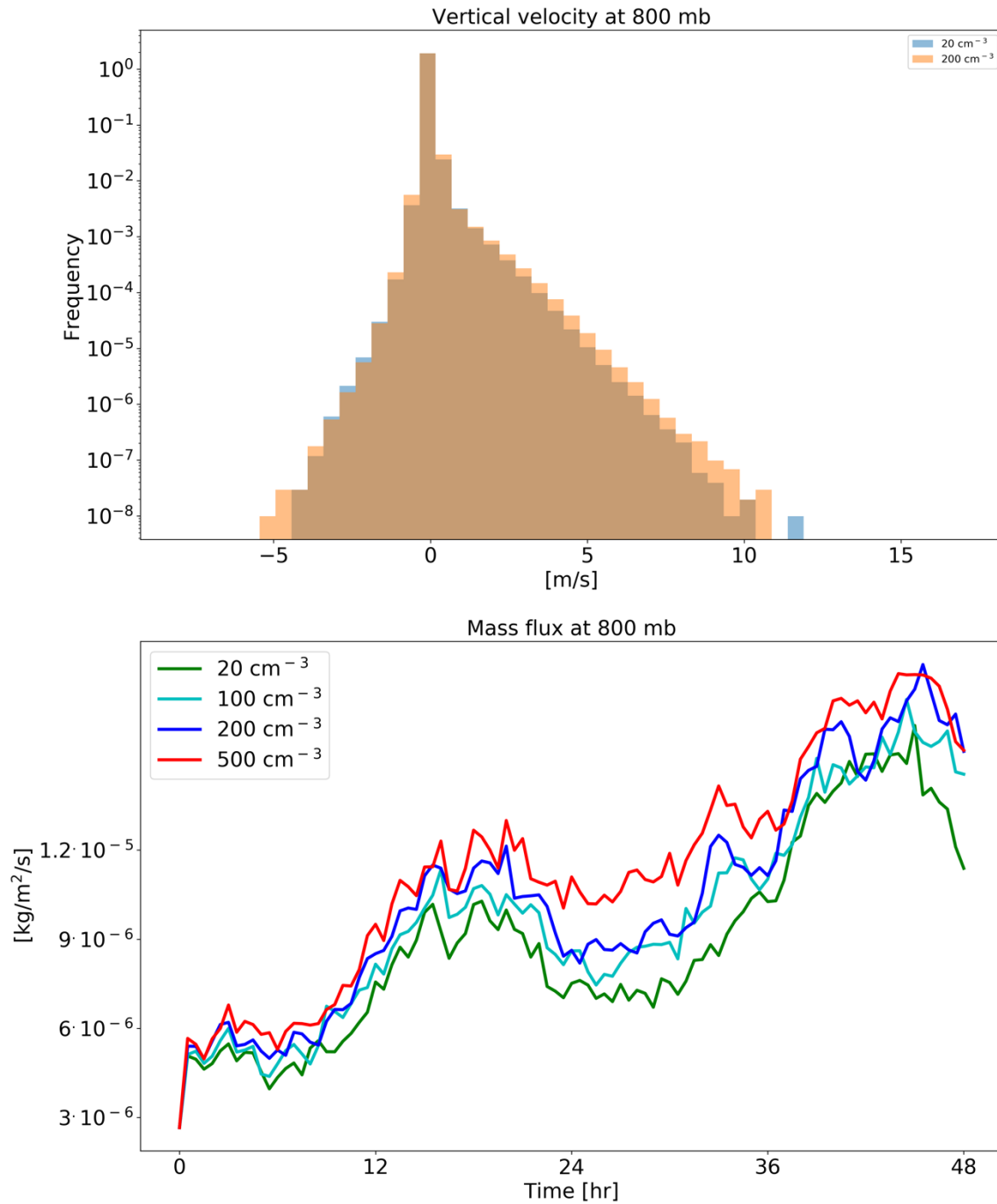
267 *“Analysis of the upward water mass flux from the warm to the cold part of the clouds (at 500*
268 *mb) in the different simulations (Fig. 19), demonstrates a substantial increase with the increase*

269 *in CDNC (Chen et al., 2017), which occur due to the increase in the water content (Fig. 17)*
270 *and the delay in the rain formation to higher levels (Heikenfeld et al., 2019), even without a*
271 *large change in the vertical velocity or cloud fraction at this level (Fig.17).”*

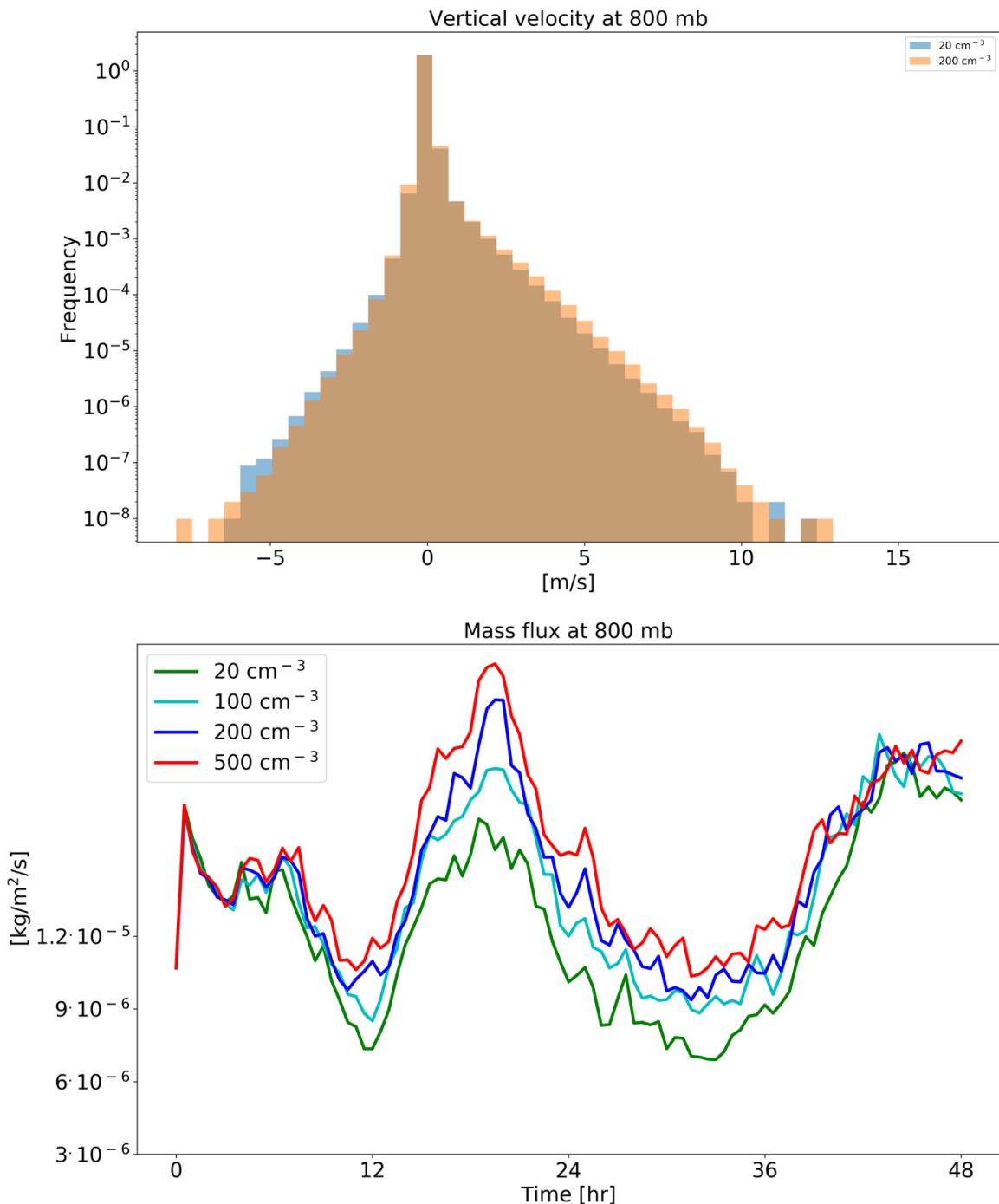
272

273 In addition, we calculated the mass flux at the level of 800 mb as the reviewer suggested (Figs.
274 R1 and R2 below). It demonstrates that in this level there is also a general increase in mass flux
275 with the increase in CDNC but to a lesser extent. The increase in mass flux is driven by a small
276 increase in water content (Figs. 9 and 17) and a small increase in vertical velocity (Figs. R1
277 and R2), while the cloud fraction is similar between the simulations (Figs. 9 and 17). In the
278 manuscript we still present the mass flux at 500 mb as it represents the transition between the
279 warm and the cold parts of the clouds.

280



281
 282 **Figure R1.** histograms of ICON simulated vertical velocity at the level of 800 mb for a clean (CDNC = 20
 283 cm⁻³) and polluted (CDNC = 200 cm⁻³) simulations (upper), and the time evolution of the net upwards water
 284 (liquid and ice) mass flux (lower) for the different CDNC simulations for the shallow-cloud dominated case
 285 (10-12/08/2016). In the histogram only two simulations are presented for clarity.
 286



287
 288 **Figure R2. histograms of ICON simulated vertical velocity at the level of 800 mb for a clean (CDNC = 20 cm⁻³) and polluted (CDNC = 200 cm⁻³) simulations (upper), and the time evolution of the net upwards water**
 289 **(liquid and ice) mass flux (lower) for the different CDNC simulations for the deep-cloud dominated case (16-**
 290 **18/08/2016). In the histogram only two simulations are presented for clarity.**

292
 293 (3) Large contribution from residuals
 294 A large contribution to the overall energy budget is within the residual term, which the authors
 295 state should reduce to zero given a long enough averaging time. How can the authors be sure

296 that this is true and that the large component in the residual term is not a "buffering" effect -
297 e.g. changing stability of the atmosphere to compensate for the changing energy budget? Can
298 the 3D distribution of the residual values be used to quantify this at all?

299 Reply: A similar argument was raised by reviewer #1 – we will repeat our reply here. What
300 was previously called a “residual” term was changes in the revised manuscript to be refer to as
301 “energy imbalance” as it better describes it. A recent study shows that in order to get close to
302 energy balance the spatial scale should be on the order of ~5000km (Jakob et al., 2019) and the
303 time scale longer than a month (we found a similar scale using GCMs). Our simulations operate
304 on smaller spatial-temporal scales than that and hence it is not surprising that we obtain an
305 imbalance.

306 The energy imbalance is composed of changes in the storage term and local divergence or
307 convergence of dry-static energy into the domain. In our case, almost the entire imbalance is
308 simply dry static energy that moves in or out of the domain. For example, in the deep-cloud
309 dominated case there is a net production of dry-static energy in the domain by precipitation
310 (which is not entirely balanced by the radiative cooling). This extra dry-static energy is then
311 advected out of the domain.

312 An explanation about this point was added to the revised manuscript:

313 *“The total column atmospheric energy budget can be described as follows:*

314
$$LP + Q_R + Q_{SH} = \text{div}(s) + ds/dt \quad (1)$$

315 *Equation 1 presents a balance between the latent heating rate (LP - latent heat of condensation*
316 *[L] times the surface precipitation rate [P]), the surface sensible heat flux (Q_{SH}), the atmospheric*
317 *radiative heating (Q_R), the divergence of dry static energy (div(s), which will become negligible*
318 *on sufficiently large spatial scales), and the dry static energy storage term (ds/dt, which will*
319 *become negligible on long [inter-annual] temporal scales). Throughout the rest of this paper we*
320 *will refer to the right-hand side of Equation 1 (div(s)+ds/dt) as the energy imbalance (which is*
321 *calculated as the residual [R] of the left-hand side).”*

322

323 *“In this shallow-cloud dominated case the radiative cooling of the atmosphere is significantly*
324 *larger than the warming due to precipitation (mean of -114.7 W/m² compared to 90.1 W/m²),*
325 *hence the energy imbalance (R) is negative. Negative R means that there must be some*
326 *convergence of dry static energy into the domain and/or decrease in the storage term, in this*
327 *case it is mostly due to convergence of dry static energy.”*

328

329 “Next, we analyse the atmospheric energy budget for the deep-cloud dominated case (Fiona
330 tropical storm – Fig. 12). As opposed to the shallow-cloud dominated case, in this case the LP
331 contribution dominates over the radiative cooling and hence the energy imbalance R is positive
332 and large, suggesting divergence of dry static energy out of the domain.”

333

334 (4) There appears to be a mismatch between TWP in Figure 8 (lower right plot) and q_t in Figure
335 9 (lower central plot). Similarly in Figures 16 & 17. The vertical profile of q_t is quite similar
336 for 3 simulations in the shallow case (Figure 9; excluding the 500 cm⁻³ line). Similarly, the q_t
337 values from 3 simulations in the deep case are also similar (Figure 17; excluding the 20 cm⁻³
338 line). However, in figure 8 & 16 there is clear separation between all the TWP lines throughout
339 the simulation. By quick calculation the spread in the TWP timeseries seems too large to be
340 explained by the differences in q_t (which are mostly between 650-400 hPa). How can this
341 difference be explained? Is the TWP only including cloud and ice, but ignoring rain water?
342 Similarly, is the LW only cloud, ignoring rain?

343 Reply: Thank you for this comment that helped us clarify this point. Indeed, the LWP include
344 the cloud mass (q_c) and not the rain mass (q_r). This is done for consistency with LWP
345 calculated from satellite observations, which are sensitive only to the cloud mass and not to the
346 rain mass (see also the reply to the next point). This is now better explained in the revised
347 manuscript:

348 “Figure 8. Domain average properties as a function of time for the different CDNC simulations for the
349 shallow-cloud dominated case. The properties that are presented here are: cloud fraction (CF), rain rate,
350 temperature in 2 m, liquid water path (LWP – based on the cloud water mass, excluding the rain mass for
351 consistency with satellite observations), ice water path (IWP) and total water path (TPW = LWP + IWP). For
352 each property, the mean difference between all combinations of simulations, normalized to a factor 5 increase
353 in CDNC, and its standard deviation appear in parenthesis.”

354

355 (5) Following from the above point: is rain water radiatively interactive in the model? If not,
356 to what extent does this removal of mass from the radiatively interactive cloud species have on
357 the Twomey effect calculations performed, given that the rain water mass is almost equal to
358 the cloud water mass at some heights?

359 Reply: As done in most atmospheric models (Hill et al., 2018), the rain mass is not included in
360 the radiative calculations. Since the rain drops are much larger than the cloud droplet, their
361 cross-section available for interaction with radiation (for a given water mass) is much smaller

362 and usually negligible (Hill et al., 2018). For example, a simple “back of the envelop”
363 calculation of the cloud optical depth (τ) as in Heus & Seifert (2013) and Spill et al. (2019)
364 follows as:

$$365 \tau = 0.19 * LWP^{5/6} * N^{1/3},$$

366 where LWP is the liquid water path and N is the drop concentration, for a given LWP for cloud
367 droplets with radius $r=10 \mu\text{m}$ and for rain drops with $r=0.5 \text{ mm}$ yield a factor of 50 decrease in
368 τ for the rain compare with the cloud. Generally, as τ is proportional to $N^{1/3}$ it decreases
369 proportional to r (for a given LWP), and since the cloud droplets and rain drops are separated
370 by 1 or 2 orders of magnitudes, the effect of the cloud droplets on the radiation is much larger
371 than that of the rain drops. This simple calculation does not account for the changes in Mie size
372 parameter between rain drops and cloud droplets but it serves to demonstrate the orders of
373 magnitude differences between the two different regimes.

374

375 (6) Impact of simplifications

376 The approach of simply modifying the CDNC instead of the aerosol concentration of the
377 atmosphere ignores several potentially important processes/feedbacks (e.g. activation of
378 CCN/IN, size distribution of aerosol, direct radiative effects) - the authors should comment on
379 these shortcomings in the conclusions.

380 Reply: Thank you. Based on this comment we have added a comment about the limitation of
381 using a fixed CDNC simulations:

382 *“The different CDNC scenarios serve as a proxy for different aerosol conditions (as the first
383 order effect of increased aerosol concentration on clouds is to increase the CDNC, Andreae,
384 2009). This also allows to separate the cloud response from the uncertainties involved in the
385 representation of the aerosols in numerical models (Ghan et al., 2011; Simpson et al., 2014;
386 Rothenberg et al., 2018). However, it limits potential feedbacks between clouds and aerosols,
387 such as the removal of aerosol levels by precipitation scavenging and potential aerosol effects
388 thereon. In addition, the fixed CDNC framework does not capture the differences in aerosol
389 activation between shallow and deep clouds, due to differences in vertical velocity. Another
390 aerosol effect that is not included in our simulations is the direct interaction between aerosol
391 and radiation. In future work we plan to examine the mutual interaction between microphysical
392 effects and the direct aerosol radiative effects.”*

393

394

395 In the conclusions:

396 *“Furthermore, we do not include the temporal evolution of the aerosol concentration.*
397 *Feedbacks between the aerosol concentration and clouds processes (such as wet scavenging),*
398 *as well as the direct effects of aerosol on radiation would add another layer of complexity that*
399 *should be accounted for in future work.”*

400

401 (7) Robustness of results

402 The authors should comment on the robustness of these results, in light of the fact that single
403 simulations (rather than ensembles) of two individual case studies are performed. The results
404 in figures 8 & 16 suggest a clear separation between all 4 CDNC concentrations from early on
405 in the simulation - however, the vertical profiles of q_i , q_t and CF in figures 9 & 17 suggest that
406 the 20 CDNC cm^{-3} simulation is the only one of the four that is substantially different
407 (particularly at upper levels, which seem to be most important in this story).

408 Reply: The robustness of our simulations, which, as the reviewer stated, are based on few
409 simulations rather than on large ensemble, occupied our mind as well. In a recent paper which
410 is currently under discussion in ACPD (Dagan and Stier, 2019) we investigate this exact
411 question. In that paper we use a smaller domain compared to the current study ($3^\circ \times 3^\circ$ rather
412 than $22^\circ \times 11^\circ$) to simulated a large ensemble of initial conditions (all together we simulate 124
413 different simulations). This large ensemble enables robust identification of the effect of CDNC
414 changes on cloud properties. We were able to show that the general conclusions which are
415 stated in the current study hold also for large statistics. Based on the following comment we
416 have added a discussion about the robustness of our results to the revised manuscript:

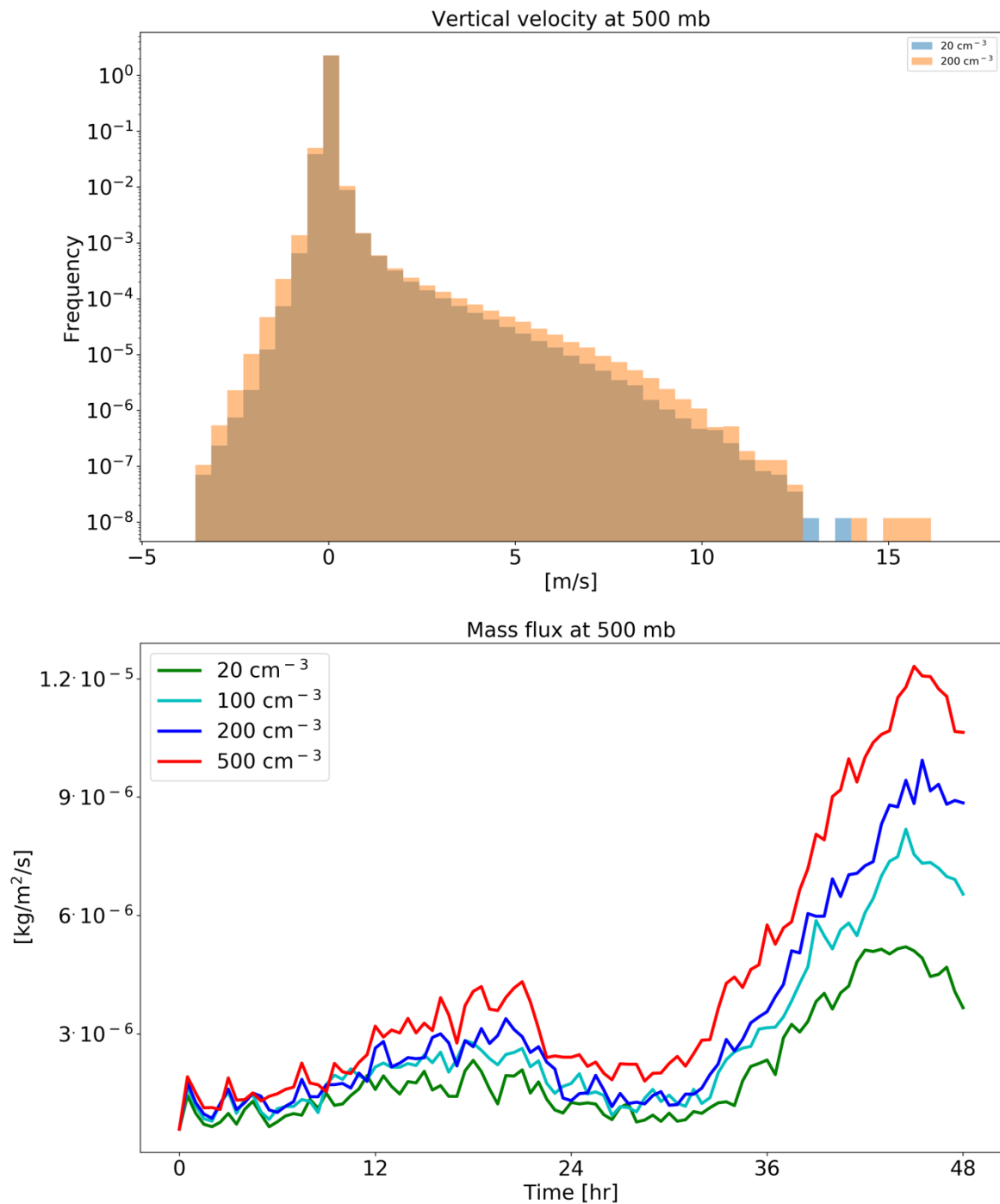
417 *“There exists a large spread in estimates of aerosol effects on clouds for different cloud types*
418 *and different environmental conditions. In this study, as we use a relatively large domain (22°*
419 *$\times 11^\circ$) and two different dates (each for two days), we sample many different local*
420 *environmental conditions and cloud types. Such more realistic setups (although with lower*
421 *spatial resolution) could provide more reliable estimates of aerosol effects on heterogeneous*
422 *cloud systems than just one-cloud-type, small domain simulations (as was done in many*
423 *previous studies, e.g (Dagan et al., 2017; Seifert et al., 2015; Ovchinnikov et al., 2014)).*
424 *However, the conclusions demonstrated here are based on two specific cases. In order to*
425 *examine the validity of our main conclusions over a wider range of initial conditions, we have*
426 *conducted a large ensemble of simulations starting from realistic initial conditions (although*
427 *with a smaller domain) in a companion paper (Dagan and Stier, 2019). These simulations*

428 demonstrate that the main conclusions presented in this paper are robust and hold also for a
429 wide range of initial conditions representative for this area.”

430

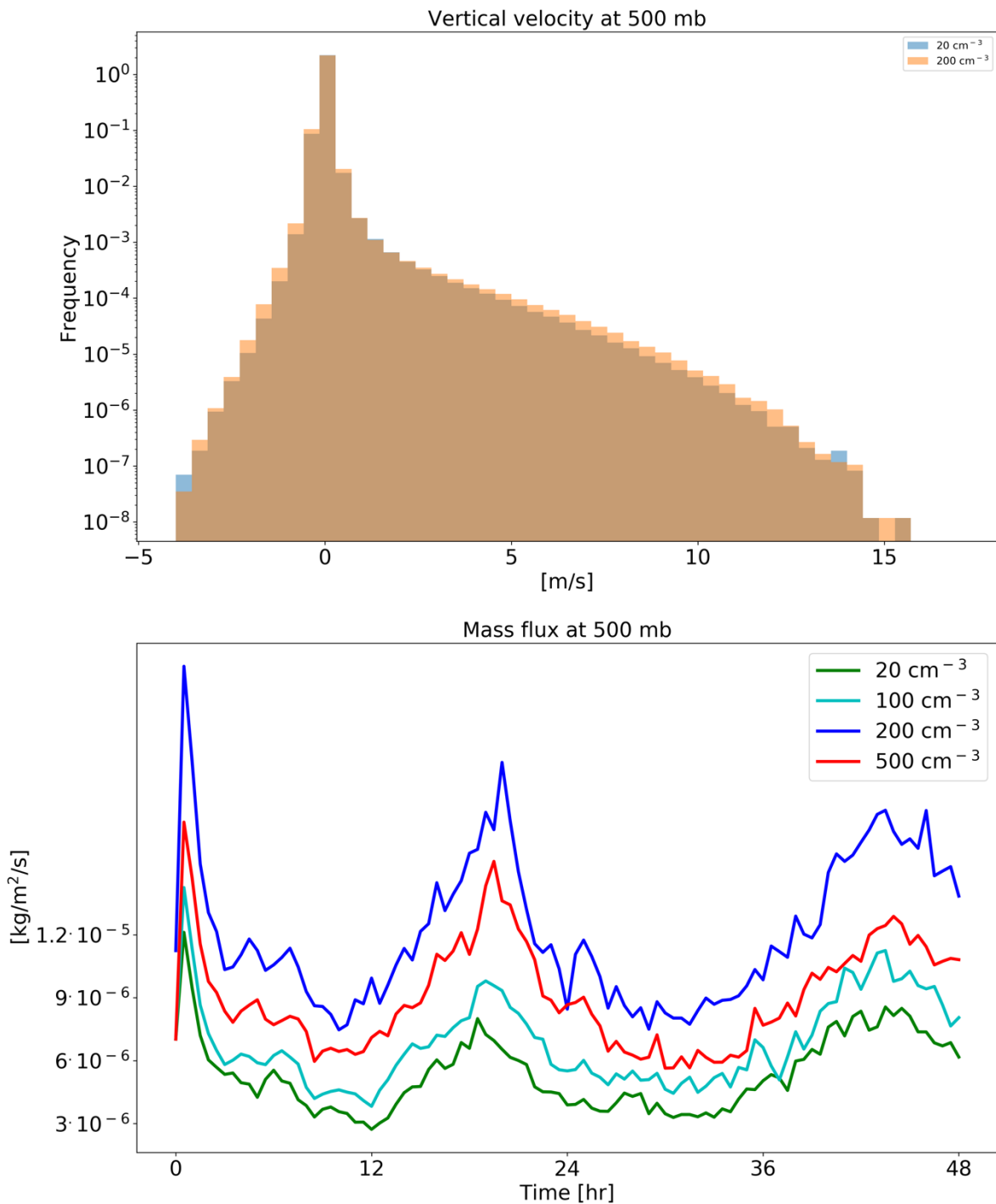
431 Minor points: please show the mass flux from all four simulations in figures 11 and 19 to be
432 consistent with the other plots in the paper.

433 Reply: The mass flux of all four simulations are now presented in Figs. 11 and 19:



434

435 **Figure 11. histograms of ICON simulated vertical velocity at the level of 500 mb for a clean (CDNC = 20 cm⁻³)**
 436 **and polluted (CDNC = 200 cm⁻³) simulations (upper), and the time evolution of the net upwards water (liquid**
 437 **and ice) mass flux (lower) for the different CDNC simulations for the shallow-cloud dominated case (10-**
 438 **12/08/2016). The 500 mb level is chosen as it represents the transition between the warm part to the cold part**
 439 **of the clouds. In the histogram only two simulations are presented for clarity.**
 440
 441



442

443 **Figure 19. histograms of ICON simulated vertical velocity at the level of 500 mb for a clean (CDNC = 20 cm⁻³)**
444 **and polluted (CDNC = 200 cm⁻³) simulations (upper), and the time evolution of the net upwards water (liquid**
445 **and ice) mass flux (lower) for the different CDNC simulations for the deep-cloud dominated case (16-**
446 **18/08/2016). The 500 mb level is chosen as it represents the transition between the warm part to the cold part**
447 **of the clouds. In the histogram only two simulations are presented for clarity.**

448

449

450 Lines 335-338: please be more quantitative about the results of the test with the offline radiation
451 calculations as to the relative contributions of the cloud fraction and TWP changes. Line 367:
452 please quantify the "vast majority" of LW flux changes due to cloudy rather than clear skies.

453 Reply: Thank you. More information was added to the revised manuscript:

454 *“For estimating the relative contribution of the changes in CF and water content to the SW*
455 *flux changes we have conducted off-line radiative transfer sensitivity tests. To quantify the*
456 *water content radiative effect, we feed the same CF vertical profile from the model into the*
457 *offline radiative transfer model BUGSrad, while allowing the water content vertical profile to*
458 *change (and visa versa to compute the CF radiative effect). This approach demonstrates that*
459 *the contribution from the small reduction in CF is negligible compared to the increased SW*
460 *reflectance caused by the increased water content (the effect of the reduction in CF compensate*
461 *only about 1% of the effect of the increase in the water content).”*

462

463 *“The increased humidity at the upper troposphere would act to decrease the outgoing LW flux,*
464 *similar to the effect of the increased ice content in the upper troposphere (Fig. 9). However,*
465 *sensitivity studies with off-line radiative transfer calculations using BUGSrad demonstrate that*
466 *the vast majority (more than 99%) of the different in F_{LW}^{TOA} between clean and polluted*
467 *conditions emerges from the cloudy skies (rather than clear-sky), suggesting that the effect of*
468 *the increased ice content at the upper troposphere dominates.”*

469

470 The plots in figures 10 and 18, currently described in the caption as Hovmöller plots, would be
471 better described as time-height plots.

472 Reply: Thanks. It was changed according to the reviewer’s suggestion.

473

474 Is there an explanation for the relative minimum of cloud water content at 650 hPa in all
475 simulations? I struggle to find a physical explanation for this.

476 Reply: We think that the relative minimum of domain-wide cloud water at 650 hPa is simply
477 due to the fact that below this level there are still quite a lot of shallow clouds while above it
478 there are anvils clouds with longer lifetime (and hence the larger cloud water mass) then the
479 liquid at lower levels.

480

481 **References**

482 Dagan, G. and Stier, P.: Ensemble daily simulations for elucidating cloud–aerosol interactions
483 under a large spread of realistic environmental conditions, *Atmos. Chem. Phys.*
484 *Discuss.*, <https://doi.org/10.5194/acp-2019-949>, in review, 2019.

485 Dagan, G., Stier, P., & Watson-Parris, D. (2019). Contrasting response of precipitation to
486 aerosol perturbation in the tropics and extra-tropics explained by energy budget
487 considerations. *Geophysical research letters*.

488 Heus, T., & Seifert, A. (2013). Automated tracking of shallow cumulus clouds in large domain,
489 long duration large eddy simulations. *Geoscientific Model Development*, 6(4), 1261-
490 1273.

491 Hill, P., Chiu, J., Allan, R., & Chern, J. D. (2018). Characterizing the radiative effect of rain
492 using a global ensemble of cloud resolving simulations. *Journal of Advances in*
493 *Modeling Earth Systems*, 10(10), 2453-2470.

494 Jakob, C., Singh, M., & Jungandreas, L. (2019). Radiative Convective Equilibrium and
495 Organized Convection: An Observational Perspective. *Journal of Geophysical*
496 *Research: Atmospheres*, 124(10), 5418-5430.

497 Spill, G., Stier, P., Field, P. R., & Dagan, G. (2019). Effects of aerosol in simulations of realistic
498 shallow cumulus cloud fields in a large domain. *Atmospheric Chemistry and Physics*.

499 Stier, P., Feichter, J., Kinne, S., Kloster, S., Vignati, E., Wilson, J., et al. (2005). The aerosol-
500 climate model ECHAM5-HAM. *Atmospheric Chemistry and Physics*, 5(4), 1125-1156.

501

502

503

504

505

506

507

508 **Atmospheric energy budget response to idealized aerosol perturbation in** 509 **tropical cloud systems**

510 **Guy Dagan¹, Philip Stier¹, Matthew Christensen¹, Guido Cioni^{2,3}, Daniel Klocke^{3,4} and Axel**
511 **Seifert⁴**

512 ¹ Atmospheric, Oceanic and Planetary Physics, Department of Physics, University of Oxford, UK

513 ² Max Planck Institute for Meteorology, Hamburg, Germany

514 ³ Hans Ertel Center for Weather Research, Offenbach am Main, Germany

515 ⁴ Deutscher Wetterdienst, Offenbach am Main, Germany

516 E-mail: guy.dagan@physics.ox.ac.uk

517

518 **Abstract**

519 The atmospheric energy budget is analysed in numerical simulations of tropical cloud systems.
520 ~~This is done in order~~ to better understand the physical processes behind aerosol effects on the
521 atmospheric energy budget. The simulations include both shallow convective clouds and deep
522 convective tropical clouds over the Atlantic Ocean. Two different sets of simulations, at different
523 dates (10-12/8/2016 and 16-18/8/2016), are ~~being~~ simulated with different dominant cloud
524 modes (shallow or deep). For each case, the cloud droplet number concentrations (CDNC) is
525 varied as a proxy for changes in aerosol concentrations. It is shown that the total column
526 atmospheric radiative cooling is substantially reduced with CDNC in the deep-cloud dominated
527 case (by ~ 10.0 W/m²), while a much smaller reduction (~ 1.6 W/m²) is shown in the shallow-
528 cloud dominated case. This trend is caused by an increase in the ice and water vapor content at
529 the upper troposphere that leads to a reduced outgoing longwave radiation, [an effect which is](#)
530 [stronger under deep-cloud dominated conditions](#). A decrease in sensible heat flux (driven by
531 increase in the near surface air temperature) reduces the warming by ~ 1.4 W/m² in both cases. It
532 is also shown that the cloud fraction response behaves in opposite ways to an increase in CDNC,
533 showing an increase in the deep-cloud dominated case and a decrease in the shallow-cloud
534 dominated case. This demonstrates that under different environmental conditions the response to
535 aerosol perturbation could be different.

536

537 **Introduction**

538 The negative anthropogenic radiative forcing due to aerosols is acting to cool the climate and to
539 compensate some of the warming due to increase in greenhouse gases (Boucher et al., 2013).
540 However, quantification of this effect is highly uncertain with a revised uncertainty range of
541 -1.60 to -0.65 W/m² (Bellouin et al., 2019). The total anthropogenic aerosol radiative forcing is
542 composed of contribution from direct interaction of aerosols with radiation (scattering and
543 absorption) and from indirect interaction with radiation due to changes in cloud properties.

544 Beside its effect on the radiation budget, aerosols may affect the precipitation distribution and
545 total amount (Levin and Cotton, 2009; Albrecht, 1989; Tao et al., 2012). A useful perspective to
546 improve our understanding of aerosol effect on precipitation, which became common in the last
547 few years, arises from constraints on the energy budget (O’Gorman et al., 2012; Muller and
548 O’Gorman, 2011; Hodnebrog et al., 2016; Samset et al., 2016; Myhre et al., 2017; Liu et al.,
549 2018; Richardson et al., 2018; Dagan et al., 2019a). On long time scales, any precipitation
550 perturbations by aerosol effects will have to be balanced by changes in radiation fluxes, sensible
551 heat flux or by divergence of dry static energy. The energy budget constraint perspective was
552 found useful to explain both global (e.g. (Richardson et al., 2018)) and regional (Liu et al., 2018;
553 Dagan et al., 2019a) precipitation response to aerosol perturbations in global scale simulations.
554 In this study, we investigate the energy budget response to aerosol perturbation on a regional
555 scale using high resolution cloud resolving simulations. This enables an improved understanding
556 of the microphysical processes controlling atmospheric energy budget perturbations. The strong
557 connection between the atmospheric energy budget and convection has long been appreciated
558 (e.g. (Arakawa and Schubert, 1974; Manabe and Strickler, 1964)) as well as the connection to
559 the general circulation of the atmosphere (Emanuel et al., 1994).

560 The total column atmospheric energy budget can be described as follows:

$$561 \quad LP + Q_R + Q_{SH} = \text{div}(s) + ds/dt \quad (1)$$

562 Equation 1 presents a balance between the latent heating rate (LP - latent heat of condensation
563 [L] times the surface precipitation rate [P]), the surface sensible heat flux (Q_{SH}), the atmospheric
564 radiative heating (Q_R), the divergence of dry static energy ($\text{div}(s)$, which will become negligible
565 on sufficiently large spatial scales), and [the](#) dry static energy storage term (ds/dt , which will
566 become negligible on long [inter-annual] temporal scales). Throughout the rest of this paper we
567 will refer to the right-hand side of Equation 1 ($\text{div}(s) + ds/dt$) as the [energy imbalance \(which is](#)
568 [calculated as the](#) residual [$\{R\}$] of the left-hand side).

569 Q_R is defined as:

$$570 \quad Q_R = (F_{SW}^{TOA} - F_{SW}^{SFC}) + (F_{LW}^{TOA} - F_{LW}^{SFC}) \quad (2)$$

571 and represents the rate of net atmospheric diabatic warming due to radiative shortwave (SW) and
572 longwave (LW) fluxes. It is expressed by the sum of the surface (SFC) and top of the atmosphere
573 (TOA) fluxes, when all fluxes are positive downwards. As in the case of TOA radiative forcing,

574 aerosols could modify the atmospheric energy budget by both direct interaction with radiation
575 and by microphysical effects on clouds. The latter is the focus of this study.

576 The microphysical effects are driven by the fact that aerosols serve as cloud condensation nuclei
577 (CCN) and ice nuclei (IN). Larger aerosol concentrations, e.g. by anthropogenic emissions, could
578 lead to larger cloud droplet and ice particle concentrations (Andreae et al., 2004; Twomey, 1977;
579 Hoose and Möhler, 2012). Changes in hydrometer concentration and size distribution were
580 shown to affect clouds' microphysical processes rates (such as condensation, evaporation,
581 freezing and collision-coalescence), which in turn could affect the dynamics of the clouds (Khain
582 et al., 2005; Koren et al., 2005; Heikenfeld et al., 2019; Chen et al., 2017; Altaratz et al., 2014;
583 Seifert and Beheng, 2006a), the rain production (Levin and Cotton, 2009; Albrecht, 1989; Tao
584 et al., 2012) and the clouds' radiative effect (Koren et al., 2010; Storelvmo et al., 2011; Twomey,
585 1977; Albrecht, 1989). The aerosol effect, and in particular its effects on the radiation budget
586 and the atmospheric energy budget, is cloud regime dependent (Altaratz et al., 2014; Lee et al.,
587 2009; Mülmenstädt and Feingold, 2018; van den Heever et al., 2011; Rosenfeld et al., 2013;
588 Glassmeier and Lohmann, 2016; Gryspeerdt and Stier, 2012; Christensen et al., 2016), time
589 dependent (Dagan et al., 2017; Gryspeerdt et al., 2015; Seifert et al., 2015; Lee et al., 2012;
590 Dagan et al., 2018c), aerosol type and size distribution dependent (Jiang et al., 2018; Lohmann
591 and Hoose, 2009) and (even for a given cloud regime) meteorological conditions dependent
592 (Dagan et al., 2015a; Fan et al., 2009; Fan et al., 2007; Kalina et al., 2014; Khain et al., 2008)
593 and was shown to be non-monotonic (Dagan et al., 2015b; Jeon et al., 2018; Gryspeerdt et al.,
594 2019; Liu et al., 2019). Hence the quantification of the global mean radiative effect is extremely
595 challenging (e.g. (Stevens and Feingold, 2009; Bellouin et al., 2019)).

596 Previous studies demonstrated that the mean aerosol effect on deep convective clouds can
597 increase the upward motion of water, and hence also increase the cloud anvil mass and extent
598 (Fan et al., 2010; Chen et al., 2017; Fan et al., 2013; Grabowski and Morrison, 2016). The
599 increase in mass flux to upper levels was explained by the convective invigoration hypothesis
600 (Fan et al., 2013; Koren et al., 2005; Rosenfeld et al., 2008; Seifert and Beheng, 2006a; Yuan
601 et al., 2011a; Williams et al., 2002), which was proposed to lead to stronger latent heat release
602 under higher aerosol concentrations and hence stronger vertical velocities. In addition to the
603 stronger vertical velocities, under polluted conditions the smaller hydrometers are being
604 transported higher in the atmosphere (for a given vertical velocity (Chen et al., 2017; Koren et
605 al., 2015; Dagan et al., 2018a)) and their lifetime at the upper troposphere is longer (Fan et al.,
606 2013; Grabowski and Morrison, 2016). The invigoration mechanism can also lead to an increase

607 in precipitation (Khain, 2009; Altaratz et al., 2014). Both the increase in precipitation and the
608 increase in anvil coverage would act to warm the atmospheric column: the increased precipitation
609 by latent heat release, and the increased anvil mass and extent by longwave radiative warming
610 (Koren et al., 2010; Storelvmo et al., 2011). However, it should be pointed out that the
611 uncertainty underlying these proposed effects remain significant (White et al., 2017; Varble,
612 2018). In addition, aerosol effects on precipitation from deep convective cloud was shown to be
613 non-monotonic and depend on the aerosol range (Liu et al., 2019).

614 In the case of shallow clouds, aerosol effect on precipitation was also shown to be non-monotonic
615 (Dagan et al., 2015a; Dagan et al., 2017). However, unlike in the deep clouds case, the mean
616 effect on precipitation, under typical modern-day conditions, is thought to be negative (Albrecht,
617 1989; Rosenfeld, 2000; Jiang et al., 2006; Xue and Feingold, 2006; Dagan and Chemke, 2016).
618 The aerosol effect on shallow cloud cover and mean water mass (measure by liquid water path -
619 LWP) might also depend on the meteorological conditions and aerosol range (Dagan et al.,
620 2015b; Dagan et al., 2017; Gryspeerd et al., 2019; Dey et al., 2011; Savane et al., 2015) and is
621 the outcome of competition between different opposing response of: rain suppression (that could
622 lead to increase in cloud lifetime and coverage (Albrecht, 1989)), warm clouds invigoration (that
623 could also lead to increase in cloud coverage and LWP (Koren et al., 2014; Kaufman et al., 2005;
624 Yuan et al., 2011b)) and increase in entrainment and evaporation (that could lead to decrease in
625 cloud coverage (Small et al., 2009; Jiang et al., 2006; Costantino and Bréon, 2013; Seigel,
626 2014)). Another addition to this complex response is the fact that the aerosol effect on warm
627 convective clouds was shown to be time dependent and affected by the clouds' feedbacks on the
628 thermodynamic conditions (Seifert et al., 2015; Dagan et al., 2016; Dagan et al., 2017; Lee et al.,
629 2012; Stevens and Feingold, 2009; Dagan et al., 2018b). Previous simulations that contained
630 several tropical cloud modes demonstrate that increase in aerosol concentrations can lead to
631 suppression of the shallow mode and invigoration of the deep mode (van den Heever et al., 2011).
632 Hence the domain mean effect, even if it is demonstrated to be small, may be the result of
633 opposing relatively large contributions from the different cloud modes (van den Heever et al.,
634 2011). The small domain mean effect may suggest that on large enough scales the energy (Muller
635 and O'Gorman, 2011; Myhre et al., 2017) or water budget (Dagan et al., 2019b) constrain
636 precipitation changes.

637 Previous studies, using global simulations (O'Gorman et al., 2012; Muller and O'Gorman, 2011;
638 Hodnebrog et al., 2016; Samset et al., 2016; Myhre et al., 2017; Liu et al., 2018; Richardson et
639 al., 2018; Dagan et al., 2019a), demonstrated the usefulness of the atmospheric energy budget

640 perspective in constraining aerosol effect on precipitation. However, the physical processes
641 behind aerosol-cloud microphysical effects on the energy budget are still far from being fully
642 understood. In this study we use cloud resolving simulations to increase our understanding of the
643 effect of microphysical aerosol-cloud interactions on the atmospheric energy budget.

644 **Methodology**

645 The icosahedral nonhydrostatic (ICON) atmospheric model (Zängl et al., 2015) is used in a
646 limited area configuration. ICON's non-hydrostatic dynamical core was evaluated with several
647 idealized cases (Zängl et al., 2015). The simulations are conducted such that they are aligned
648 with the NARVAL 2 (Next-generation Aircraft Remote-Sensing for Validation Studies (Klepp
649 et al., 2014; Stevens et al., 2019; Stevens et al., 2016)) campaign, which took place during August
650 2016 in the western part of the northern tropical Atlantic. We use existing NARVAL 2
651 convection-permitting simulations (Klocke et al., 2017) as initial and boundary conditions for
652 our simulations.

653 The domain covers $\sim 22^\circ$ in the zonal direction ($25^\circ - 47^\circ$ W) and $\sim 11^\circ$ in the meridional direction
654 ($6^\circ - 17^\circ$ N) and therefore a large fraction of the northern tropical Atlantic (Fig. 1). During August
655 2016, the intertropical convergence zone (ITCZ) was located in the southern part of the domain
656 while the northern part mostly contains trade cumulus clouds. Hence, this case study provides
657 an opportunity to study heterogenous clouds systems. Daily variations in the deep/shallow cloud
658 modes in our domain were observed, but it always included both cloud modes, albeit in different
659 relative fraction. Two different dates are chosen, one representing a shallow-cloud dominated
660 mode (10-12/8/2016 – see Fig. 2, and Figs S1 and S3, supporting information- SI), and one that
661 represents a deep-cloud dominated mode (16-18/8/16 – see Fig. 3 and Figs. S2 and S3, SI). In
662 the shallow-cloud dominated case, most of the domain is covered by trade cumulus clouds that
663 are being advected with the trade winds from north-east to south-west. In the southern part of the
664 domain, throughout most of the simulation, there is a zonal band of deep convective clouds (Fig.
665 2) that contribute on average $\sim 25\%$ out of the total cloud cover (Fig. S3, SI). The deep-cloud
666 dominated case represents the early stages of the development of the tropical storm Fiona (Fig.
667 3). Fiona formed in the eastern tropical Atlantic and moved toward the west-north-west. It started
668 as a tropical depression at 16/8/2016 18:00 UTC while its centre was located at 12.0° N 32.2° W.
669 It kept moving towards the north-west and reach a level of a tropical storm at 17/8/2016 12UTC,
670 while its centre was located at 13.7° N 36.0° W
671 (https://www.nhc.noaa.gov/data/tcr/AL062016_Fiona.pdf). The general propagation speed and

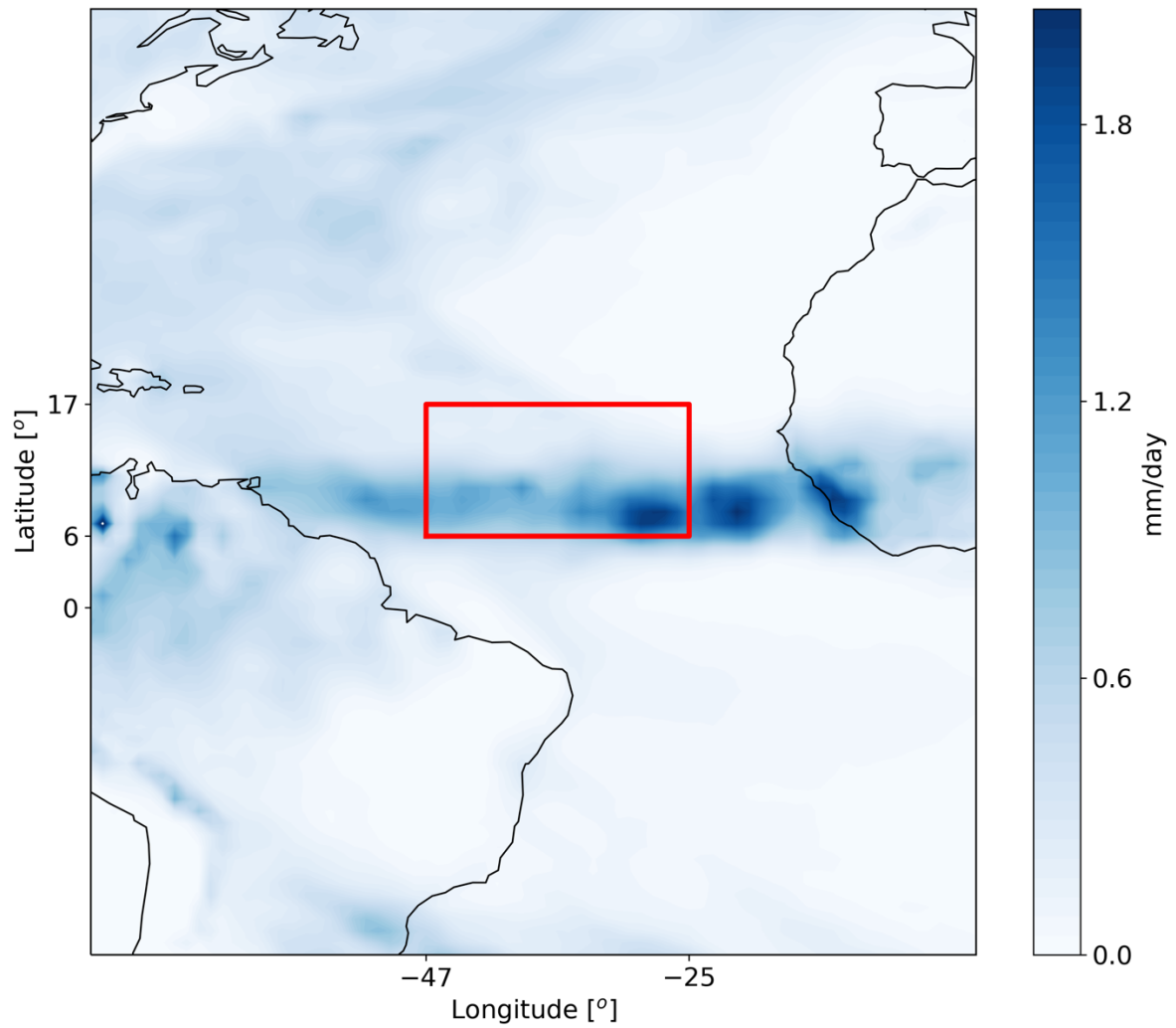
672 direction, strength (measure by maximal surface wind speed) and location of the storm are
673 predicted well by the model. However, the model produces more anvil clouds than what was
674 observed from the satellite (Fig. 3). These two different cases, representing different atmospheric
675 energy budget initial state (see also Figs. 4 and 12 below), enable the investigation of the aerosol
676 effect on the energy budget under different initial conditions.

677 We use a two-moment bulk microphysical scheme (Seifert and Beheng, 2006b). For each case,
678 four different simulations with different prescribed cloud droplet number concentrations
679 (CDNC) of 20, 100, 200, and 500 cm^{-3} are conducted. The different CDNC scenarios serve as
680 a proxy for different aerosol-~~concentration~~ conditions (as the first order effect of increased
681 aerosol concentration on clouds is to increase the CDNC, (Andreae, 2009)). This also allows
682 to separate the cloud response from and avoid the uncertainties involved in the representation
683 of the aerosols in numerical models (Ghan et al., 2011; Simpson et al., 2014; Rothenberg et al.,
684 2018). However, it limits potential feedbacks between clouds and aerosols, such as the removal
685 of aerosol levels by precipitation scavenging and potential aerosol effects thereon. In addition,
686 the fixed CDNC framework does not capture the differences in aerosol activation-~~fraction~~
687 between shallow and deep clouds, due to differences in vertical velocity. Another aerosol effect
688 that is not included in our simulations is the direct interaction between aerosol and radiation.
689 In future work we plan to examine the mutual interaction between the microphysical effects
690 and the direct aerosol radiative effects.

691 For calculation of the difference between high CDNC (polluted) conditions and low CDNC
692 (clean) conditions, the simulations with CDNC of 200 and 20 cm^{-3} are chosen as they represent
693 the range typically observed over the ocean (see for example the CDNC range presented in
694 recent observational-based studies (Rosenfeld et al., 2019; Gryspeerd et al., 2019)). Each
695 simulation is conducted for 48 hours starting from 12 UTC. The horizontal resolution is set to
696 1200 m and 75 vertical levels are used. The temporal resolution is 12 sec and the output interval
697 is 30 min. Interactive radiation is calculated every 12 min using the RRTM-G scheme (Clough
698 et al., 2005; Iacono et al., 2008; Mlawer et al., 1997). We have added a coupling between the
699 microphysics and the radiation to include the Twomey effect (Twomey, 1977). This was done
700 by including the information of the cloud liquid droplet effective radius, calculated in the
701 microphysical scheme, in the radiation calculations. No Twomey effect due to changes in the
702 ice particles size distribution was considered due to the large uncertainty involved in the ice
703 microphysics and morphology. Additional details, such as the surface and atmospheric physics

704 parameterizations, are described in Klocke et al., (2017) and include an interactive surface flux
705 scheme and a fixed sea surface temperature (SST). We note that using a fixed SST does not
706 include feedbacks of aerosols on the SST evolution that could change the surface fluxes.
707 However, due to the large heat capacity of the ocean, we do not expect the SST to dramatically
708 change over the two days simulations.

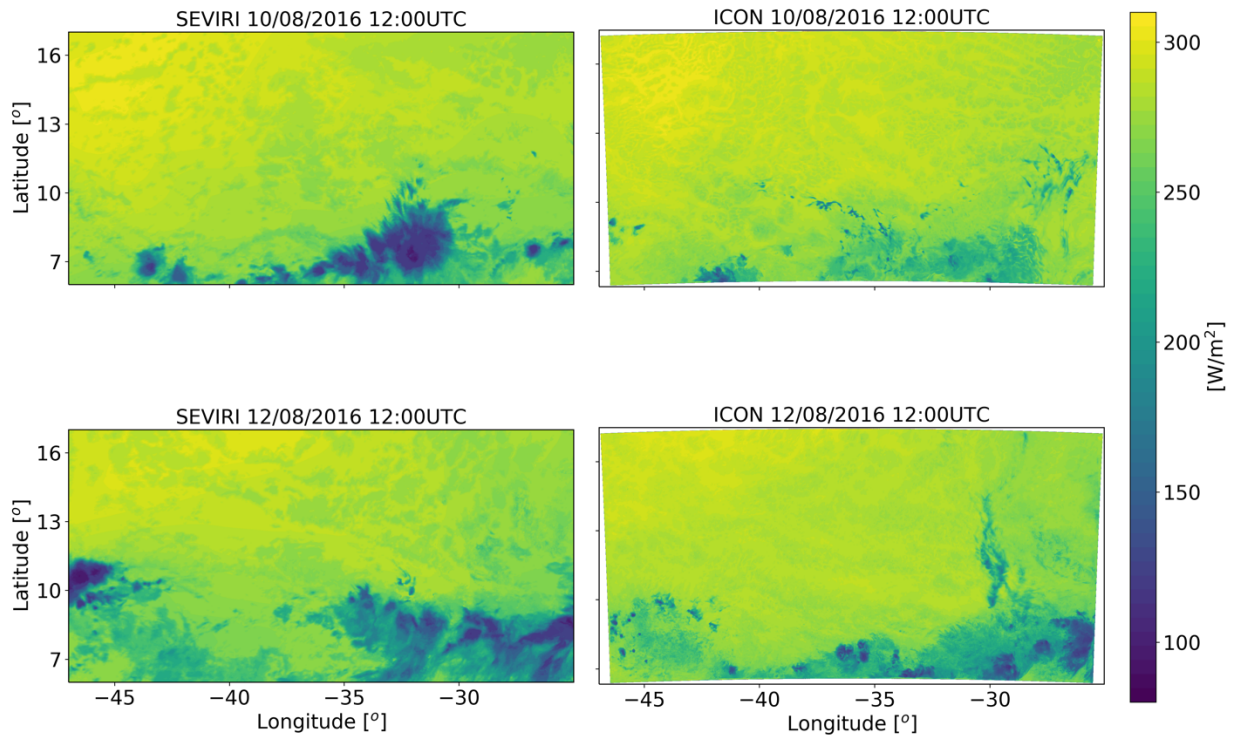
709 For comparing the outgoing longwave flux from the simulations and observations we use
710 imager data from the SEVIRI instrument onboard the Meteosat Second Generation (MSG)
711 geostationary satellite (Aminou, 2002). The outgoing longwave flux is calculated using the
712 Optimal Retrieval for Aerosol and Cloud (ORAC) algorithm (Sus et al. 2017; McGarragh, et
713 al. 2017). Cloud optical (thickness, effective radius, water path) and thermal (cloud top
714 temperature and pressure) properties are retrieved from ORAC using an optimal estimation-
715 based approach. These retrievals and reanalysis profiles of temperature, humidity and ozone
716 are then ingested into BUGSrad, a two-stream correlated-k broadband flux algorithm (Stephens
717 et al., 2001) that outputs the fluxes at the top and bottom of the atmosphere and shown to have
718 excellent agreement when applied to both active (CloudSat) and passive (Advanced Along
719 Track Scanning Radiometer) satellite sensors compared to Clouds and the Earth's Radiant
720 Energy System (Henderson et al. 2013; Stengel et al. 2019). In addition, off-line sensitivity
721 radiative transfer tests using vertical profiles from our model were conducted with BUGSrad
722 to identify the source of the differences in fluxes between clean and polluted conditions.



723

724 **Figure 1. Domain of the ICON simulations (red rectangle) ~~for the NARVAL 2 case study~~ overlaid on the**
725 **August 2016 ECMWF era-interim reanalysis (Dee et al., 2011) mean precipitation rate.**

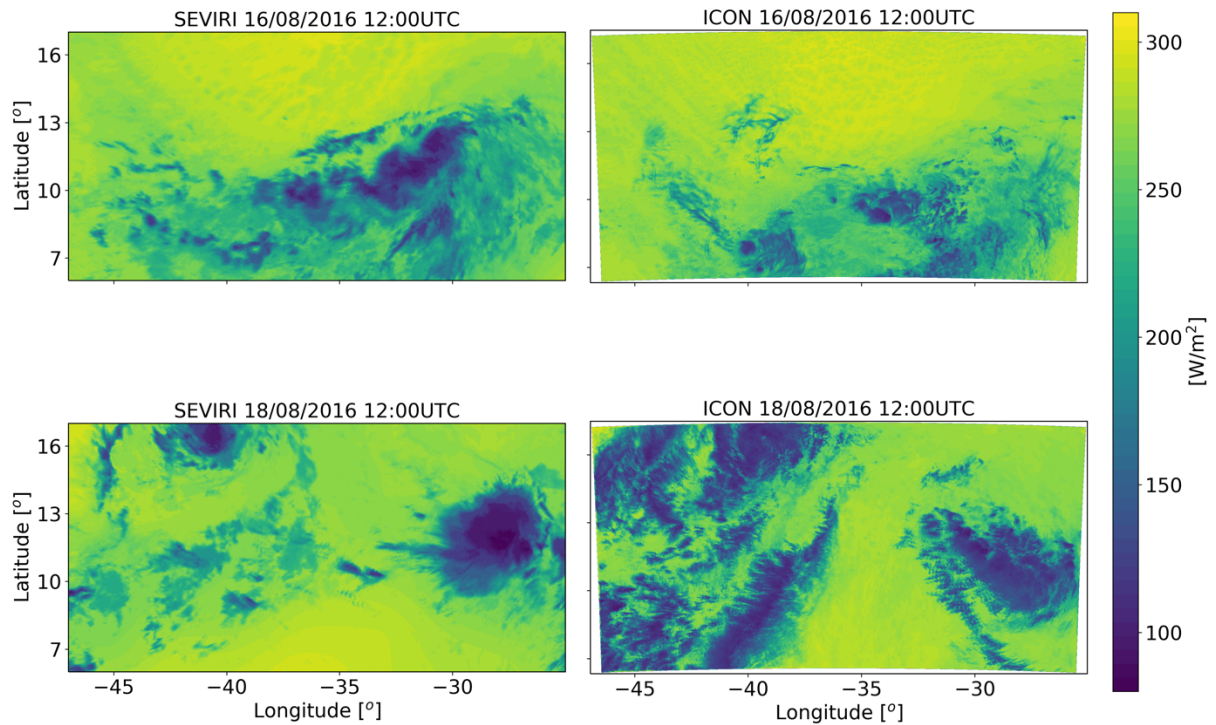
726



727
 728 **Figure 2. Outgoing longwave flux at the top of atmosphere at the initial stage (upper row) and the last stage**
 729 **(lower row – each average over 30 minutes) of the simulation of the shallow-cloud dominated case (10-**
 730 **12/08/2016) from geo-stationary satellite (SEVIRI-MSG – right column) and the ICON model simulation with**
 731 **CDNC of 20 cm^{-3} (left column).**

732

733



734

735 **Figure 3.** similar to Figure 2 but for the deep-cloud dominated case (16-18/08/2016).

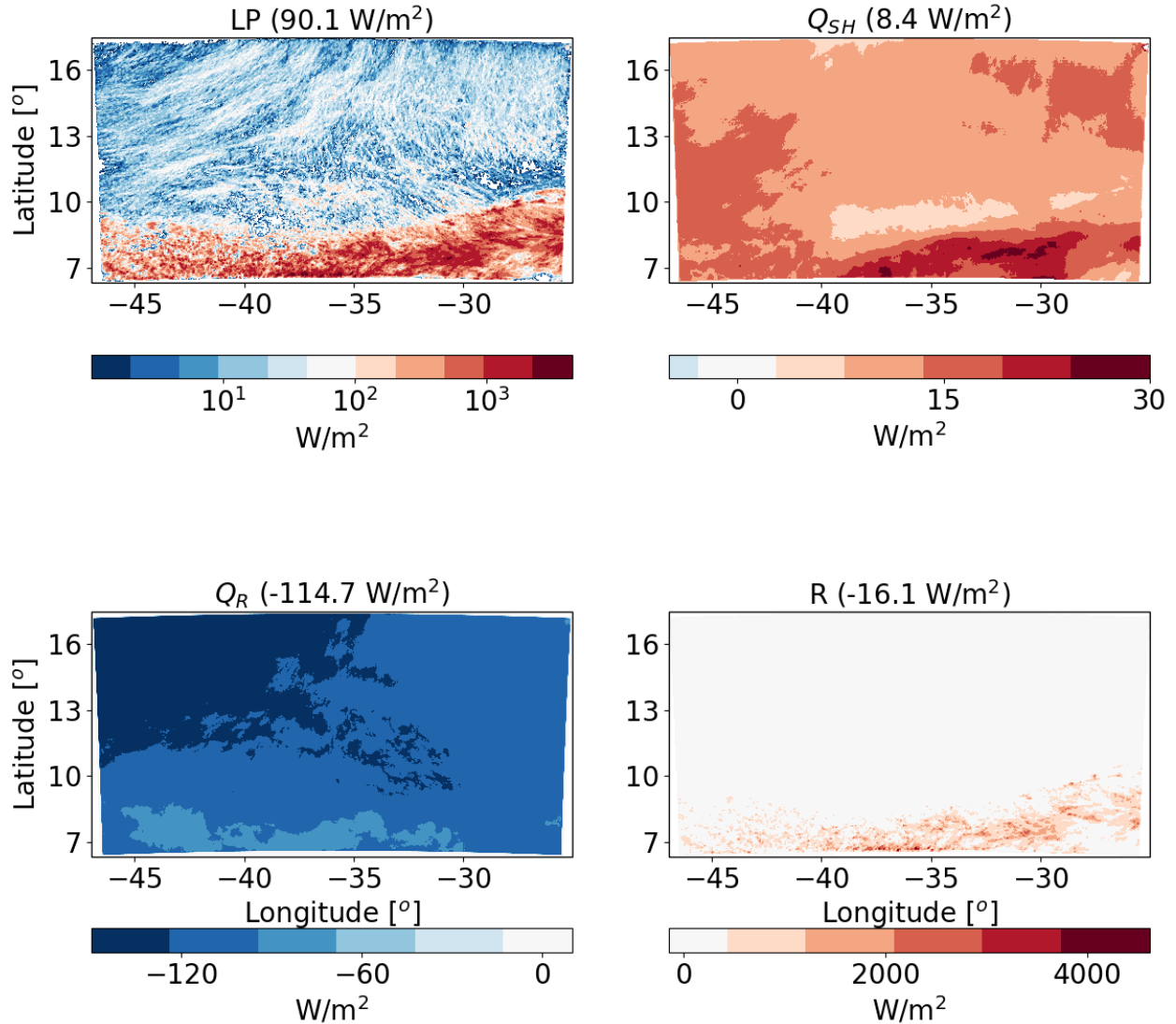
736 **Results**

737 **Shallow-cloud dominated case -10-12/08/2016**

738 We start with energy budget analysis of the shallow-cloud dominated case base simulations
 739 (CDNC = 20 cm⁻³). Figure 4 presents the time mean (over the two days simulation) of the
 740 different terms of the energy budget (Equation 1). As expected, LP dominates the warming of
 741 the atmosphere while Q_R dominate the cooling. The sensible heat flux (Q_{SH}) is positive (act to
 742 warm the atmosphere) but it is an order of magnitude smaller than the LP and Q_R magnitudes. In
 743 this shallow-cloud dominated case the radiative cooling of the atmosphere is significantly larger
 744 than the warming due to precipitation (mean of -114.7 W/m² compared to with 90.1 W/m²), hence
 745 the energy imbalance-residual (R) is negative. Negative R means that there must be some
 746 convergence of dry static energy into the domain and/or decrease in the storage term, in this case
 747 it is mostly due to convergence of dry static energy.

748 We note that there is a significant difference in the spatial distribution of LP and Q_R (Jakob et al., 2019). While the Q_R is more uniformly distributed, the LP is mostly concentrated at the south
 749 part of the domain (where the deep convective clouds are formed) and it has a dotted structure.
 750 Locally, at the core of a deep convective clouds, the LP contribution can reach a few 1000 W/m²
 751 (1 mm/hr of precipitation is equivalent to 628 W/m²), however, the vast majority of the domain
 752

753 contributes very little in terms of LP . Q_R also presents some spatial structure in which there is a
 754 weak atmospheric cooling at the south part of the domain (the region of the deep convective
 755 clouds) and a strong cooling at the rest of the domain.



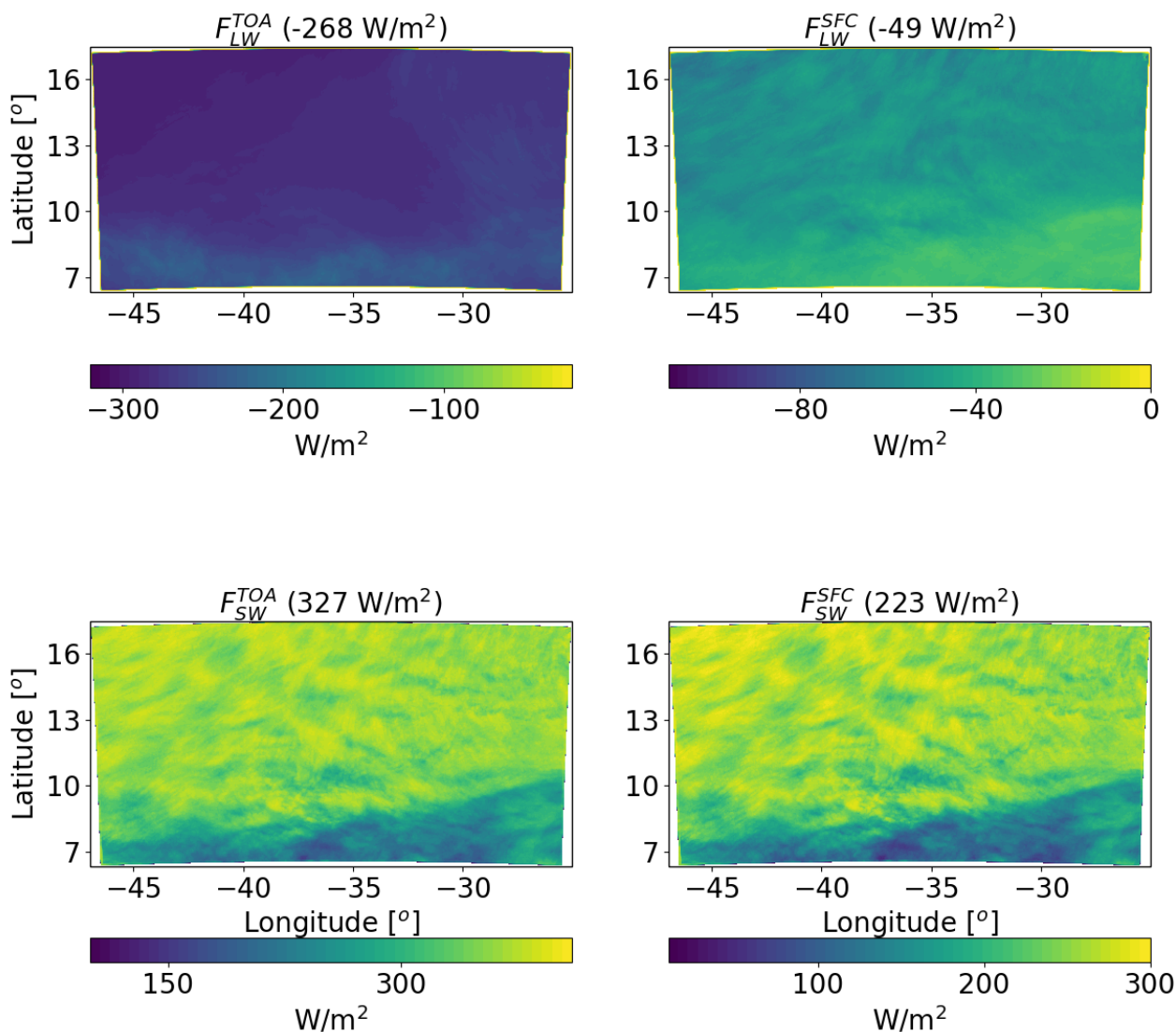
756
 757 **Figure 4.** Spatial distribution of the time mean of the different terms of the energy budget for the ICON
 758 simulation of the shallow-cloud dominated case (10-12/08/2016) with $CDNC = 20 \text{ cm}^{-3}$. The terms that appear
 759 here are: LP - latent heat by precipitation, Q_{SH} - sensible heat flux, Q_R - atmospheric radiative warming, and
 760 R – the [residual energy imbalance](#). The domain and time-mean value of each term appears in parenthesis.

761

762 For understanding the spatial structure of Q_R , next we examine the spatial distribution of the LW
 763 and SW radiative fluxes at the TOA and surface (Fig. 5). We note that the smaller radiative
 764 cooling in the region of deep clouds in the south of the domain is mostly contributed by a
 765 decrease in F_{LW}^{TOA} . The SW fluxes also demonstrate a strong south-north gradient, as the deep

766 convective clouds in the south are more reflective than the shallow trade cumulus (with the lower
 767 mean cloud fraction) in the rest of the domain.

768



769
 770 **Figure 5. Spatial distribution of ICON simulated time-mean longwave (LW) and shortwave (SW) radiation**
 771 **fluxes at the top of atmosphere (TOA) and surface (SFC) for a simulation of the shallow-cloud dominated**
 772 **case (10-12/08/2016) with CDNC = 20 cm⁻³. The domain and time mean value of each term appears in**
 773 **parenthesis.**

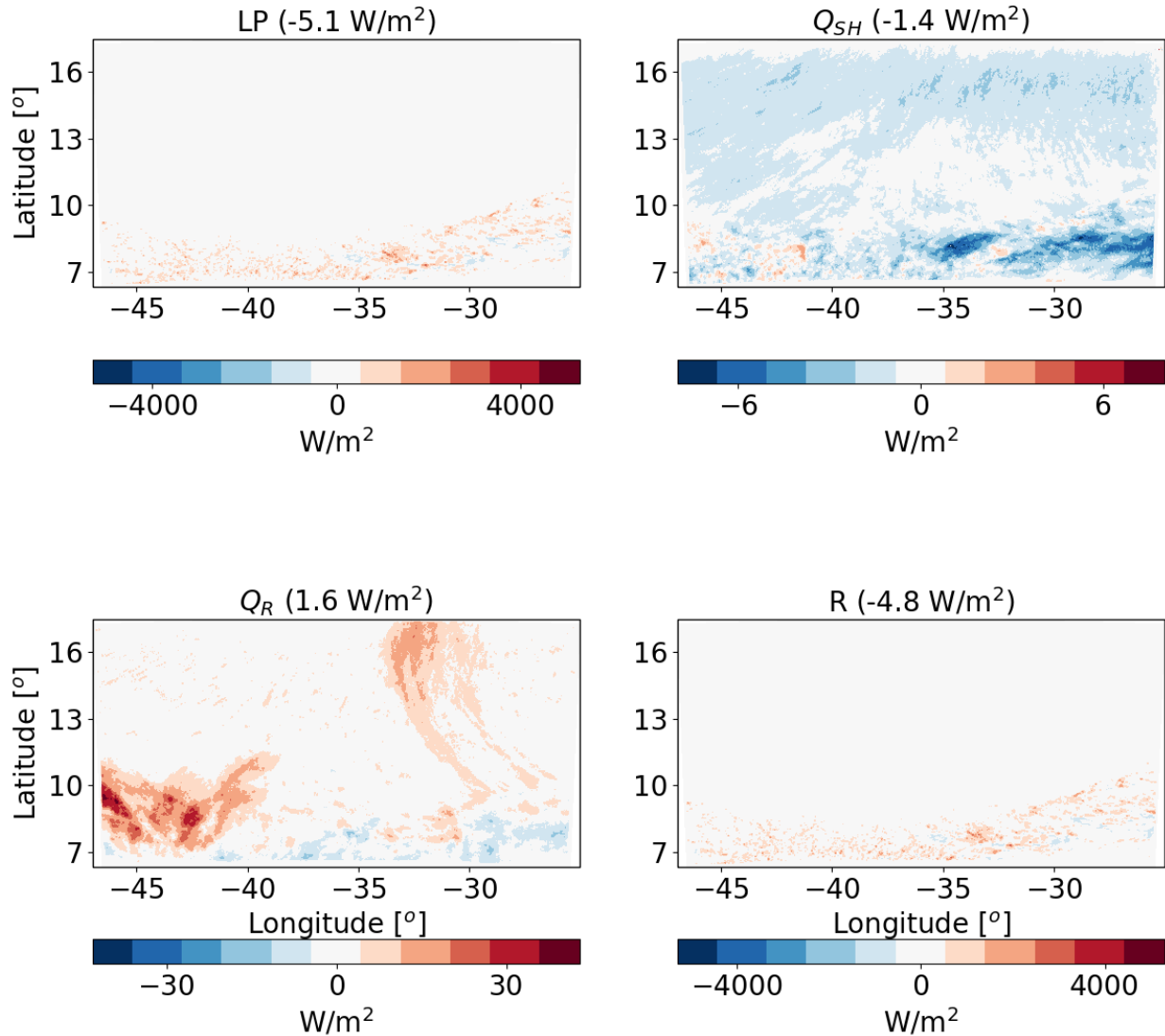
774

775 **Response to aerosol perturbation – shallow-cloud dominated case**

776 Next, we analyse the response of the atmospheric energy budget of this case to perturbations in
 777 CDNC. Figure 6 presents the differences in the different terms of the energy budget between a
 778 polluted simulation (CDNC = 200 cm⁻³) and a clean simulation (CDNC = 20 cm⁻³). It

779 demonstrates that the LP differences between the different CDNC scenarios contribute 5.1 W/m^2
780 less to warm the atmosphere in the polluted vs. the clean simulation. We note that this apparently
781 large effect is caused by a small, non-statistically significant, precipitation difference ($\sim 0.4 \text{ mm}$
782 over the two days of simulation - see Fig. 8 below). The strong sensitivity of the atmospheric
783 energy budget to small precipitation changes (recalling that 1 mm/hr is equivalent to 628 W/m^2)
784 exemplifies the caution one needs to take when looking on precipitation response in terms of
785 energy budget perspective. The Q_R differences lead to relative warming of the atmosphere of the
786 polluted case compared to the clean case by 1.6 W/m^2 . We note that most of the Q_R differences
787 are located in the south-west part of the domain. The Q_{SH} changes counteracts 1.4 W/m^2 of the
788 atmospheric warming by Q_R and so the end result is a deficit of 4.8 W/m^2 in the atmospheric
789 energy budget in the polluted simulation compared to the clean simulation. The decrease in the
790 Q_{SH} is driven by an increase in the near surface air temperature (see Fig. 8).

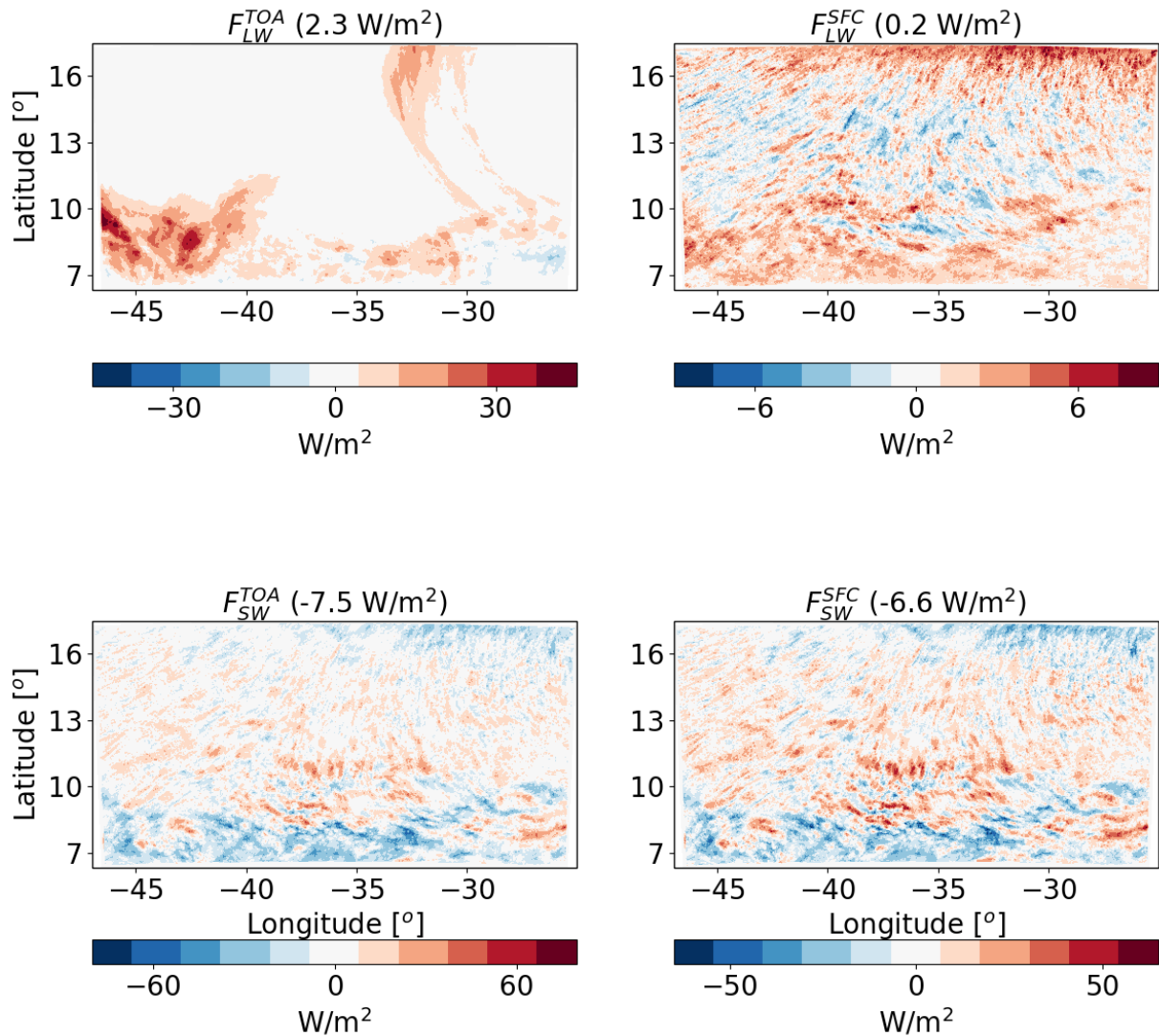
791



792
 793 **Figure 6.** The differences between polluted ($\text{CDNC} = 200 \text{ cm}^{-3}$) and clean ($\text{CDNC} = 20 \text{ cm}^{-3}$) ICON simulations
 794 of the time-mean terms of the energy budget for the shallow-cloud dominated case (10-12/08/2016). The terms
 795 that appears here are: LP - latent heat by precipitation, Q_{SH} - sensible heat flux, Q_R - atmospheric radiative
 796 warming, and R – the [residual energy imbalance](#). The domain and time mean value of each term appears in
 797 parenthesis.

798 To understand the response of Q_R to the CDNC perturbation, we next examine the response of
 799 the different radiative fluxes. Figure 7 demonstrates that most of the relative atmospheric
 800 radiative heating in the polluted case compared to the clean case is contributed by changes in the
 801 F_{LW}^{TOA} fluxes. The changes in F_{LW}^{SFC} are an order of magnitude smaller. The SW fluxes change both
 802 at the TOA and SFC are larger than the F_{LW}^{TOA} changes, however, in terms of the atmospheric energy
 803 budget, they almost cancel each other out and the net SW atmospheric effect is only -0.9 W/m^2 .
 804 Most of the reduction in SW fluxes (both at TOA and the surface) comes from the deep
 805 convective regions in the south of the domain while the shallow cloud regions experience some

806 increase in SW fluxes. This can be attributed to the increase in deep convective cloud fraction
 807 and a decrease in the shallow cloud fraction with the increase in CDNC (see Fig. 9 below). The
 808 TOA net radiative effect for the entire system (as opposed to the atmospheric energy budget that
 809 take into consideration the surface radiative fluxes changes) is about -5.2 W/m^2 .



810
 811 **Figure 7.** The differences between polluted ($\text{CDNC} = 200 \text{ cm}^{-3}$) and clean ($\text{CDNC} = 20 \text{ cm}^{-3}$) ICON simulations
 812 of the time mean radiative longwave (LW) and shortwave (SW) fluxes at the top of atmosphere (TOA) and
 813 surface (SFC) for the shallow-cloud dominated case (10-12/08/2016). The domain and time mean value of
 814 each term appears in parenthesis.

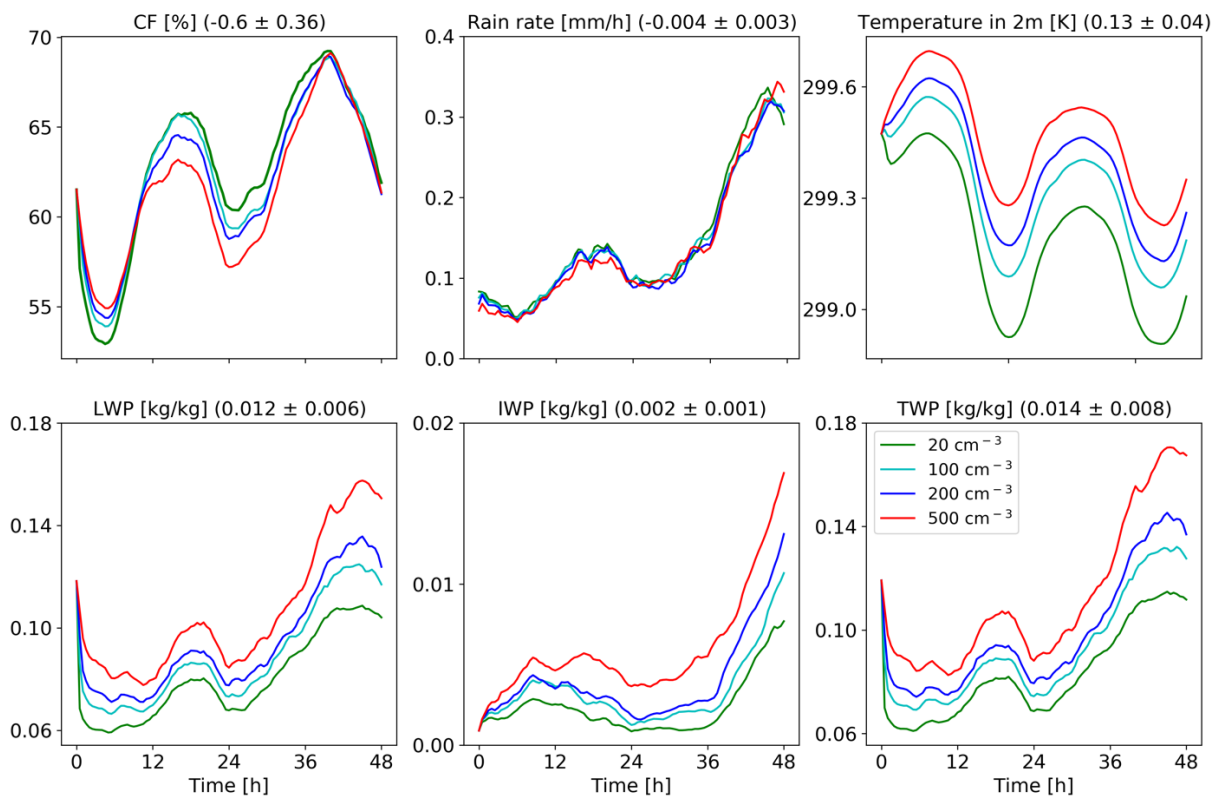
815
 816 The differences in the energy (Fig. 6) and radiation (Fig. 7) budgets between the clean and
 817 polluted cases shown above, could be explained by the differences in the cloud mean properties.
 818 Figure 8 presents the time evolution of some of the domain mean properties while Fig. 9 presents
 819 time and horizontal mean vertical profiles. To examine the robustness of the trends we add here

820 two more CDNC cases of 100 and 500 cm^{-3} (on top of the two that were examine above – 20 and
821 200 cm^{-3}). Figure 8 demonstrates that the domain mean cloud fraction (CF) generally decreases
822 with the increase in CDNC (except for the first ~10 hours of the simulations). Examining the
823 vertical structure of the CF response (Fig. 9), demonstrates that with the increase in CDNC there
824 is a reduction in the low level (below 800 mb) CF concomitantly with an increase in CF at the
825 middle and upper troposphere. The differences in rain rate between the different simulations are
826 small. However, both the liquid water path (LWP) and the ice water path (IWP) show a consistent
827 increase with CDNC. Accordingly, also the total water path (TWP), which is the sum of the LWP
828 and the IWP, substantial increases with CDNC. The vertical profiles of the different hydrometers
829 (Fig. 9) indicate, as expected, that the cloud droplet mass mixing ration (q_c - droplet with radius
830 smaller than 40 μm) increases with CDNC, while the rain mass mixing ratio (q_r - drops with
831 radius larger than 40 μm) decreases due to the shift in the droplet size distribution to smaller
832 sizes under larger CDNC conditions. As this case is dominated by shallow clouds, there exists
833 only a comparably small amount of ice mixing ration (q_i) (c.f. Fig. 17), but its concentration
834 increases with the CDNC increase. The combined effect of the increase in CDNC is to
835 monotonically increase the total water mixing ratio (q_t) above 800 mb (Fig. 9). The relative
836 increase in q_t with CDNC becomes larger at higher levels.

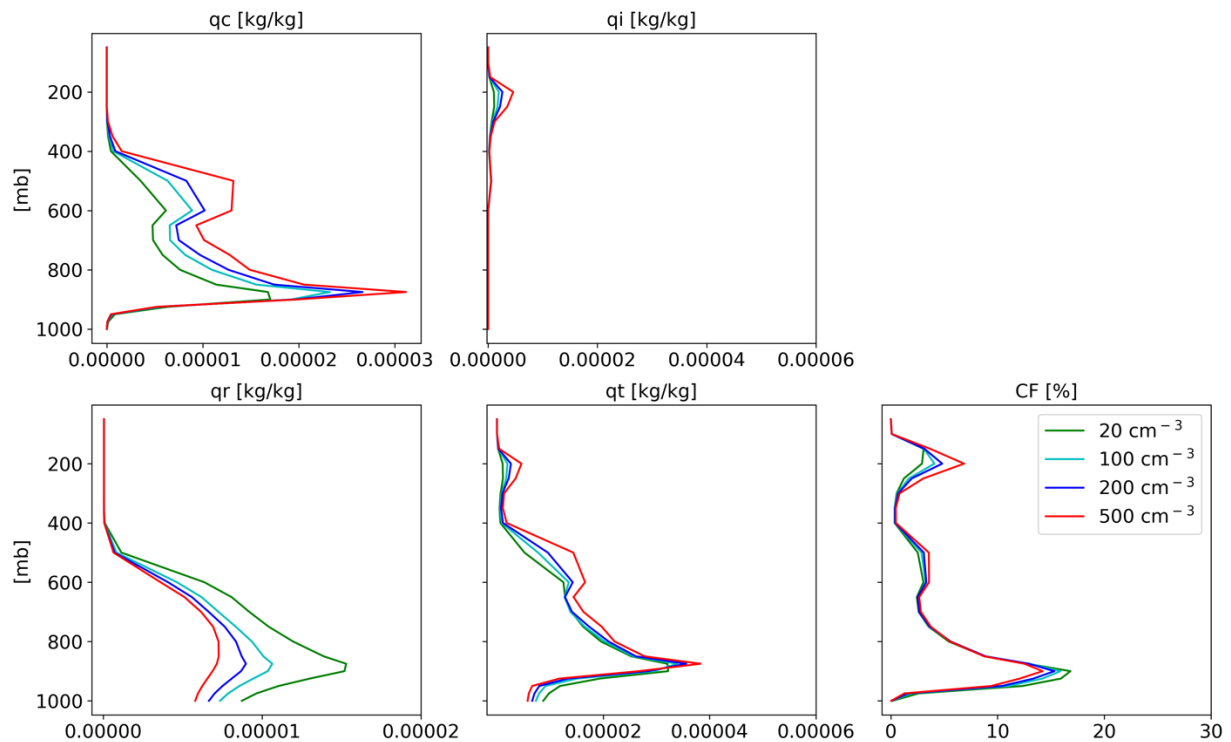
837 The increase in cloud water with increasing CDNC can explain both the reductions in the net
838 downward SW fluxes (both at TOA and surface) and the decrease in outgoing LW flux at TOA
839 (Fig. 7), as it results in more SW reflection concomitantly with more LW trapping in the
840 atmosphere (Koren et al., 2010). Another contributor to the SW flux reduction (more reflectance)
841 at the TOA is the Twomey effect (Twomey, 1977), while, the decrease in the low-level CF
842 compensates some of this effect. Here we present the outcome of these contradicting effects on
843 the SW fluxes, which shows a reduction at both the TOA and surface (Fig. 7). For estimating the
844 relative contribution of the Twomey effect compare to the cloud adjustments (CF and TWP
845 effects) to the SW flux changes, we have re-run the simulations with the Twomey effect turned
846 off (the radiation calculations do not consider the changes in effective radius between the
847 different simulations). It demonstrates that without the Twomey effect the TOA SW difference
848 is only -1.7 W/m^2 as compared to -7.5 W/m^2 with the Twomey effect, demonstrating the
849 predominant role of the Twomey effect. For estimating the relative contribution of the changes
850 in CF and [TWP–water content](#) to the SW flux changes we have conducted off-line radiative
851 transfer sensitivity tests. To quantify the [water content](#)[TWP](#) radiative effect, we feed the same
852 CF vertical profile from the model into [the offline radiative transfer model](#) BUGSrad, while

853 allowing the [water content](#)^{FWP} vertical profile to change (and visa versa to compute the CF
 854 radiative effect). This approach demonstrates that the contribution from the small reduction in
 855 CF is negligible compared to the increased SW reflectance caused by the increased ~~in~~ [water](#)
 856 [content](#)^{FWP} (the effect of the reduction in CF compensate only about 1% of the effect of the
 857 [increase in the water content](#)).

858 We also note a monotonic increase in the near surface temperature with CDNC (see also Fig. 10
 859 below). This trend can be explained by warm rain suppression with increasing CDNC that leads
 860 to less evaporative cooling (see the decrease in the total amount of water mass mixing ration just
 861 above the surface in Fig. 9, (Dagan et al., 2016; Albrecht, 1993; Seigel, 2014; Seifert and Heus,
 862 2013; Lebo and Morrison, 2014)). In addition, it was shown that under polluted conditions the
 863 rain drops below cloud base are larger, hence evaporating less efficiently (Lebo and Morrison,
 864 2014; Dagan et al., 2016). The increase in the near surface temperature drives the decrease in the
 865 Q_{SH} (Fig. 6).



866
 867 **Figure 8. Domain average properties as a function of time for the different CDNC simulations for the shallow-**
 868 **cloud dominated case. The properties that are presented here are: cloud fraction (CF), rain rate, temperature**
 869 **in 2 m, liquid water path (LWP – based on the cloud water mass, excluding the rain mass for consistency**
 870 **with satellite observations), ice water path (IWP) and total water path (TPW = LWP + IWP). For each**
 871 **property, the mean difference between all combinations of simulations, normalized to a factor 5 increase in**
 872 **CDNC, and its standard deviation appear in parenthesis.**



874

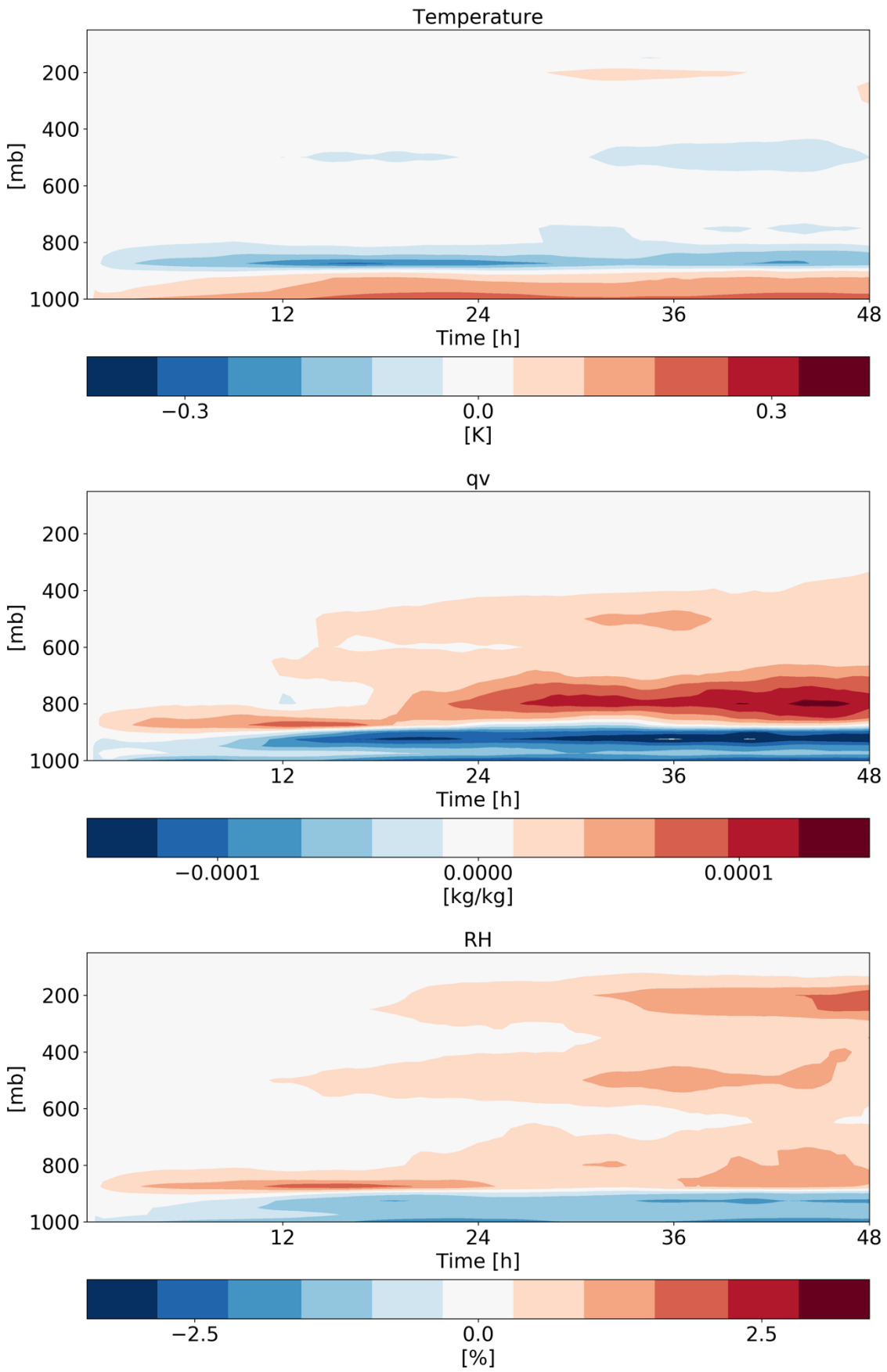
875 **Figure 9. Domain and time average vertical profiles for the different CDNC simulations for the shallow-cloud**
 876 **dominated case. The properties that are presented here are: cloud droplet mass mixing ratio (q_c – for clouds’**
 877 **droplets with radius smaller than $40\ \mu\text{m}$), ice mass mixing ratio (q_i), rain mass mixing ratio (q_r - for clouds’**
 878 **drops with radius larger than $40\ \mu\text{m}$), total water mass mixing ratio ($q_t = q_c + q_i + q_r$), and cloud fraction (CF).**
 879 **The x-axis ranges are identical as for the deep-cloud dominated case – Fig. 17.**

880

881 In addition to the clouds’ effect on the radiation fluxes, changes in humidity could also contribute
 882 (Fig. 10). We note that increase in CDNC leads to increase in relative humidity (RH) and specific
 883 humidity (q_v) at the middle and upper troposphere without a significant temperature change. The
 884 increased humidity at the upper troposphere would act to decrease the outgoing LW flux, a
 885 similar to the effect of as the increased ice content in the upper troposphere has (Fig. 9).
 886 However, sensitivity studies with off-line radiative transfer calculations using BUGSrad,
 887 demonstrate that the vast majority (more than 99%) of the different in F_{LW}^{TOA} between clean and
 888 polluted conditions emerges from the cloudy skies (rather than clear-sky), suggesting that the
 889 effect of the increased ice content at the upper troposphere dominates predominant.

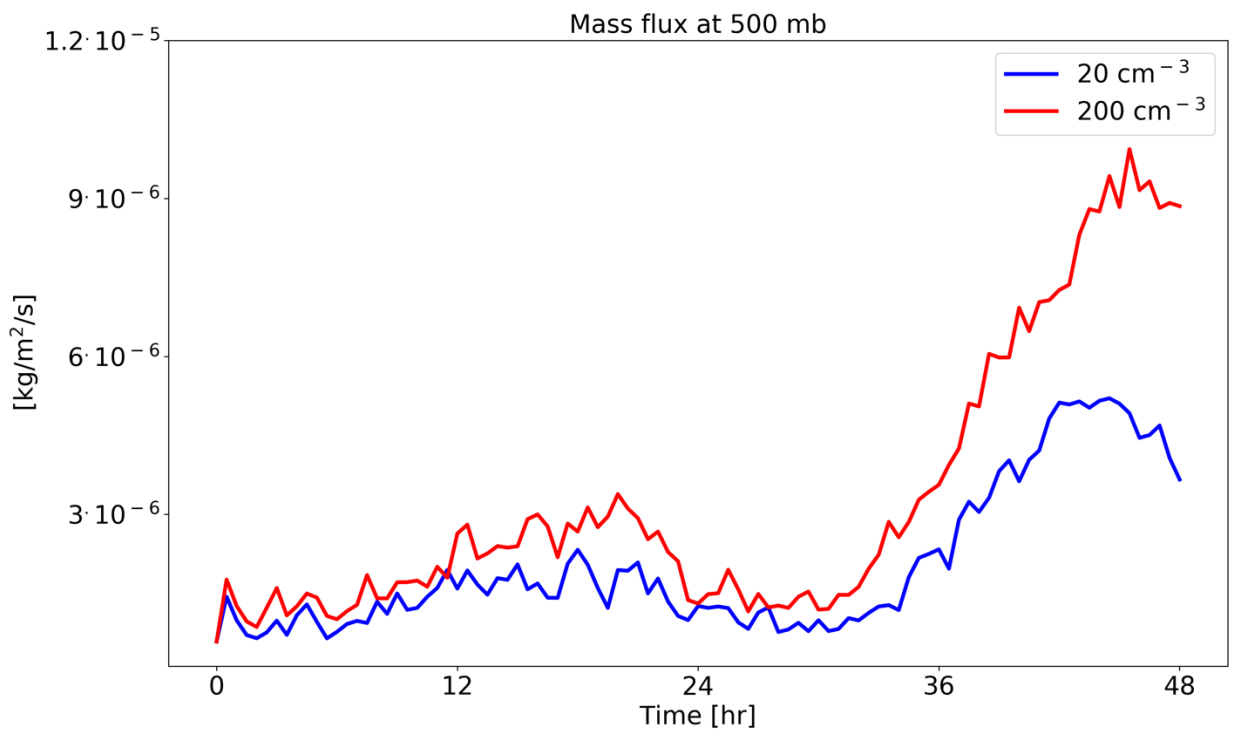
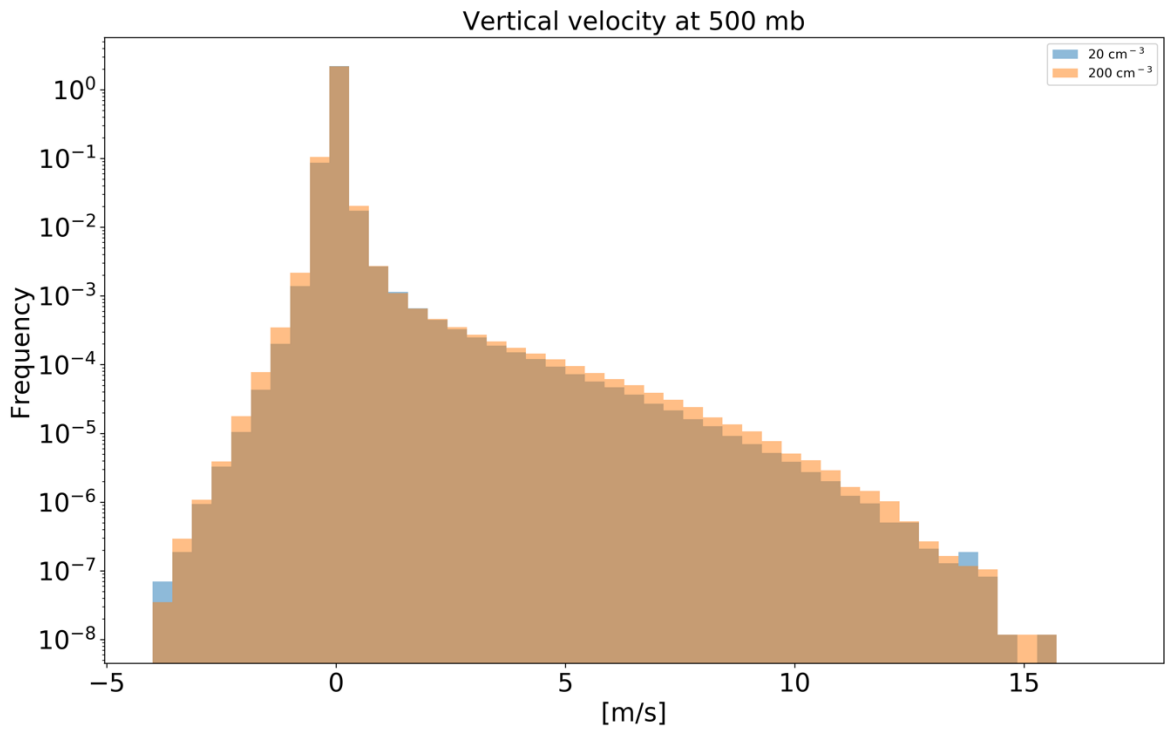
890 Both the increase in water vapor and ice content in the upper troposphere are driven by an
 891 increase in upward water (liquid and ice) mass flux with increasing CDNC to these levels (Fig.

892 11). [An increase in mass flux could be caused by an increase in vertical velocities and/or by an](#)
893 [increase in cloud \(or updraft\) fraction and/or by an increase in cloud water content. In our case,](#)
894 [tThe increaseincreases](#) in mass flux is driven partially by the small increase in vertical velocity
895 (especially for updraft between 5 and 10 m/s – [Fig. 11](#)), [partially by the small increase in cloud](#)
896 [fraction at this level \(Fig. 9\)](#) and mostly due to the larger water mass mixing ratio (Fig. 9) that
897 leads to an increase in mass flux even for a given vertical velocity. The increased relative
898 humidity at the upper troposphere, further increases the ice particle lifetime at these levels (in
899 addition to the microphysical effect (Grabowski and Morrison, 2016)) as the evaporation rate
900 decreases. In addition, the differences in the thermodynamics evolution between the different
901 simulations (Fig. 10) demonstrate drying and warming of the boundary layer with increasing
902 CDNC, due to reduction in rain evaporation below cloud base and deepening of the boundary
903 layer (Dagan et al., 2016; Lebo and Morrison, 2014; Seifert et al., 2015; Spill et al., 2019). The
904 drying of the boundary layer could explain the reduction in the low cloud fraction (Fig. 9 (Seifert
905 et al., 2015)).

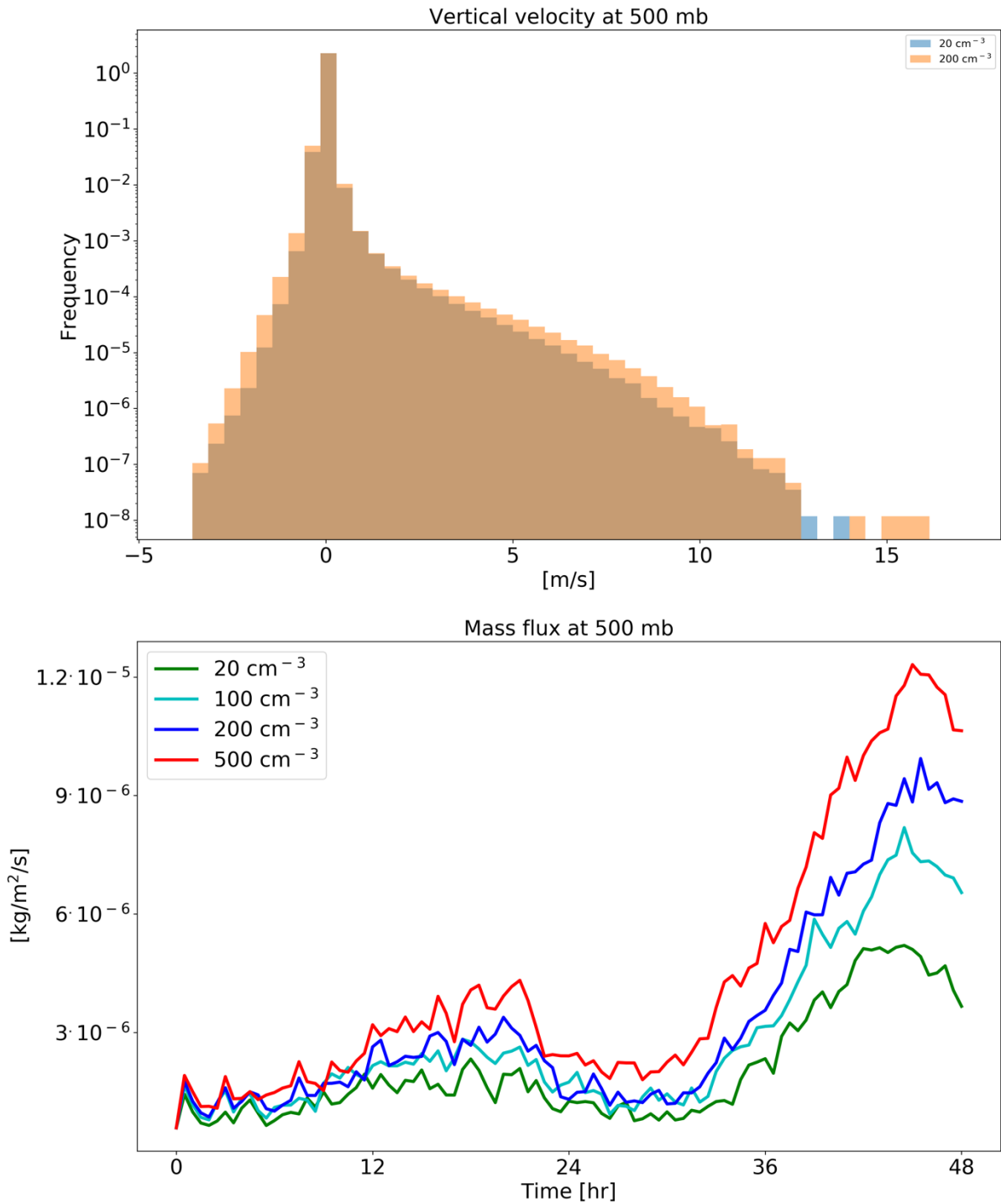


907 **Figure_10. [Time-heightHovmöller](#) diagrams of the differences in the domain mean temperature, specific**
908 **humidity (qv) and relative humidity (RH) vertical profiles between polluted (CDNC = 200 cm⁻³) and clean**
909 **(CDNC = 20 cm⁻³) simulations for the shallow-cloud dominated case (10-12/08/2016).**

910



911



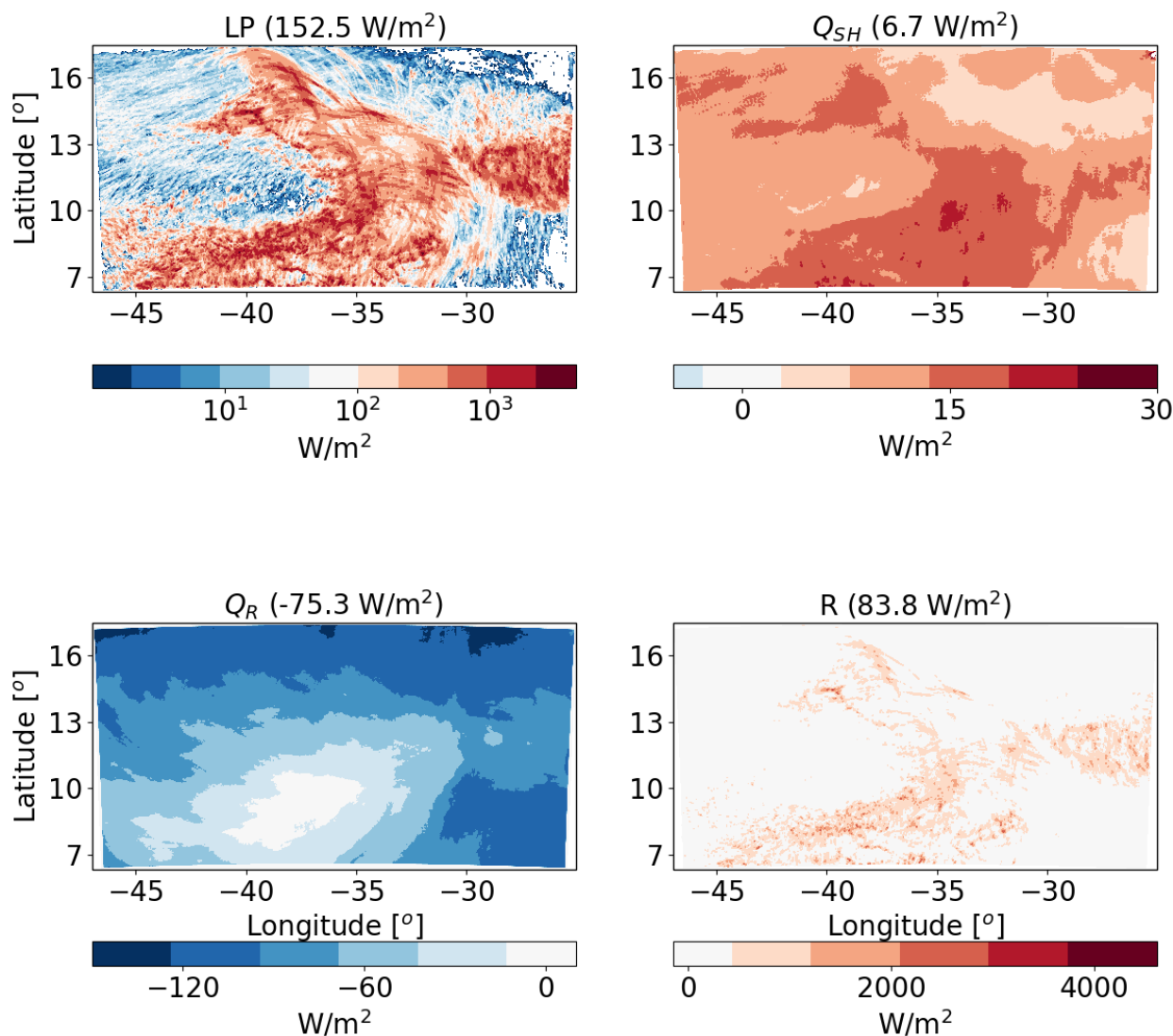
912

913 **Figure 11. histograms of ICON simulated vertical velocity at the level of 500 mb for a clean (CDNC = 20 cm^{-3})**
 914 **and polluted (CDNC = 200 cm^{-3}) simulations** (upper), and the time evolution of the net upwards water (liquid
 915 **and ice) mass flux (lower) for the different CDNC simulations for a clean (CDNC = 20 cm^{-3}) and polluted**
 916 **(CDNC = 200 cm^{-3}) simulations** for the shallow-cloud dominated case (10-12/08/2016). The 500 mb level is
 917 **chosen as it represents the transition between the warm part to the cold part of the clouds. In the histogram**
 918 **only two simulations are presented for clarity.**

919

920 **Deep-cloud dominated case -16-18/08/2016**

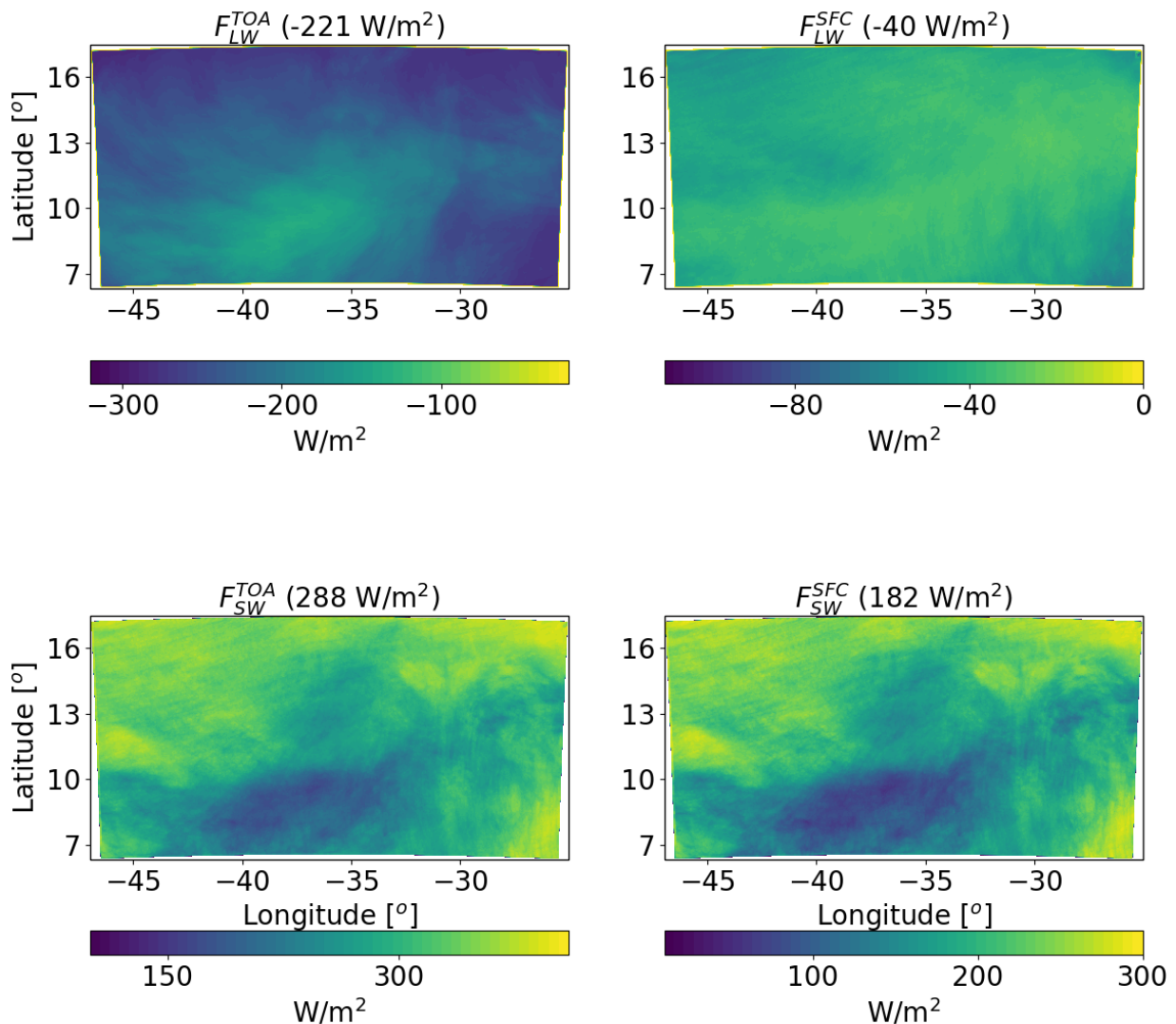
921 Next, we analyse the atmospheric energy budget for the deep-cloud dominated case (Fiona
 922 tropical storm – Fig. 12). As opposed to the shallow-cloud dominated case, in this case the LP
 923 contribution dominates over the radiative cooling and hence the energy imbalance-residual R is
 924 positive and large, suggesting divergence of dry static energy out of the domain. This difference
 925 in the base line atmospheric energy budget between the different cases simulated here, enable an
 926 examination of the aerosol effect on the atmospheric energy budget under contrasting initial
 927 conditions. As in the shallow-cloud dominated case, the Q_R values varies between small values
 928 (especially at the regions that were mostly covered by deep clouds) to larger negative values
 929 (dominated at the regions that were covered by shallow clouds). The Q_{SH} is positive and an order
 930 of magnitude smaller than the Q_R and LP , similar to the shallow-cloud dominated case.



931

932 **Figure 12. Spatial distribution of the time mean of the different terms of the energy budget for the ICON**
 933 **simulation of the deep-cloud dominated case (16-18/08/2016) with CDNC = 20 cm⁻³. The terms that appear**
 934 **here are: *LP* - latent heat by precipitation, *Q_{SH}* - sensible heat flux, *Q_R* - atmospheric radiative warming, and**
 935 ***R* – the [residual energy imbalance](#). The domain and time-mean value of each term appears in parenthesis.**

936
 937 Further examination of the radiative fluxes (Fig. 13) demonstrates again the resemblance in the
 938 spatial structure between *Q_R* and *F_{LW}^{TOA}*. As compared to the shallow-cloud dominated case, since
 939 the clouds are more opaque and cover larger fraction of the sky, there is a decrease in the
 940 magnitude of all fluxes (in different amount). For example, *F_{SW}^{SFC}* is lower by 41 W/m²
 941 (representing larger SW reflectance back to space) and the magnitude of *F_{LW}^{TOA}* by 47 W/m² as
 942 compare to the shallow-cloud dominated case. The combined effect of the radiative flux
 943 differences between the two cases is a decrease of the atmospheric radiative cooling by 39.6
 944 W/m² (-114.7 compare with -75.3 W/m² – see Figs. 5 and 13).



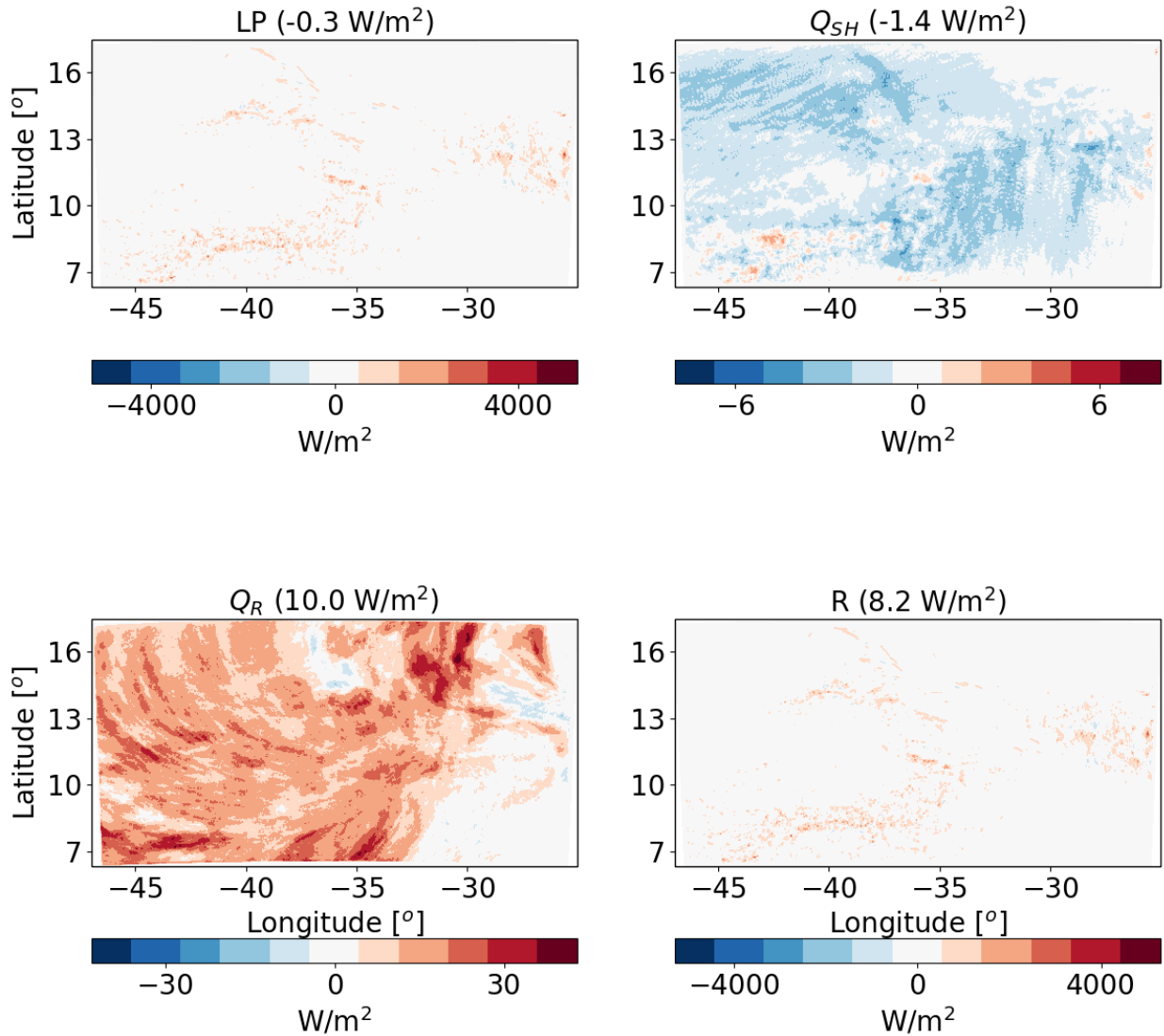
945

946 **Figure 13. Spatial distribution of ICON simulated time-mean longwave (LW) and shortwave (SW) radiation**
947 **fluxes at the top of atmosphere (TOA) and surface (SFC) for a simulation of the deep-cloud dominated case**
948 **(16-18/08/2016) with CDNC = 20 cm⁻³. The domain and time mean value of each term appears in parenthesis.**

949

950 **Response to aerosol perturbation – deep-cloud dominated case**

951 For the deep-cloud dominated case, an increase in CDNC results in a decrease in LP by -0.3
952 W/m². Again, this difference is due to [a](#) non-statistically significant precipitation changes (see
953 also Fig. 16 below). A similar Q_{SH} decrease as in the shallow-cloud dominated case is observed
954 in the deep-clouds dominated case (see Figs. 14 and 6). The predominant difference in the
955 response between the two cases is in Q_R , which increases much more in the deep-cloud dominated
956 case: 10.0 W/m² (Fig. 14) compared with 1.6 W/m² in the shallow-cloud dominated case (Fig.
957 6).

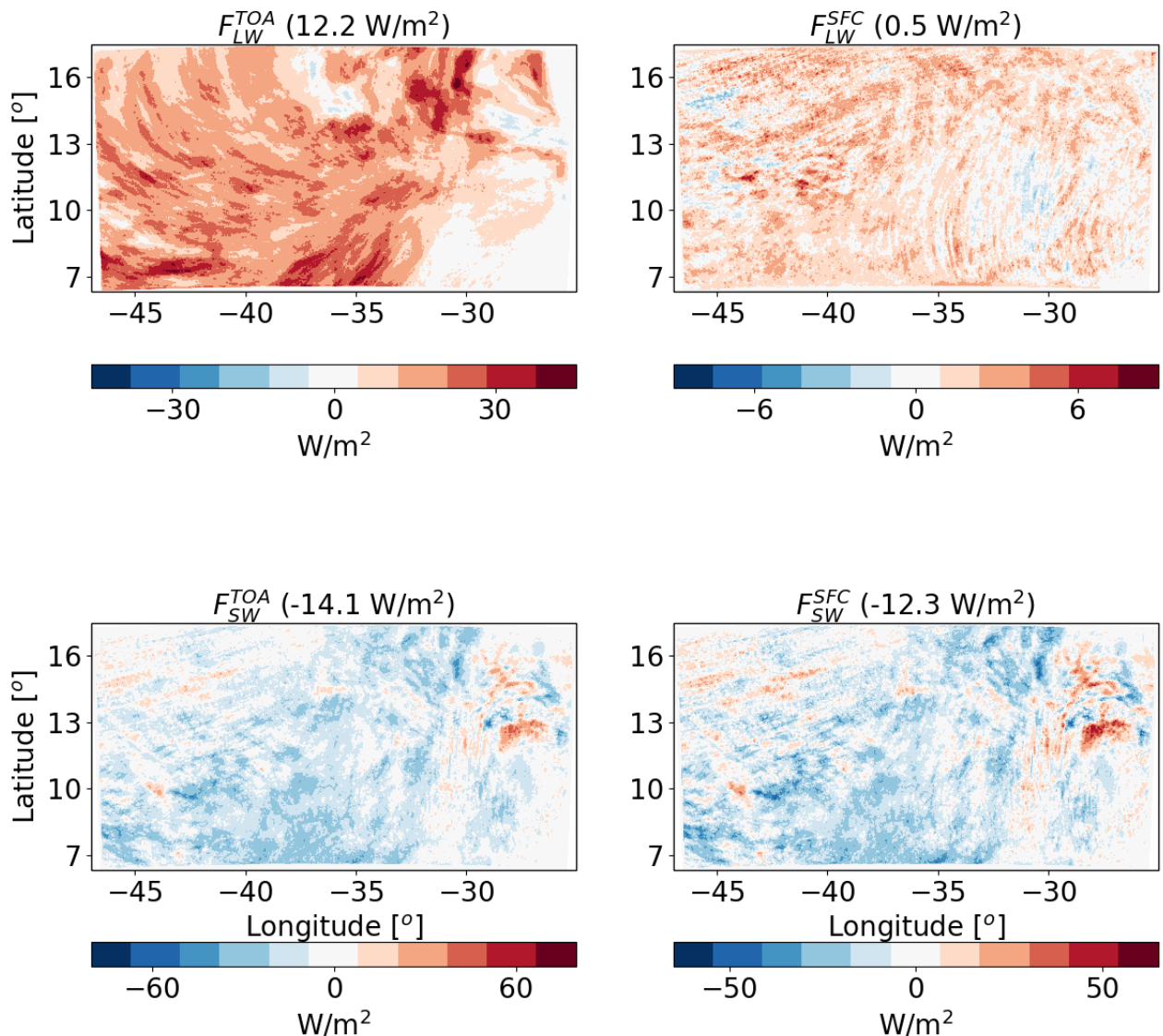


958
 959 **Figure 14.** The differences between polluted (CDNC = 200 cm⁻³) and clean (CDNC = 20 cm⁻³) ICON
 960 simulations of the time-mean terms of the energy budget for the deep-cloud dominated case (16-18/08/2016).
 961 The terms that appears here are: *LP* - latent heat by precipitation, *Q_{SH}* - sensible heat flux, *Q_R* - atmospheric
 962 radiative warming, and *R* - the [residual energy imbalance](#). The domain and time mean value of each term
 963 appears in parenthesis.

964

965 The large increase in *Q_R* is caused mostly by the increase in F_{LW}^{TOA} (which becomes less negative
 966 i.e. less outgoing LW radiation under polluted conditions – Fig. 15). The CDNC effect on F_{LW}^{SFC}
 967 has a much smaller magnitude. The SW fluxes changes are substantial (-14.1 W/m² at TOA and
 968 -12.3 W/m² at the surface), however, in terms of the atmospheric energy budget, since clouds do
 969 not absorb much in the SW, the TOA and surface changes almost cancel each other out and the
 970 net effect is only ~1.8 W/m² atmospheric radiative cooling (which decrease some of the LW

971 warming). The net TOA total (SW+LW) radiative flux change is about -1.9 W/m^2 . The trends in
 972 the mean cloud properties (Figs. 16 and 17 below) can explain this large radiative response.



973
 974 **Figure 15. The differences between polluted (CDNC = 200 cm⁻³) and clean (CDNC = 20 cm⁻³) ICON**
 975 **simulations of the time mean radiative longwave (LW) and shortwave (SW) fluxes at the top of atmosphere**
 976 **(TOA) and surface (SFC) for the deep-cloud dominated case (16-18/08/2016). The domain and time mean**
 977 **value of each term appears in parenthesis.**

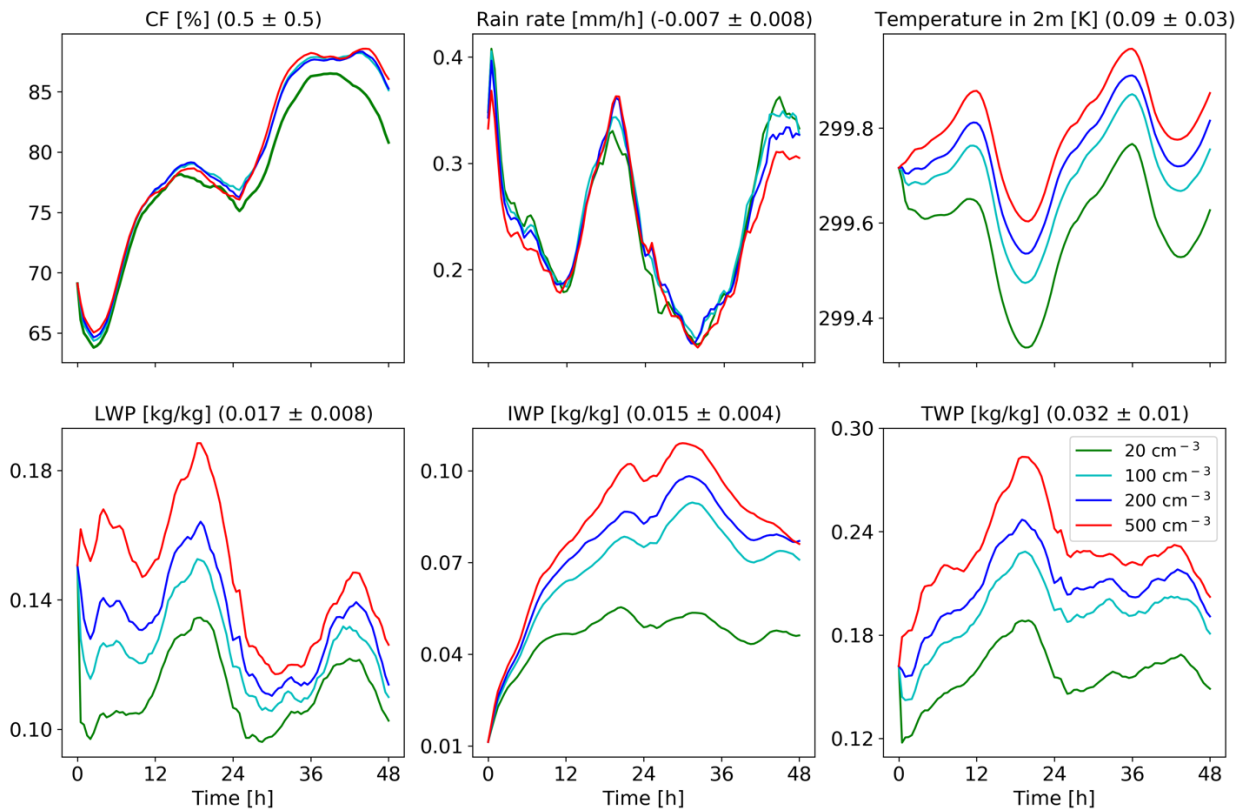
978
 979 Figure 16 presents some of the domain mean properties as a function of time for the deep-cloud
 980 dominated case. It demonstrates an increase in CF with CDNC which is more significant during
 981 the second day of the simulation. This is opposite to the CF reduction in the shallow-cloud
 982 dominated case (Fig. 8). It also demonstrates a very significant increase in LWP and, even more

983 (in relative terms), in IWP and thus also in TWP. The increase in CF and water content can
984 explain the decrease in SW fluxes both at TOA and surface (Fig. 15) as more SW is being
985 reflected back to space. The larger SW reflection under increased CDNC is also contributed to
986 by the Twomey effect (Twomey, 1977). Re-running the simulations without the Twomey effect
987 result in 9.6 W/m² reduction in the TOA SW flux as compare to 14.1 W/m² with the Twomey
988 effect on. We note that the relative role of the Twomey effect (compare to the cloud adjustments
989 – CF and TWP) is larger in the shallow-cloud dominated case as compared to the deep-cloud
990 dominated case (-14.19.6 W/m² and -9.614.1 W/m² for simulations with and without the Twomey
991 effect in the deep-cloud dominated case, compare to -1.77.5 W/m² and -1.77.5 W/m² in the
992 shallow-cloud dominated case, respectively). However, it should be noted that the Twomey
993 effect due to changes in the ice particles size distribution was not considered. In this case, unlike
994 in the shallow-cloud dominated case, the three contributions to the SW changes (CF, Twomey
995 and LWP/IWP, e.g. (Goren and Rosenfeld, 2014)) all contribute to the SW flux reduction (Fig.
996 15 presents the results of all contributors). Off-line sensitivity tests demonstrate that the relative
997 contribution of the TWP-water content and the CF to the increase in SW reflectance is roughly
998 $\frac{3}{4}$ and $\frac{1}{4}$, respectively.

999 The vertical profile changes with CDNC (Fig. 17) demonstrate a consistent picture of a decrease
1000 in CF in low clouds and a significant increase in CF and liquid and ice content at the mid and
1001 upper troposphere. The CF increase at the upper troposphere, and especially the increase in the
1002 ice content, can explain the decrease in the outgoing LW radiation (Fig. 15). The increase in ice
1003 content at the upper troposphere is in agreement with recent observational studies (Gryspeerd et
1004 al., 2018; Sourdeval et al., 2018; Christensen et al., 2016). Analysis of the upward water mass
1005 flux from the warm to the cold part of the clouds (at 500 mb) in the different simulations (Fig.
1006 19), demonstrates a substantial increase with the increase in CDNC (Chen et al., 2017), which
1007 occurs due to the increase in the water content (Fig. 17) and the delay in the rain formation to
1008 higher levels (Heikenfeld et al., 2019), even without a large change in the vertical velocity or
1009 cloud fraction at this level (Fig. 17)~~due to the increase in the water content (Fig. 17) and the delay~~
1010 ~~in the rain formation to higher levels (Heikenfeld et al., 2019)~~. Similar to the shallow-cloud
1011 dominated case (Fig. 8), the near surface temperature monotonically increases with CDNC, while
1012 the effect on the mean rain rate is small.

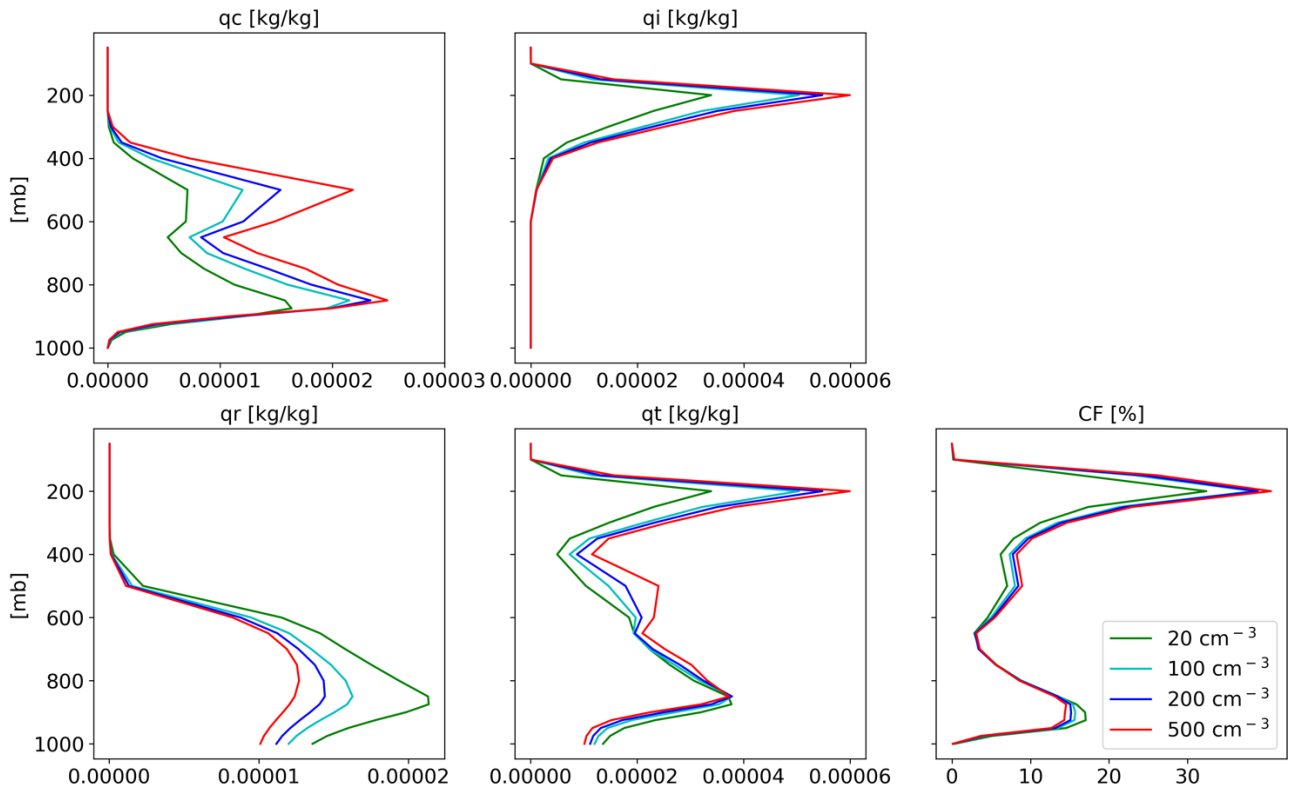
1013 The differences in the thermodynamic evolution between polluted and clean conditions for this
1014 case (Fig. 18), demonstrate the same trend as in the shallow-cloud dominated case (Fig. 10).
1015 Here again, we note an increase in the humidity at the mid and upper troposphere, that contribute

1016 to the reduction in the outgoing LW flux. The deepening, drying and warming of the boundary
 1017 layer are observed in this case as well. Both the increase in humidity at the mid-upper troposphere
 1018 and the deepening of the boundary layer (Seifert et al., 2015) could cause a reduction of the
 1019 outgoing LW flux. To distinguished the effect of clouds and humidity at the different levels on
 1020 the outgoing LW flux, we have conducted sensitivity off-line radiative transfer calculations using
 1021 BUGSrad. As in the shallow-cloud dominated case, the difference in outgoing LW flux between
 1022 clean and polluted conditions primarily emerges from the CDNC effect on clouds. The small
 1023 remaining effect of the clear sky ($\sim 0.2 \text{ W/m}^2$) is contributed by the change in the humidity at the
 1024 mid and upper troposphere rather than by the deepening of the boundary layer (which would lead
 1025 to LW emission from lower temperatures and is expected to be more significant under lower free
 1026 troposphere humidity conditions).

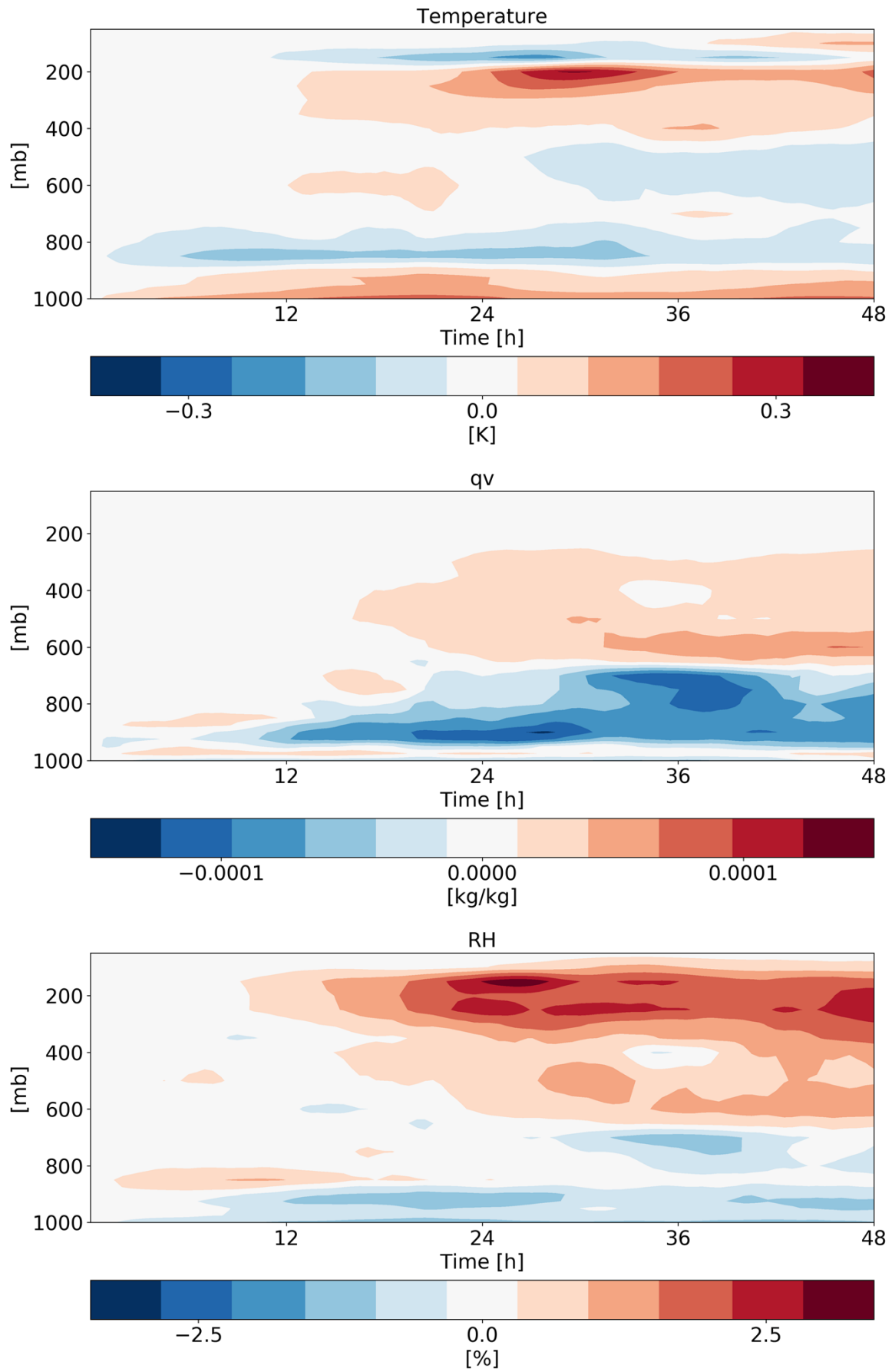


1027
 1028 **Figure 16. Domain average properties as a function of time for the different CDNC simulations for the deep-**
 1029 **cloud dominated case. The properties that are presented here are: cloud fraction (CF), rain rate, temperature**
 1030 **in 2 m, liquid water path (LWP – based on the cloud water mass, excluding the rain mass for consistency**
 1031 **with satellite observations), ice water path (IWP) and total water path (TPW = LWP + IWP). For each**
 1032 **property, the mean difference between all combinations of simulations, normalized to a factor 5 increase in**
 1033 **CDNC, and its standard deviation appear in parenthesis.**

1034



1035
 1036 **Figure 17. Domain and time average vertical profiles for the different CDNC simulations for the shallow-**
 1037 **cloud dominated case. The properties that are presented here are: cloud droplet mass mixing ratio (q_c – for**
 1038 **clouds’ droplets with radius smaller than $40\ \mu\text{m}$), ice mass mixing ratio (q_i), rain mass mixing ratio (q_r - for**
 1039 **clouds’ drops with radius larger than $40\ \mu\text{m}$), total water mass mixing ratio ($q_t = q_c + q_i + q_r$), and cloud**
 1040 **fraction (CF).**

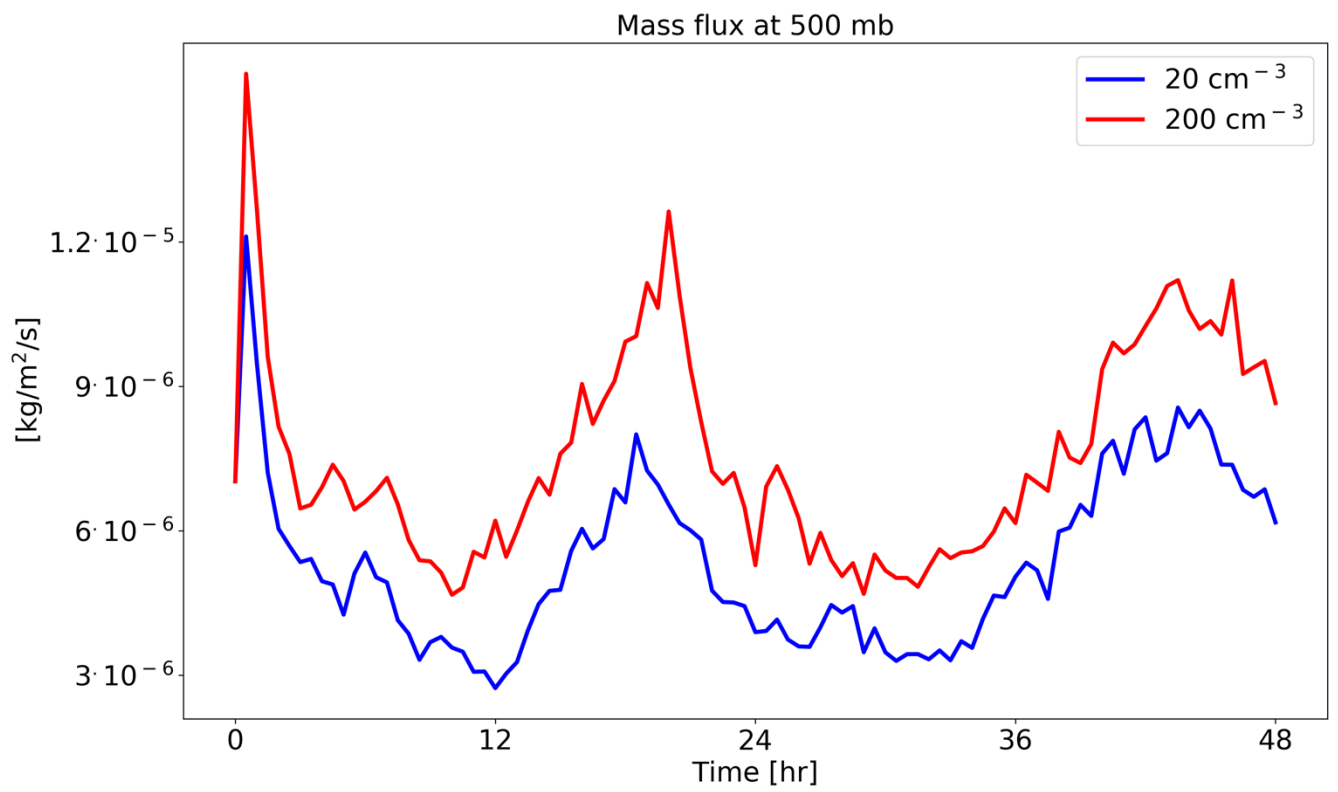
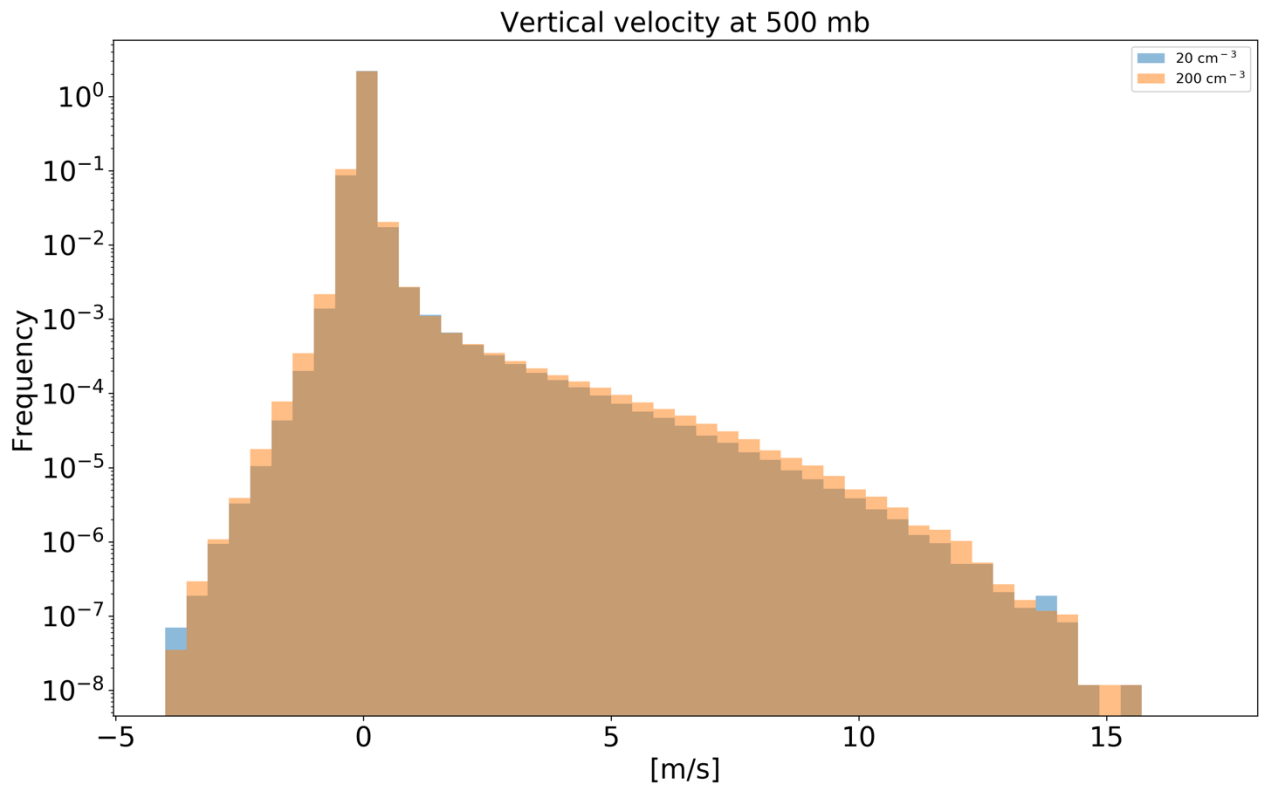


1041
1042

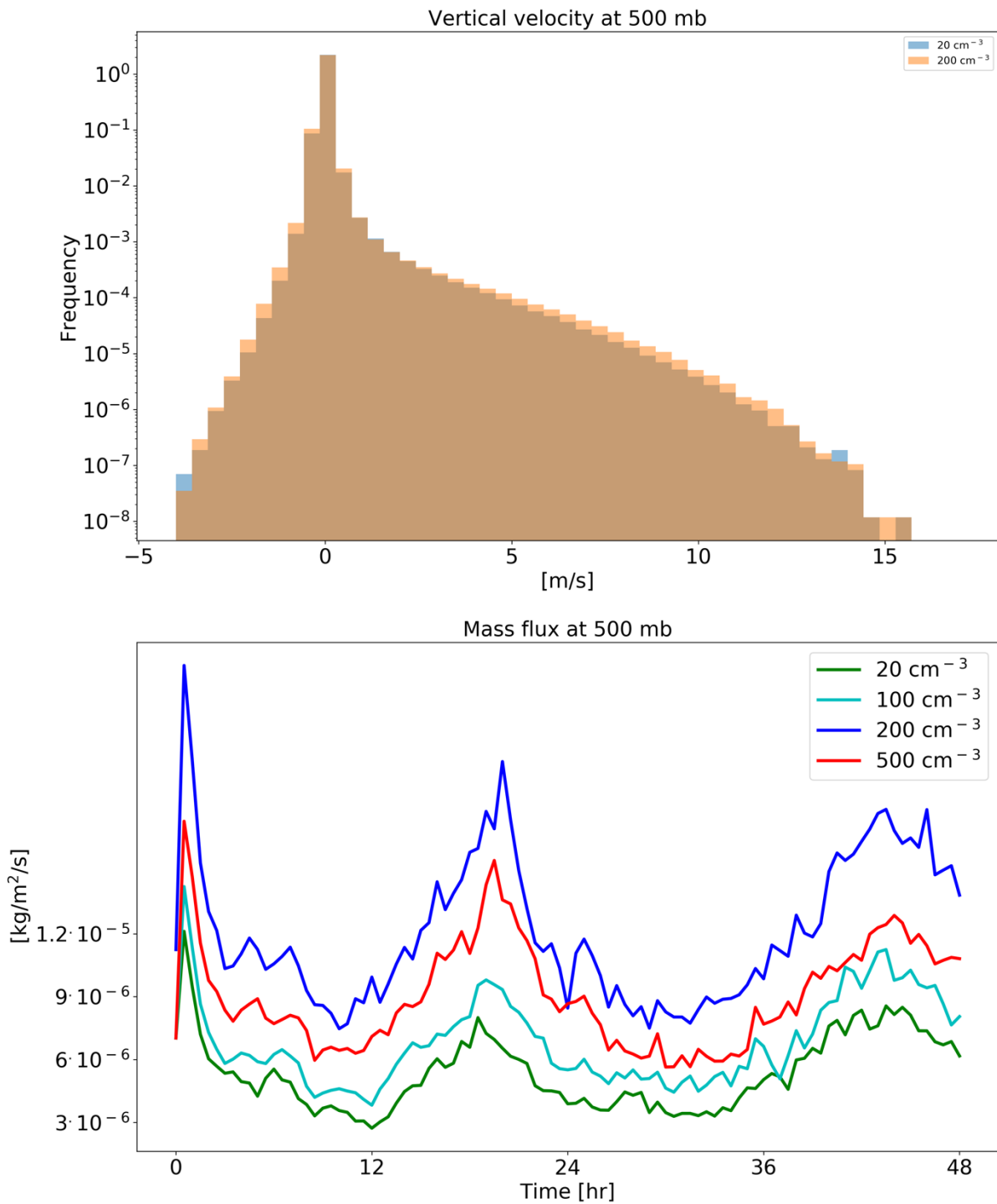
Figure 18. [Time-height Hovmöller](#) diagrams of the differences in the domain mean temperature, specific

1043 **humidity (q_v) and relative humidity (RH) vertical profiles between polluted ($CDNC = 200 \text{ cm}^{-3}$) and clean**
1044 **($CDNC = 20 \text{ cm}^{-3}$) simulations for the deep-cloud dominated case (16-18/08/2016).**

1045



1046



1047

1048 **Figure 19.- histograms of ICON simulated vertical velocity at the level of 500 mb for a clean (20 cm^{-3}) and polluted (200 cm^{-3}) simulations (upper), and the time evolution of the net upwards water (liquid and ice) mass flux (lower) for the different CDNC simulations for the deep-cloud dominated case (16-18/08/2016). The 500 mb level is chosen as it represents the transition between the warm part to the cold part of the clouds. In the histogram only two simulations are presented for clarity, histograms of ICON simulated vertical velocity at the level of 500 mb (upper), and the time evolution of the net upwards water (liquid and ice) mass flux (lower) for a clean (20 cm^{-3}) and polluted (200 cm^{-3}) simulations for the deep-**

1055 ~~cloud dominated case (16-18/08/2016). The 500 mb level is chosen as it represents the transition between the~~
1056 ~~warm part to the cold part of the clouds.~~

1057

1058 **Summary and conclusions**

1059 Two different case studies of tropical cloud systems over the Atlantic Ocean were simulated
1060 using the ICON numerical model in a cloud resolving configuration with 1.2 km resolution and
1061 a relatively large domain ($\sim 22^\circ \times 11^\circ$). The cases represent dates from the NARVAL 2 field
1062 campaign that took place during August 2016 and have different dominant cloud types and
1063 different dominating terms in their energy budget. The first case (10-12/8/2016) is shallow-cloud
1064 dominated and hence dominated by radiative cooling, while the second case (16-18/8/2016) is
1065 dominated by deep convective clouds and hence dominated by precipitation warming. The main
1066 objective of this study is to analyse the response of the atmospheric energy budget to changes in
1067 cloud droplet number concentration (CDNC), which serve as a proxy for (or idealized
1068 representation of) changes in aerosol concentration. This enables better understanding of the
1069 processes acting in global-scale studies trying to constrain aerosol effect on precipitation changes
1070 using the energy budget perspective (O’Gorman et al., 2012; Muller and O’Gorman, 2011;
1071 Hodnebrog et al., 2016; Samset et al., 2016; Myhre et al., 2017; Liu et al., 2018; Richardson et
1072 al., 2018; Dagan et al., 2019a). Our results demonstrate that regional atmospheric energy budgets
1073 can be significantly perturbed by changes in CDNC and that the magnitude of the effect is cloud
1074 regime dependent (even for a given geographical region and given time of the year as the two
1075 cases are separated by less than a week).

1076 Figure 20 summarizes the energy and radiation response of the two simulated cases to CDNC
1077 perturbations. It shows that the atmosphere in the deep-cloud dominated case experiences a very
1078 strong atmospheric warming due to an increase in CDNC (10.0 W/m^2). Most of this warming is
1079 caused by a reduction in the outgoing LW radiation at the TOA. The SW radiative fluxes (both
1080 at the TOA and surface) is also significantly modified but their net effect on the atmospheric
1081 column energy budget is small. The net TOA radiative fluxes change in this case is -1.9 W/m^2 .
1082 Beside the atmospheric radiative warming, changes in precipitation ($\sim -0.3 \text{ W/m}^2$), and in sensible
1083 heat flux (Q_{SH} , -1.4 W/m^2) also contribute to the total trend as a response of increase in CDNC.
1084 We note that since 1 mm/hr of rain is equivalent to 628 W/m^2 , even negligible changes in
1085 precipitation of less than 0.5 mm over 48 hr (as seen in our simulations) can still appear as
1086 significant changes in the atmospheric energy budget and contribute a few W/m^2 .

1087 The response of the radiative fluxes can be explained by the changes in the mean cloud and
1088 thermodynamic properties in the domain. The mean cloud fraction (CF) increases with the
1089 increase in CDNC (Fig. 16) while the vertical structure of it indicates a reduction in the low
1090 cloud fraction (below 800 mb) and an increase in the mid and upper troposphere CF (Fig. 17).
1091 The water content (both liquid and ice) also increase with the increase in CDNC (Figs. 16 and
1092 17) with increasing amount with height. These changes in the mean cloud properties drive both
1093 the reduction in SW fluxes at TOA and surface and LW flux at TOA as the clouds become more
1094 opaque (Koren et al., 2010; Storelvmo et al., 2011) and cover a larger fraction of the sky. In
1095 addition to cloud responses, the domain-mean thermodynamic conditions change as well (Fig.
1096 18). Specifically, the humidity content at the mid and upper troposphere increases with higher
1097 CDNC, (due to increase mass flux to the upper troposphere) which further decreases the outgoing
1098 LW flux at the TOA. However, the vast majority of the LW effect emerges from the changes in
1099 clouds.

1100 Both the increase in water vapor and ice content ~~inat~~ the upper troposphere are driven by an
1101 increase in water mass flux with increasing CDNC to these levels (Fig. 19, (Koren et al., 2005;
1102 Rosenfeld et al., 2008; Altaratz et al., 2014; Chen et al., 2017)), which is caused mostly by the
1103 increase in the water mixing ratio ~~inat~~ the mid-troposphere rather than by increase in vertical
1104 velocity (Figs. ~~11 and~~ 19) or in cloud fraction (Fig. 17). The ice content ~~inat~~ the upper
1105 troposphere is also increased due to reduction in the ice falling speed (Grabowski and Morrison,
1106 2016), while the increased relative humidity at these levels, further increases the ice particle
1107 lifetime due to slower evaporation. However, the increase in water mass flux to the upper layers
1108 is not accompanied with an increase in precipitation as predicted by the classical “invigoration”
1109 paradigm (Altaratz et al., 2014; Rosenfeld et al., 2008), which suggest that some compensating
1110 mechanisms are operating (Stevens and Feingold, 2009).

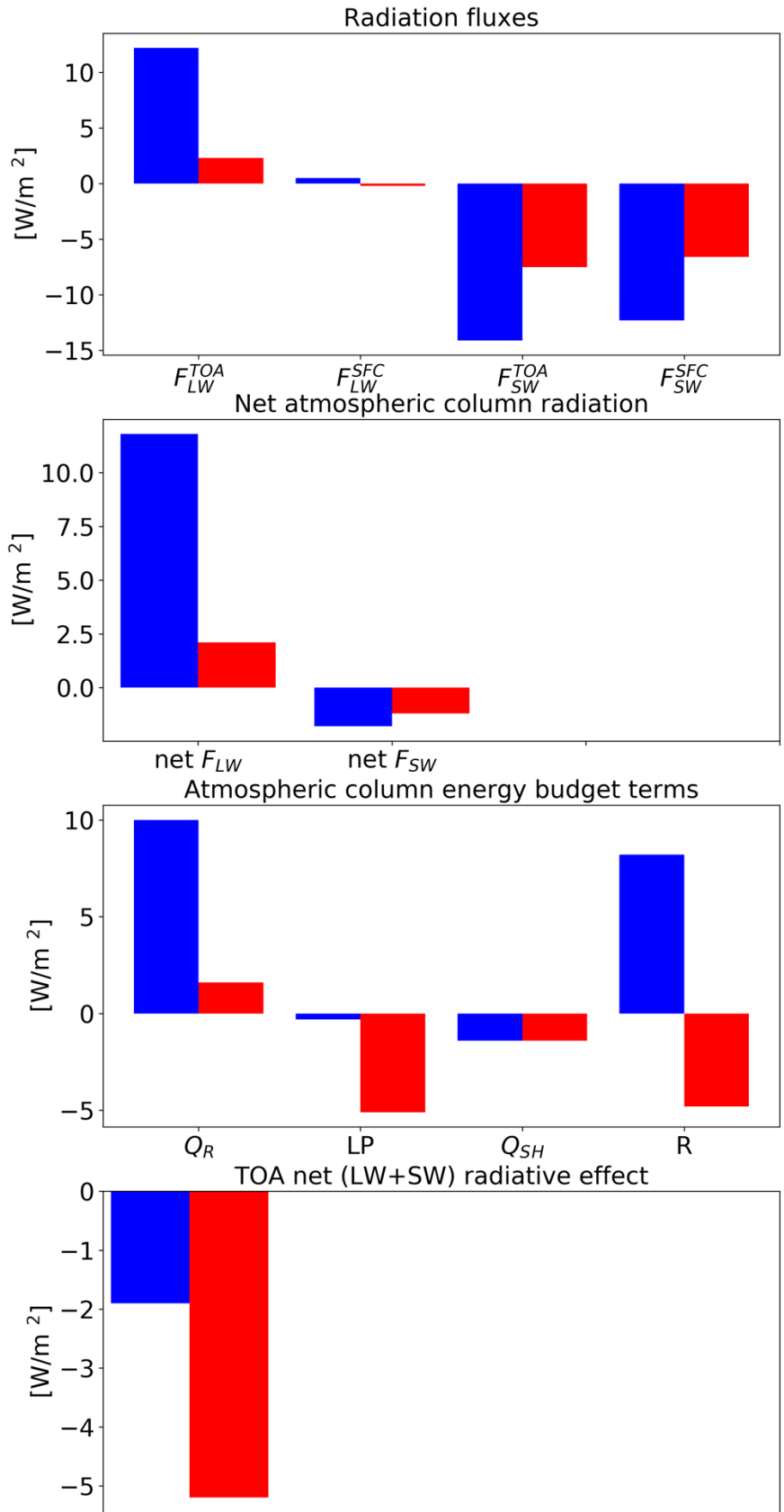
1111 In the shallow-cloud dominated case (which also contains a significant amount of deep
1112 convection), the response of Q_R is weaker but still substantial (a total decrease in the atmospheric
1113 radiative cooling of 1.6 W/m^2 - Fig. 20). The weaker total response under the shallow-cloud
1114 dominated conditions is due to the smaller role of the ice part in this case. Here again, the changes
1115 in Q_{SH} decrease about -1.4 W/m^2 of this atmospheric warming. As in the deep-cloud dominated
1116 case, most of the atmospheric radiative warming is caused by reduction in the outgoing LW flux,
1117 while the surface and TOA SW fluxes changes are non-negligible but cancel each other out (in
1118 terms of the atmospheric energy budget – reflecting small SW atmospheric absorption changes).
1119 However, a significant TOA net (SW+LW) radiative flux change of $\sim -5.2 \text{ W/m}^2$ remains. In this

1120 case, the cloud-mean effect on radiation is more complicated. While CF decreases with
1121 increasing CDNC, the mean water path (both LWP and IWP) increases (Fig. 8). As in the deep-
1122 cloud dominated case, the increase in the water content occurs mostly at the mid and upper
1123 troposphere, while the decrease in CF occurs mostly in the lower troposphere (Fig. 9). In terms
1124 of the SW fluxes, the effect of the decrease in low CF (decrease SW reflections) and the increase
1125 in water mass (increase SW reflections) would partially compensate, while the Twomey effect
1126 (Twomey, 1977) adds to the increase SW reflections. In this case, the net effect is more SW
1127 reflected back to space at TOA and a net negative flux change (including also the LW).

1128 There exists a large spread in estimates of aerosol effects on clouds for different cloud types and
1129 different environmental conditions. In this study, as we use a relatively large domain ($22^\circ \times 11^\circ$)
1130 and two different dates (each for two days), we sample many different local environmental
1131 conditions and cloud types. Such more realistic setups (although with lower spatial resolution)
1132 could provide more reliable estimates of aerosol effects on heterogeneous cloud systems than
1133 just one-cloud-type, small domain simulations (as was done in many previous studies, e.g (Dagan
1134 et al., 2017; Seifert et al., 2015; Ovchinnikov et al., 2014)). [However, the conclusions](#)
1135 [demonstrated here are based on two specific cases. In order to examine the validity of our main](#)
1136 [conclusions over a wider range of initial conditions, we have conducted a large ensemble of](#)
1137 [simulations starting from realistic initial conditions \(although with a smaller domain\) in a](#)
1138 [companion paper \(Dagan and Stier, 2019\). These simulations demonstrate that the main](#)
1139 [conclusions presented in this paper are robust and hold also for a wide range of initial conditions](#)
1140 [representative for this area.](#) In addition, the realistic setup with the continuously changing
1141 boundary conditions and systems that pass through the domain, [which are used here](#), prevent
1142 conclusions that might be valid only in cyclic double periodic large eddy simulations, as the
1143 background meteorological conditions change more realistically (Dagan et al., 2018b). Another
1144 uncertainty in the assessment of the aerosol response are the large differences between different
1145 models and microphysical schemes (White et al., 2017; Fan et al., 2016; Khain et al., 2015;
1146 Heikenfeld et al., 2019). In this study, as we use only one model, we do not address this
1147 uncertainty. In future work we intend to examine the response in multiple models. In addition,
1148 more detailed observational constraints on the models are needed. Furthermore, we do not
1149 include [the](#) temporal evolution of the aerosol concentration. Feedbacks between the aerosol
1150 concentration and clouds processes (such as wet scavenging), [as well as the direct effects of](#)
1151 [aerosol on radiation](#) would add another layer of complexity that should be accounted for in future
1152 work.

1153 Generally, the global mean aerosol radiative forcing is estimated to be negative (Boucher et al.,
1154 2013; Bellouin et al., 2019). However, these global aerosol forcing estimates have so far not
1155 included the radiative forcing associated with potential effects of aerosols on deep convection –
1156 and these effects are not represented in most current climate models due to limitations in
1157 convection parameterisations, with only a few exceptions (Kipling et al., 2017; Labbouz et al.,
1158 2018). Here we demonstrate the existence of non-negligible aerosol radiative effects (of -5.2 and
1159 -1.9 W/m² for the shallow and deep cloud dominated cases, respectively) in tropical cloud
1160 systems, that contained both deep and shallow convective clouds, with significant SW and LW
1161 contributions. From the (limited) two cases simulated here, it appears that (in agreement with
1162 previous studies) the aerosol effect may be regime dependent and that even within a given cloud
1163 regime the effect may vary with the meteorological conditions.

1164 Finally, we hypothesise that the aerosol impact shown on the atmospheric energy balance, with
1165 increasing divergence of dry static energy from deep convective regions concomitantly with
1166 increased convergence in shallow clouds regions, can have effects on the large-scale circulation.
1167 This should be investigated in future work.



1168

1169 **Figure 20. Summary of the radiation and energy response to CDNC perturbation in the two different cases.**

1170 **Blue represent the deep-cloud dominated case while red the shallow-cloud dominated case.**

1171 **Author contributions.** G. D. carried out the simulations and analyses presented. G.C., D.K. and
1172 A.S. assisted with the simulations. M.C. assisted with the radiative transfer calculations and
1173 comparison with observations. P. S. and A.S. assisted with the design and interpretation of the
1174 analyses. G. D. prepared the manuscript with contributions from all co-authors.

1175 **Acknowledgements:**

1176 This research was supported by the European Research Council (ERC) project constRaining
1177 the EffeCts of Aerosols on Precipitation (RECAP) under the European Union's Horizon 2020
1178 research and innovation programme with grant agreement No 724602. The simulations were
1179 performed using the ARCHER UK National Supercomputing Service. ECMWF is
1180 acknowledged for providing Era-interim data set (<https://apps.ecmwf.int/datasets/>). We
1181 acknowledge MPI, DWD and DKRZ for the NARVAL simulations. [The data presented in the](https://zenodo.org/record/3611366#.Xi7rHC-cbUI)
1182 [paper can be find in: https://zenodo.org/record/3611366#.Xi7rHC-cbUI](https://zenodo.org/record/3611366#.Xi7rHC-cbUI)
1183 [DOI:10.5281/zenodo.3611366](https://doi.org/10.5281/zenodo.3611366)

1184

1185 **References**

1186 Albrecht, B. A.: Aerosols, cloud microphysics, and fractional cloudiness, *Science* (New York, NY), 245,
1187 1227, DOI: 10.1126/science.245.4923.1227, 1989.
1188 Albrecht, B. A.: Effects of precipitation on the thermodynamic structure of the trade wind boundary
1189 layer, *Journal of Geophysical Research: Atmospheres* (1984–2012), 98, 7327-7337,
1190 <https://doi.org/10.1029/93JD00027>, 1993.
1191 Altaratz, O., Koren, I., Remer, L., and Hirsch, E.: Review: Cloud invigoration by aerosols—Coupling
1192 between microphysics and dynamics, *Atmospheric Research*, 140, 38-60,
1193 <https://doi.org/10.1016/j.atmosres.2014.01.009>, 2014.
1194 Aminou, D.: MSG's SEVIRI instrument, *ESA Bulletin* (0376-4265), 15-17, 2002.
1195 Andreae, M. O., Rosenfeld, D., Artaxo, P., Costa, A. A., Frank, G. P., Longo, K. M., and Silva-Dias, M. A.
1196 F.: Smoking rain clouds over the Amazon, *Science*, 303, 1337-1342, 10.1126/science.1092779, 2004.
1197 Andreae, M. O.: Correlation between cloud condensation nuclei concentration and aerosol optical
1198 thickness in remote and polluted regions, *Atmospheric Chemistry and Physics*, 9.2, 543-556, 2009.
1199 Arakawa, A., and Schubert, W. H.: Interaction of a cumulus cloud ensemble with the large-scale
1200 environment, Part I, *Journal of the Atmospheric Sciences*, 31, 674-701, 1974.
1201 Bellouin, N., Quaas, J., Gryspeerdt, E., Kinne, S., Stier, P., Watson-Parris, D., Boucher, O., Carslaw, K.,
1202 Christensen, M., and Daniau, A.-L.: Bounding aerosol radiative forcing of climate change, *Reviews of*
1203 *Geophysics*, <http://hdl.handle.net/21.11116/0000-0003-9D8D-E>, 2019.
1204 Boucher, O., Randall, D., Artaxo, P., Bretherton, C., Feingold, G., Forster, P., Kerminen, V., Kondo, Y.,
1205 Liao, H., and Lohmann, U.: Clouds and aerosols, *Climate Change*, 571-657, 2013.
1206 Chen, Q., Koren, I., Altaratz, O., Heiblum, R. H., Dagan, G., and Pinto, L.: How do changes in warm-
1207 phase microphysics affect deep convective clouds?, *Atmospheric Chemistry and Physics*, 17, 9585-
1208 9598, <https://doi.org/10.5194/acp-17-9585-2017>, 2017.

1209 Christensen, M. W., Chen, Y. C., and Stephens, G. L.: Aerosol indirect effect dictated by liquid clouds,
1210 Journal of Geophysical Research: Atmospheres, 121, <https://doi.org/10.1002/2016JD025245>, 2016.
1211 Clough, S., Shephard, M., Mlawer, E., Delamere, J., Iacono, M., Cady-Pereira, K., Boukabara, S., and
1212 Brown, P.: Atmospheric radiative transfer modeling: a summary of the AER codes, Journal of
1213 Quantitative Spectroscopy and Radiative Transfer, 91, 233-244,
1214 <https://doi.org/10.1016/j.jqsrt.2004.05.058>, 2005.
1215 Costantino, L., and Bréon, F.-M.: Aerosol indirect effect on warm clouds over South-East Atlantic,
1216 from co-located MODIS and CALIPSO observations, Atmospheric Chemistry and Physics, 13, 69-88,
1217 2013.
1218 Dagan, G., Koren, I., and Altaratz, O.: Aerosol effects on the timing of warm rain processes,
1219 Geophysical Research Letters, 42, 4590-4598, [10.1002/2015GL063839](https://doi.org/10.1002/2015GL063839), 2015a.
1220 Dagan, G., Koren, I., and Altaratz, O.: Competition between core and periphery-based processes in
1221 warm convective clouds—from invigoration to suppression, Atmospheric Chemistry and Physics, 15,
1222 2749-2760, <https://doi.org/10.5194/acp-15-2749-2015>, 2015b.
1223 Dagan, G., and Chemke, R.: The effect of subtropical aerosol loading on equatorial precipitation,
1224 Geophysical Research Letters, 43, <https://doi.org/10.1002/2016GL071206>, 2016.
1225 Dagan, G., Koren, I., Altaratz, O., and Heiblum, R. H.: Aerosol effect on the evolution of the
1226 thermodynamic properties of warm convective cloud fields, Scientific Reports, 6, 38769, DOI:
1227 [10.1038/srep38769](https://doi.org/10.1038/srep38769), 2016.
1228 Dagan, G., Koren, I., Altaratz, O., and Heiblum, R. H.: Time-dependent, non-monotonic response of
1229 warm convective cloud fields to changes in aerosol loading, Atmos. Chem. Phys., 17, 7435-7444,
1230 [10.5194/acp-17-7435-2017](https://doi.org/10.5194/acp-17-7435-2017), 2017.
1231 Dagan, G., Koren, I., and Altaratz, O.: Quantifying the effect of aerosol on vertical velocity and
1232 effective terminal velocity in warm convective clouds, Atmospheric Chemistry and Physics, 18, 6761-
1233 6769, <https://doi.org/10.5194/acp-18-6761-2018>, 2018a.
1234 Dagan, G., Koren, I., Altaratz, O., and Lehahn, Y.: Shallow convective cloud field lifetime as a key
1235 factor for evaluating aerosol effects, iScience, 10, 192-202,
1236 <https://doi.org/10.1016/j.isci.2018.11.032>, 2018b.
1237 Dagan, G., Koren, I., Kostinski, A., and Altaratz, O.: Organization and oscillations in simulated shallow
1238 convective clouds, Journal of Advances in Modeling Earth Systems,
1239 <https://doi.org/10.1029/2018MS001416>, 2018c.
1240 Dagan, G., Stier, P., and Watson-Parris, D.: Contrasting response of precipitation to aerosol
1241 perturbation in the tropics and extra-tropics explained by energy budget considerations, Geophysical
1242 Research Letters, <https://doi.org/10.1029/2019GL083479>, 2019a.
1243 Dagan, G., Stier, P., and Watson-Parris, D.: Analysis of the atmospheric water budget for elucidating
1244 the spatial scale of precipitation changes under climate change, Geophysical Research Letters,
1245 <https://doi.org/10.1029/2019GL084173>, 2019b
1246 [Dagan, G. and Stier, P.: Ensemble daily simulations for elucidating cloud–aerosol interactions under a](https://doi.org/10.5194/acp-2019-949)
1247 [large spread of realistic environmental conditions, Atmos. Chem. Phys. Discuss.,](https://doi.org/10.5194/acp-2019-949)
1248 <https://doi.org/10.5194/acp-2019-949>, in review, 2019.
1249 Dee, D., Uppala, S., Simmons, A., Berrisford, P., Poli, P., Kobayashi, S., Andrae, U., Balmaseda, M.,
1250 Balsamo, G., and Bauer, P.: The ERA-Interim reanalysis: Configuration and performance of the data
1251 assimilation system, Quarterly Journal of the royal meteorological society, 137, 553-597,
1252 <https://doi.org/10.1002/qj.828>, 2011.

1253 Dey, S., Di Girolamo, L., Zhao, G., Jones, A. L., and McFarquhar, G. M.: Satellite-observed
1254 relationships between aerosol and trade-wind cumulus cloud properties over the Indian Ocean,
1255 *Geophysical Research Letters*, 38, <https://doi.org/10.1029/2010GL045588>, 2011.

1256 Emanuel, K. A., Neelin, J. D., and Bretherton, C. S.: On large-scale circulations in convecting
1257 atmospheres, *Quarterly Journal of the Royal Meteorological Society*, 120, 1111-1143, 1994.

1258 Fan, J., Zhang, R., Li, G., and Tao, W.-K.: Effects of aerosols and relative humidity on cumulus clouds,
1259 *Journal of Geophysical Research-Atmospheres*, 112, 10.1029/2006jd008136, 2007.

1260 Fan, J., Yuan, T., Comstock, J. M., Ghan, S., Khain, A., Leung, L. R., Li, Z., Martins, V. J., and
1261 Ovchinnikov, M.: Dominant role by vertical wind shear in regulating aerosol effects on deep
1262 convective clouds, *Journal of Geophysical Research-Atmospheres*, 114, 10.1029/2009jd012352,
1263 2009.

1264 Fan, J., Comstock, J. M., and Ovchinnikov, M.: The cloud condensation nuclei and ice nuclei effects
1265 on tropical anvil characteristics and water vapor of the tropical tropopause layer, *Environmental*
1266 *Research Letters*, 5, 10.1088/1748-9326/5/4/044005, 2010.

1267 Fan, J., Leung, L. R., Rosenfeld, D., Chen, Q., Li, Z., Zhang, J., and Yan, H.: Microphysical effects
1268 determine macrophysical response for aerosol impacts on deep convective clouds, *Proceedings of*
1269 *the National Academy of Sciences*, 110, E4581-E4590, <https://doi.org/10.1073/pnas.1316830110>,
1270 2013.

1271 Fan, J., Wang, Y., Rosenfeld, D., and Liu, X.: Review of aerosol–cloud interactions: Mechanisms,
1272 significance, and challenges, *Journal of the Atmospheric Sciences*, 73, 4221-4252,
1273 <https://doi.org/10.1175/JAS-D-16-0037.1>, 2016.

1274 Ghan, S. J., Abdul-Razzak, H., Nenes, A., Ming, Y., Liu, X., Ovchinnikov, M., Shipway, B., Meskhidze,
1275 N., Xu, J., and Shi, X.: Droplet nucleation: Physically-based parameterizations and comparative
1276 evaluation, *Journal of Advances in Modeling Earth Systems*, 3,
1277 <https://doi.org/10.1029/2011MS000074>, 2011.

1278 Glassmeier, F., and Lohmann, U.: Constraining precipitation susceptibility of warm-, ice-, and mixed-
1279 phase clouds with microphysical equations, *Journal of the Atmospheric Sciences*, 73, 5003-5023,
1280 <https://doi.org/10.1175/JAS-D-16-0008.1>, 2016.

1281 Goren, T., and Rosenfeld, D.: Decomposing aerosol cloud radiative effects into cloud cover, liquid
1282 water path and Twomey components in marine stratocumulus, *Atmospheric research*, 138, 378-393,
1283 <https://doi.org/10.1016/j.atmosres.2013.12.008>, 2014.

1284 Grabowski, W. W., and Morrison, H.: Untangling microphysical impacts on deep convection applying
1285 a novel modeling methodology. Part II: Double-moment microphysics, *Journal of the Atmospheric*
1286 *Sciences*, 73, 3749-3770, <https://doi.org/10.1175/JAS-D-15-0367.1>, 2016.

1287 Gryspeerdt, E., and Stier, P.: Regime-based analysis of aerosol-cloud interactions, *Geophysical*
1288 *Research Letters*, 39, <https://doi.org/10.1029/2012GL053221>, 2012.

1289 Gryspeerdt, E., Stier, P., White, B., and Kipling, Z.: Wet scavenging limits the detection of aerosol
1290 effects on precipitation, *Atmospheric Chemistry and Physics*, 15, 7557-7570,
1291 <https://doi.org/10.5194/acp-15-7557-2015>, 2015.

1292 Gryspeerdt, E., Sourdeval, O., Quaas, J., Delanoë, J., Krämer, M., and Kühne, P.: Ice crystal number
1293 concentration estimates from lidar–radar satellite remote sensing–Part 2: Controls on the ice crystal
1294 number concentration, *Atmospheric Chemistry and Physics*, 18, 14351-14370,
1295 <https://doi.org/10.5194/acp-18-14351-2018>, 2018b.

1296 Gryspeerd, E., Goren, T., Sourdeval, O., Quaas, J., Mülmenstädt, J., Dipu, S., Unglaub, C., Gettelman,
1297 A., and Christensen, M.: Constraining the aerosol influence on cloud liquid water path, *Atmospheric*
1298 *Chemistry and Physics*, 19, 5331-5347, <https://doi.org/10.5194/acp-19-5331-2019>, 2019.

1299 Heikenfeld, M., White, B., Labbouz, L., and Stier, P.: Aerosol effects on deep convection: the
1300 propagation of aerosol perturbations through convective cloud microphysics, *Atmospheric*
1301 *Chemistry and Physics*, 19, 2601-2627, <https://doi.org/10.5194/acp-19-2601-2019>, 2019.

1302 Henderson, D. S., L'Ecuyer, T., Stephens, G., Partain, P., and Sekiguchi, M.: A Multisensor Perspective
1303 on the Radiative Impacts of Clouds and Aerosols, *J. Appl. Meteorol. Clim.*, 52, 853– 871,
1304 <https://doi.org/10.1175/JAMC-D-12-025.1>, 2013.

1305 Hodnebrog, O., Myhre, G., Forster, P. M., Sillmann, J., and Samset, B. H.: Local biomass burning is a
1306 dominant cause of the observed precipitation reduction in southern Africa, *Nat Commun*, 7,
1307 10.1038/ncomms11236, 2016.

1308 Hoose, C., and Möhler, O.: Heterogeneous ice nucleation on atmospheric aerosols: a review of
1309 results from laboratory experiments, *Atmospheric Chemistry and Physics*, 12, 9817–9854. 2012.

1310 Iacono, M. J., Delamere, J. S., Mlawer, E. J., Shephard, M. W., Clough, S. A., and Collins, W. D.:
1311 Radiative forcing by long-lived greenhouse gases: Calculations with the AER radiative transfer
1312 models, *Journal of Geophysical Research: Atmospheres*, 113,
1313 <https://doi.org/10.1029/2008JD009944>, 2008.

1314 Jakob, C., Singh, M., and Jungandreas, L.: Radiative Convective Equilibrium and Organized
1315 Convection: An Observational Perspective, *Journal of Geophysical Research: Atmospheres*, 124,
1316 5418-5430, 2019.

1317 Jeon, Y.-L., Moon, S., Lee, H., Baik, J.-J., and Lkhamjav, J.: Non-Monotonic Dependencies of Cloud
1318 Microphysics and Precipitation on Aerosol Loading in Deep Convective Clouds: A Case Study Using
1319 the WRF Model with Bin Microphysics, *Atmosphere*, 9, 434, <https://doi.org/10.3390/atmos9110434>,
1320 2018.

1321 Jiang, H., Xue, H., Teller, A., Feingold, G., and Levin, Z.: Aerosol effects on the lifetime of shallow
1322 cumulus, *Geophysical Research Letters*, 33, 10.1029/2006gl026024, 2006.

1323 Jiang, J. H., Su, H., Huang, L., Wang, Y., Massie, S., Zhao, B., Omar, A., and Wang, Z.: Contrasting
1324 effects on deep convective clouds by different types of aerosols, *Nature communications*, 9, 3874,
1325 2018.

1326 Kalina, E. A., Friedrich, K., Morrison, H., and Bryan, G. H.: Aerosol effects on idealized supercell
1327 thunderstorms in different environments, *Journal of the Atmospheric Sciences*, 71, 4558-4580,
1328 <https://doi.org/10.1175/JAS-D-14-0037.1>, 2014.

1329 Kaufman, Y. J., Koren, I., Remer, L. A., Rosenfeld, D., and Rudich, Y.: The effect of smoke, dust, and
1330 pollution aerosol on shallow cloud development over the Atlantic Ocean, *Proceedings of the*
1331 *National Academy of Sciences of the United States of America*, 102, 11207-11212,
1332 10.1073/pnas.0505191102, 2005.

1333 Khain, A., Rosenfeld, D., and Pokrovsky, A.: Aerosol impact on the dynamics and microphysics of
1334 deep convective clouds, *Quarterly Journal of the Royal Meteorological Society*, 131, 2639-2663,
1335 10.1256/qj.04.62, 2005.

1336 Khain, A., Beheng, K., Heymsfield, A., Korolev, A., Krichak, S., Levin, Z., Pinsky, M., Phillips, V.,
1337 Prabhakaran, T., and Teller, A.: Representation of microphysical processes in cloud-resolving models:
1338 spectral (bin) microphysics vs. bulk parameterization, *Reviews of Geophysics*,
1339 <https://doi.org/10.1002/2014RG000468>, 2015.

1340 Khain, A. P., BenMoshe, N., and Pokrovsky, A.: Factors determining the impact of aerosols on surface
1341 precipitation from clouds: An attempt at classification, *Journal of the Atmospheric Sciences*, 65,
1342 1721-1748, 10.1175/2007jas2515.1, 2008.

1343 Khain, A. P.: Notes on state-of-the-art investigations of aerosol effects on precipitation: a critical
1344 review, *Environmental Research Letters*, 4, 015004 (015020 pp.)-015004 (015020 pp.),
1345 10.1088/1748-9326/4/1/015004, 2009.

1346 Kipling, Z., Stier, P., Labbouz, L., and Wagner, T.: Dynamic subgrid heterogeneity of convective cloud
1347 in a global model: description and evaluation of the Convective Cloud Field Model (CCFM) in
1348 ECHAM6–HAM2, *Atmospheric Chemistry and Physics*, 17, 327-342, [https://doi.org/10.5194/acp-17-](https://doi.org/10.5194/acp-17-327-2017)
1349 [327-2017](https://doi.org/10.5194/acp-17-327-2017), 2017.

1350 Klepp, C., Ament, F., Bakan, S., Hirsch, L., and Stevens, B.: The NARVAL Campaign Report, 2014.

1351 Klocke, D., Brueck, M., Hohenegger, C., and Stevens, B.: Rediscovery of the doldrums in storm-
1352 resolving simulations over the tropical Atlantic, *Nature Geoscience*, 10, 891, 2017.

1353 Koren, I., Kaufman, Y. J., Rosenfeld, D., Remer, L. A., and Rudich, Y.: Aerosol invigoration and
1354 restructuring of Atlantic convective clouds, *Geophysical Research Letters*, 32,
1355 10.1029/2005gl023187, 2005.

1356 Koren, I., Remer, L. A., Altaratz, O., Martins, J. V., and Davidi, A.: Aerosol-induced changes of
1357 convective cloud anvils produce strong climate warming, *Atmospheric Chemistry and Physics*, 10,
1358 5001-5010, 10.5194/acp-10-5001-2010, 2010.

1359 Koren, I., Dagan, G., and Altaratz, O.: From aerosol-limited to invigoration of warm convective
1360 clouds, *science*, 344, 1143-1146, DOI: 10.1126/science.1252595, 2014.

1361 Koren, I., Altaratz, O., and Dagan, G.: Aerosol effect on the mobility of cloud droplets, *Environmental*
1362 *Research Letters*, 10, 104011, doi:10.1088/1748-9326/10/10/104011, 2015.

1363 Labbouz, L., Kipling, Z., Stier, P., and Protat, A.: How Well Can We Represent the Spectrum of
1364 Convective Clouds in a Climate Model? Comparisons between Internal Parameterization Variables
1365 and Radar Observations, *Journal of the Atmospheric Sciences*, 75, 1509-1524,
1366 <https://doi.org/10.1175/JAS-D-17-0191.1>, 2018.

1367 Lebo, Z. J., and Morrison, H.: Dynamical effects of aerosol perturbations on simulated idealized
1368 squall lines, *Monthly Weather Review*, 142, 991-1009, 2014.

1369 Lee, S.-S., Feingold, G., and Chuang, P. Y.: Effect of aerosol on cloud–environment interactions in
1370 trade cumulus, *Journal of the Atmospheric Sciences*, 69, 3607-3632, 2012.

1371 Lee, S. S., Donner, L. J., and Phillips, V. T. J.: Sensitivity of aerosol and cloud effects on radiation to
1372 cloud types: comparison between deep convective clouds and warm stratiform clouds over one-day
1373 period, *Atmospheric Chemistry and Physics*, 9, 2555-2575, 2009.

1374 Levin, Z., and Cotton, W. R.: *Aerosol pollution impact on precipitation: A scientific review*, Springer,
1375 2009.

1376 Liu, H., Guo, J., Koren, I., Altaratz, O., Dagan, G., Wang, Y., Jiang, J. H., Zhai, P., and Yung, Y. L.: Non-
1377 Monotonic Aerosol Effect on Precipitation in Convective Clouds over Tropical Oceans, *Scientific*
1378 *Reports*, 9, 7809, 2019.

1379 Liu, L., Shawki, D., Voulgarakis, A., Kasoar, M., Samset, B., Myhre, G., Forster, P., Hodnebrog, Ø.,
1380 Sillmann, J., and Aalbergsjø, S.: A PDRMIP Multimodel Study on the impacts of regional aerosol
1381 forcings on global and regional precipitation, *Journal of Climate*, 31, 4429-4447, 2018.

1382 Lohmann, U., and Hoose, C.: Sensitivity studies of different aerosol indirect effects in mixed-phase
1383 clouds, *Atmospheric Chemistry and Physics*, 9, 8917-8934, 2009.

1384 Manabe, S., and Strickler, R. F.: Thermal equilibrium of the atmosphere with a convective
1385 adjustment, *Journal of the Atmospheric Sciences*, 21, 361-385, 1964

1386 Mlawer, E. J., Taubman, S. J., Brown, P. D., Iacono, M. J., and Clough, S. A.: Radiative transfer for
1387 inhomogeneous atmospheres: RRTM, a validated correlated-k model for the longwave, *Journal of*
1388 *Geophysical Research: Atmospheres*, 102, 16663-16682, 1997.

1389 Muller, C., and O’Gorman, P.: An energetic perspective on the regional response of precipitation to
1390 climate change, *Nature Climate Change*, 1, 266, 2011.

1391 Mülmenstädt, J., and Feingold, G.: The Radiative Forcing of Aerosol–Cloud Interactions in Liquid
1392 Clouds: Wrestling and Embracing Uncertainty, *Current Climate Change Reports*, 4, 23-40,
1393 <https://doi.org/10.1007/s40641-018-0089-y>, 2018.

1394 Myhre, G., Forster, P., Samset, B., Hodnebrog, Ø., Sillmann, J., Aalbergsjø, S., Andrews, T., Boucher,
1395 O., Faluvegi, G., and Fläschner, D.: PDRMIP: a precipitation driver and response model
1396 intercomparison project—protocol and preliminary results, *Bulletin of the American Meteorological*
1397 *Society*, 98, 1185-1198, 2017.

1398 O’Gorman, P. A., Allan, R. P., Byrne, M. P., and Previdi, M.: Energetic Constraints on Precipitation
1399 Under Climate Change, *Surveys in Geophysics*, 33, 585-608, [https://doi.org/10.1007/s10712-011-](https://doi.org/10.1007/s10712-011-9159-6)
1400 [9159-6](https://doi.org/10.1007/s10712-011-9159-6), 2012.

1401 Ovchinnikov, M., Ackerman, A. S., Avramov, A., Cheng, A., Fan, J., Fridlind, A. M., Ghan, S.,
1402 Harrington, J., Hoose, C., and Korolev, A.: Intercomparison of large-eddy simulations of Arctic
1403 mixed-phase clouds: Importance of ice size distribution assumptions, *Journal of Advances in*
1404 *Modeling Earth Systems*, 6, 223-248, <https://doi.org/10.1002/2013MS000282>, 2014.

1405 Richardson, T., Forster, P., Andrews, T., Boucher, O., Faluvegi, G., Fläschner, D., Hodnebrog, Ø.,
1406 Kasoar, M., Kirkevåg, A., and Lamarque, J.-F.: Drivers of precipitation change: An energetic
1407 understanding, *Journal of Climate*, 31, 9641-9657, <https://doi.org/10.1175/JCLI-D-17-0240.1>, 2018.

1408 Rosenfeld, D.: Suppression of rain and snow by urban and industrial air pollution, *Science*, 287, 1793-
1409 1796, [10.1126/science.287.5459.1793](https://doi.org/10.1126/science.287.5459.1793), 2000.

1410 Rosenfeld, D., Lohmann, U., Raga, G. B., O’Dowd, C. D., Kulmala, M., Fuzzi, S., Reissell, A., and
1411 Andreae, M. O.: Flood or drought: How do aerosols affect precipitation?, *Science*, 321, 1309-1313,
1412 [10.1126/science.1160606](https://doi.org/10.1126/science.1160606), 2008.

1413 Rosenfeld, D., Wood, R., Donner, L. J., and Sherwood, S. C.: Aerosol cloud-mediated radiative forcing:
1414 highly uncertain and opposite effects from shallow and deep clouds, in: *Climate Science for Serving*
1415 *Society*, Springer, 105-149, https://doi.org/10.1007/978-94-007-6692-1_5, 2013.

1416 Rosenfeld, D., Zhu, Y., Wang, M., Zheng, Y., Goren, T., and Yu, S.: Aerosol-driven droplet
1417 concentrations dominate coverage and water of oceanic low-level clouds, *Science*, 363, eaav0566,
1418 DOI: [10.1126/science.aav0566](https://doi.org/10.1126/science.aav0566), 2019.

1419 Rothenberg, D., Avramov, A., and Wang, C.: On the representation of aerosol activation and its
1420 influence on model-derived estimates of the aerosol indirect effect, *Atmos. Chem. Phys*, 18, 7961-
1421 7983, <https://doi.org/10.5194/acp-18-7961-2018>, 2018.

1422 Samset, B., Myhre, G., Forster, P., Hodnebrog, Ø., Andrews, T., Faluvegi, G., Flaeschner, D., Kasoar,
1423 M., Kharin, V., and Kirkevåg, A.: Fast and slow precipitation responses to individual climate forcings: A
1424 PDRMIP multimodel study, *Geophysical Research Letters*, 43, 2782-2791,
1425 <https://doi.org/10.1002/2016GL068064>, 2016.

1426 Savane, O. S., Vant-Hull, B., Mahani, S., and Khanbilvardi, R.: Effects of Aerosol on Cloud Liquid
1427 Water Path: Statistical Method a Potential Source for Divergence in Past Observation Based
1428 Correlative Studies, *Atmosphere*, 6, 273-298, <https://doi.org/10.3390/atmos6030273>, 2015.

1429 Seifert, A., and Beheng, K.: A two-moment cloud microphysics parameterization for mixed-phase
1430 clouds. Part 2: Maritime vs. continental deep convective storms, *Meteorology and Atmospheric*
1431 *Physics*, 92, 67-82, <https://doi.org/10.1007/s00703-005-0113-3>, 2006a.

1432 Seifert, A., and Beheng, K. D.: A two-moment cloud microphysics parameterization for mixed-phase
1433 clouds. Part 1: Model description, *Meteorology and atmospheric physics*, 92, 45-66,
1434 <https://doi.org/10.1007/s00703-005-0112-4>, 2006b.

1435 Seifert, A., and Heus, T.: Large-eddy simulation of organized precipitating trade wind cumulus
1436 clouds, *Atmos. Chem. Phys*, 13, 5631-5645, doi:10.5194/acpd-13-1855-2013, 2013.

1437 Seifert, A., Heus, T., Pincus, R., and Stevens, B.: Large-eddy simulation of the transient and near-
1438 equilibrium behavior of precipitating shallow convection, *Journal of Advances in Modeling Earth*
1439 *Systems*, <https://doi.org/10.1002/2015MS000489>, 2015.

1440 Seigel, R. B.: Shallow Cumulus Mixing and Subcloud Layer Responses to Variations in Aerosol
1441 Loading, *Journal of the Atmospheric Sciences*, <https://doi.org/10.1175/JAS-D-13-0352.1>, 2014.

1442 Simpson, E., Connolly, P., and McFiggans, G.: An investigation into the performance of four cloud
1443 droplet activation parameterisations, *Geoscientific Model Development*, 7, 1535-1542,
1444 doi:10.5194/gmd-7-1535-2014, 2014.

1445 Small, J. D., Chuang, P. Y., Feingold, G., and Jiang, H.: Can aerosol decrease cloud lifetime?,
1446 *Geophysical Research Letters*, 36, <https://doi.org/10.1029/2009GL038888>, 2009.

1447 Sourdeval, O., Gryspeerdt, E., Krämer, M., Goren, T., Delanoë, J., Afchine, A., Hemmer, F., and Quaas,
1448 J.: Ice crystal number concentration estimates from lidar–radar satellite remote sensing–Part 1:
1449 Method and evaluation, <https://doi.org/10.5194/acp-18-14327-2018> 2018.

1450 Spill, G., Stier, P., Field, P. R., and Dagan, G.: Effects of aerosol in simulations of realistic shallow
1451 cumulus cloud fields in a large domain, *Atmospheric Chemistry and Physics*,
1452 <https://doi.org/10.5194/acp-2019-432>, 2019.

1453 Stephens, G. L., Gabriel, P. M., and Partain, P. T.: Parameterization of atmospheric radiative transfer.
1454 Part I: Validity of simple models, *Journal of the atmospheric sciences*, 58, 3391-3409,
1455 [https://doi.org/10.1175/1520-0469\(2001\)058%3C3391:POARTP%3E2.0.CO;2](https://doi.org/10.1175/1520-0469(2001)058%3C3391:POARTP%3E2.0.CO;2), 2001.

1456 Stevens, B., and Feingold, G.: Untangling aerosol effects on clouds and precipitation in a buffered
1457 system, *Nature*, 461, 607-613, 10.1038/nature08281, 2009.

1458 Stevens, B., Farrell, D., Hirsch, L., Jansen, F., Nuijens, L., Serikov, I., Brüggmann, B., Forde, M., Linne,
1459 H., and Lonitz, K.: The Barbados Cloud Observatory: Anchoring investigations of clouds and
1460 circulation on the edge of the ITCZ, *Bulletin of the American Meteorological Society*, 97, 787-801,
1461 2016.

1462 Stevens, B., Ament, F., Bony, S., Crewell, S., Ewald, F., Gross, S., Hansen, A., Hirsch, L., Jacob, M., and
1463 Kölling, T.: A high-altitude long-range aircraft configured as a cloud observatory—the NARVAL
1464 expeditions, *Bulletin of the American Meteorological Society*, <https://doi.org/10.1175/BAMS-D-18-0198.1>, 2019.

1466 Storelvmo, T., Hoose, C., and Eriksson, P.: Global modeling of mixed-phase clouds: The albedo and
1467 lifetime effects of aerosols, *Journal of Geophysical Research: Atmospheres*, 116,
1468 <https://doi.org/10.1029/2010JD014724>, 2011.

1469 Tao, W.-K., Chen, J.-P., Li, Z., Wang, C., and Zhang, C.: Impact of aerosols on convective clouds and
1470 precipitation, *Reviews of Geophysics*, 50, RG2001, <https://doi.org/10.1029/2011RG000369>, 2012.

1471 Twomey, S.: The influence of pollution on the shortwave albedo of clouds, *Journal of the*
1472 *atmospheric sciences*, 34, 1149-1152, 1977.

1473 van den Heever, S. C., Stephens, G. L., and Wood, N. B.: Aerosol Indirect Effects on Tropical
1474 Convection Characteristics under Conditions of Radiative-Convective Equilibrium, *Journal of the*
1475 *Atmospheric Sciences*, 68, 699-718, [10.1175/2010jas3603.1](https://doi.org/10.1175/2010jas3603.1), 2011.

1476 Varble, A.: Erroneous attribution of deep convective invigoration to aerosol concentration, *Journal*
1477 *of the Atmospheric Sciences*, 75, 1351-1368, <https://doi.org/10.1175/JAS-D-17-0217.1>, 2018.

1478 White, B., Gryspeerdt, E., Stier, P., Morrison, H., Thompson, G., and Kipling, Z.: Uncertainty from
1479 choice of microphysics scheme in convection-permitting models significantly exceeds aerosol effects,
1480 *Atmospheric Chemistry and Physics*, 7, <https://doi.org/10.5194/acp-17-12145-2017>, 2017.

1481 Williams, E., Rosenfeld, D., Madden, N., Gerlach, J., Gears, N., Atkinson, L., Dunnemann, N.,
1482 Frostrom, G., Antonio, M., and Biazon, B.: Contrasting convective regimes over the Amazon:
1483 Implications for cloud electrification, *J. Geophys. Res.*, 107, <https://doi.org/10.1029/2001JD000380>,
1484 2002.

1485 Xue, H., and Feingold, G.: Large-eddy simulations of trade wind cumuli: Investigation of aerosol
1486 indirect effects, *Journal of the atmospheric sciences*, 63, 1605-1622,
1487 <https://doi.org/10.1175/JAS3706.1>, 2006.

1488 Yuan, T., Remer, L. A., Pickering, K. E., and Yu, H.: Observational evidence of aerosol enhancement of
1489 lightning activity and convective invigoration, *Geophysical Research Letters*, 38,
1490 [10.1029/2010gl046052](https://doi.org/10.1029/2010gl046052), 2011a.

1491 Yuan, T., Remer, L. A., and Yu, H.: Microphysical, macrophysical and radiative signatures of volcanic
1492 aerosols in trade wind cumulus observed by the A-Train, *Atmospheric Chemistry and Physics*, 11,
1493 7119-7132, [10.5194/acp-11-7119-2011](https://doi.org/10.5194/acp-11-7119-2011), 2011b.

1494 Zängl, G., Reinert, D., Rípodas, P., and Baldauf, M.: The ICON (ICOsahedral Non-hydrostatic)
1495 modelling framework of DWD and MPI-M: Description of the non-hydrostatic dynamical core,
1496 *Quarterly Journal of the Royal Meteorological Society*, 141, 563-579,
1497 <https://doi.org/10.1002/qj.2378>, 2015.

1498